

IMPLEMENTATION AND ASSESSMENT TECHNIQUES FOR THE
APPLICATIONS OF ADVANCED DISTRIBUTION MANAGEMENT SYSTEM

by

Md Shakawat Hossan

A dissertation submitted to the faculty of
The University of North Carolina at Charlotte
in partial fulfillment of the requirements
for the degree of Doctor of Philosophy in
Electrical Engineering

Charlotte

2018

Approved by:

Dr. Badrul Chowdhury

Dr. Asis Nasipuri

Dr. Valentina Cecchi

Dr. Churlzu Lim

©2018
Md Shakawat Hossan
ALL RIGHTS RESERVED

ABSTRACT

MD SHAKAWAT HOSSAN. Implementation and Assessment Techniques for the Applications of Advanced Distribution Management System. (Under the direction of DR. BADRUL CHOWDHURY)

In recent years, massive numbers of distributed energy resources are being installed in distribution feeders at both the utility and customer levels. These integrations are creating bi-directional power flow complexities in all the existing applications of distribution management system (DMS) and outage management system (OMS). Therefore, a significant interest is growing among utilities to combine all the DMS and OMS functionalities with distributed energy resources management system. This combined structure is known as advanced distribution management system (ADMS). ADMS is comprised of three major applications: conservation voltage reduction (CVR), demand response(DR), and fault location, isolation, and service restoration (FLISR). In this dissertation, some critical challenges for ADMS applications are defined with the proposed solutions. The objectives of this dissertation are: (1) Selection of appropriate load model for the assessment of CVR in a time-varying manner; (2) Implementation and assessment of CVR with the integration of DER and considering time varying stochasticity; (3) A combined framework of CVR and DR for maximizing the energy efficiency; (4) Fault location scheme for FLISR with very high penetration of DER.

The first objective of this dissertation is to select the most appropriate voltage sensitive composite load model. The selection of an appropriate load model can lead to the calculation of energy savings precisely with near accurate CVR factor. In addition, appropriate load model can help to calculate the voltage sensitivity factor more precisely which can help the utility to identify improvements in voltage profile throughout a distribution feeder during CVR deployment. Therefore, two widely used voltage sensitive load models- exponential and ZIP load model are extensively

analyzed and compared. Two different dual-stage filtering techniques are discussed for retrieving load coefficients for individual models.

The second objective defines a model of CVR deployment where voltage sensitive loads and smart inverter interfaced DERs are considered for effective CVR planning. Voltage control strategies of smart inverters provide additional benefits for flattening the voltage profile while deploying CVR. In addition, a lower voltage set point at the substation helps to deploy deeper CVR deployment and more energy savings. Moreover, a time-varying stochastic CVR deployment is also shown for advanced planning which might help the utility to know about the most beneficial times if short-term CVR deployment is intended.

The third objective develops a framework to maximize the energy efficiency by integrating CVR and DR both. This framework considers the deepest CVR deployment possible, such as objective two, with the addition of load shifting based DR. In addition, DR program in this model considers different tariff/incentive plans and provides the most suitable one for each customer. The entire model also depicts an energy management plan for individual customers. The model considers the integration of PV based DERs and battery energy storage systems. Stochasticity in load consumption and DER injection is also considered.

The final objective of this dissertation is to demonstrate a fault location scheme for FLISR. The scheme is developed based on the collected data of wireless sensors and smart meters when faults occur. The scheme considers bi-directional power flows with high penetration of DERs. In addition, simultaneous occurrence of faults at different locations of a distribution feeder is considered in case of any natural calamity. The model is independent of building an impedance matrix. Instead, it uses a graph theory based method to narrow the search space of suspected faults.

These objectives are beneficial for both utility and customers in terms of energy efficiency, reliability, and resiliency. All these objectives are developed theoretically

and tested in utility scale distribution feeders. In addition, the future challenges are also described for the modernization of the envisioned distribution system.

ACKNOWLEDGEMENTS

The journey of PhD is a challenging but mesmerizing experience. This journey would have not been fulfilled without the ever-ending inspiration and support of many people. At this point, I would like to take the opportunity to extend my heartiest appreciation.

At first, I would like to express my sincere gratitude to my advisor, Dr. Badrul Chowdhury. It would have not been possible to finish this dissertation without his tremendous support. His enormous knowledge and motivational endorsement have led me to solve difficult problems and eventually complete this dissertation. Moreover, his challenging comments and careful direction on every part of my doctoral study have helped me to gain deeper understanding on modern power systems and to improve my technical and communication skills. I am also grateful to Dr. Valentina Cecchi, Dr. Asis Nasipuri, and Dr. Churlzu Lim for serving in my doctoral committee and for their valuable time in reviewing this dissertation. It would have not been possible to submit this dissertation in its present form without their extremely valuable feedback. Energy Production and Infrastructure Center (EPIC) of UNC Charlotte, Center for Applied Power and Energy Research (CAPER), and Savannah River National Lab (SRNL) deserve much appreciation for providing financial support to complete this dissertation.

Next, I would like to thank Rajib and Juma for their continuous support and heartiest affection as an elder brother and sister throughout our stay at Charlotte. I would also like to mention my friends- Hasan, Tapu, Ucchash, and Rony for their ever ending love and support for my passions. In addition, I would like to thank Mesbah and Maliha for being there in any need. Mentioning Adnan and Muhib throughout this journey is noteworthy. Apart from these beautiful souls, other Bangladeshi graduate students at UNC Charlotte have been very helpful.

Most of all, I would like to extend a special thanks to my family. My wife, Bably,

has made countless sacrifices to help me to reach at this point. Without her extreme support and patience, It would have not been possible for me to complete this dissertation. I am thankful to my mother, mother-in-law, father-in-law, and my younger brother for believing in me. Inspirational words of my late father are unforgettable which have created the pathways of my life.

Finally, I would like to utter that the write ups of late Dr. Humayun Ahmed and the music of Steven Wilson have helped me to think about life and it's goal. Their work have motivated me so far and will continue to do so for the years to live.

TABLE OF CONTENTS

LIST OF FIGURES	xi
LIST OF TABLES	xiv
LIST OF SYMBOLS	1
CHAPTER 1: INTRODUCTION	1
1.1. Conservation Voltage Reduction (CVR)	2
1.1.1. Implementation of CVR	2
1.1.2. Assessment of CVR	3
1.1.3. Challenges in CVR deployment	4
1.2. Demand Response	7
1.2.1. Implementation of DR	7
1.2.2. Challenges in DR program	9
1.3. Fault location, isolation, and service restoration (FLISR)	10
1.3.1. Implementation of FLISR	10
1.3.2. Challenges in FLISR	11
CHAPTER 2: Assessment and Implementation of Conservation Voltage Reduction	13
2.1. Comparison of Load Models for Assessing CVR deployment	13
2.1.1. Overview	13
2.1.2. Load Modeling	18
2.1.3. Dual-Stage Filtering	20
2.1.4. Factor Estimation	26
2.1.5. Simulation and Results	29

	ix
2.1.6. Summary	38
2.2. Time-Varying Stochastic and Analytical Assessment of CVR	40
2.2.1. Overview	40
2.2.2. Distribution System Modeling	41
2.2.3. Uncertainty Modeling	45
2.2.4. Analytical Approach	47
2.2.5. Simulation and Results	48
2.2.6. Summary	53
2.3. Effective CVR planning with Smart DERs	54
2.3.1. Overview	56
2.3.2. Var Control Using Smart Inverter	57
2.3.3. Formulation Methodology	58
2.3.4. Results and Analysis	62
2.3.5. Summary	69
CHAPTER 3: Integrated CVR and Demand Response Framework for Distribution System	70
Nomenclature	70
3.1. Overview	73
3.2. Problem Formulation	76
3.2.1. Objective Function	76
3.2.2. Load Modeling	76
3.2.3. Distribution Feeder Modeling	79
3.2.4. DER Modeling	80

	x
3.2.5. Capacitor Bank Modeling	81
3.2.6. Voltage Control	82
3.2.7. Electricity Pricing	82
3.3. Prediction Uncertainty	83
3.4. Numerical Analysis	86
3.5. Summary	89
CHAPTER 4: Data-Driven Fault Location Scheme for FLISR Program	91
4.1. Overview	91
4.2. Proposed Fault Location Method	95
4.3. Search Space Reduction	96
4.3.1. Ratio Test	98
4.3.2. Modified depth first search(MDFS)	102
4.4. Voltage Profile Analysis	103
4.5. Simulation Results	107
4.6. Summary	110
CHAPTER 5: Conclusion	113
REFERENCES	117

LIST OF FIGURES

FIGURE 1.1: ADMS platform for envisioned distribution system.	2
FIGURE 1.2: CVR deployment with different load types; a. Voltage difference, b. Power difference.	6
FIGURE 2.1: Dual-stage filtering for CVRF and VSF estimation.	28
FIGURE 2.2: (a).Schematic diagram of the simulation. (b).Converted feeder	30
FIGURE 2.3: CYME vs OpenDSS (a). Short circuit (b). Power Flow (c). Short-circuit histogram (d). Power flow histogram.	31
FIGURE 2.4: Phase A voltage profile of a February week.	32
FIGURE 2.5: Phase A CVRoff voltage distribution for a February week.	32
FIGURE 2.6: Usage of dual-stage RLS (a) CVRF in first stage (TEXP), (b) CVRF in second stage (TZIP), (c) VSF in first stage (TEXP), (d) VSF in second stage (TZIP).	34
FIGURE 2.7: Usage of dual-stage KF (a) CVRF in first stage (TEXP), (b) CVRF in second stage (TZIP), (c) VSF first stage (TEXP), (d) VSF in second stage (TZIP).	35
FIGURE 2.8: Estimation error for CVRF (a) using dual-stage RLS, (b) using dual-stage KF; Estimation error for VSF (c) using dual-stage RLS, (d) using dual-stage KF.	36
FIGURE 2.9: (a) Measured and simulated active power on February 7 th ; (b) Zoomed part 1 of Fig. 2.9(a); (c) Zoomed part 2 of Fig. 2.9(a).	38
FIGURE 2.10: Long term CVR vs short term CVR.	40
FIGURE 2.11: Efficiency vs Power and Derating factor vs Temperature relationship.	43
FIGURE 2.12: Modified dynamic volt-var curve.	44
FIGURE 2.13: Typical discretization of the PDF of load forecast error.	46
FIGURE 2.14: Hierarchy of time alternatives of AHP.	49

FIGURE 2.15: Ranking strategy for CVR deployment benefits.	49
FIGURE 2.16: CDF of CVRoff voltage profile for winter.	50
FIGURE 2.17: Average secondary system voltage profile: (a). Case 1. (b). Case 2.	51
FIGURE 2.18: Factor Weights: (a). Case 1. (b). Case 2.	52
FIGURE 2.19: UWF for case 1 a. CVRF and LF. b. CVRF and VSF.	53
FIGURE 2.20: UWF for case 1 a. CVRF and LF. b. CVRF and VSF.	54
FIGURE 2.21: Conceptual system diagram.	59
FIGURE 2.22: Modified ieee37 bus test system.	63
FIGURE 2.23: Average voltage profile of the system (Operating voltage=1.04 p.u.).	63
FIGURE 2.24: a. Time vs Temp b. Time vs Load Shape c. Time vs Irradiance.	64
FIGURE 2.25: Source voltage shape (Smart PV).	65
FIGURE 2.26: Feeder voltage profile (smart PV) a. Summer b. Winter.	66
FIGURE 2.27: Smart PV generation a. active Power b. reactive Power.	66
FIGURE 2.28: Node voltage at interconnection points.	67
FIGURE 2.29: Inverter droop settings.	67
FIGURE 2.30: Source voltage shape (Conventional PV).	67
FIGURE 2.31: Feeder voltage profile (Conventional PV) a. Summer b. Winter.	68
FIGURE 2.32: Conventional PV active power generation.	68
FIGURE 3.1: Load consumption with integrated CVR and DR.	75
FIGURE 3.2: Conceptual diagram of radial distribution feeder.	80

FIGURE 3.3: Modified IEEE37 bus test system.	86
FIGURE 3.4: Price deviation for three demand response plans.	87
FIGURE 3.5: Aggregated load consumption for three cases; a. critical day, b. typical weekday, c. typical weekend.	88
FIGURE 3.6: Mean voltage profile for three cases; a. critical day, b. typical weekday, c. typical weekend.; SVR operation for three cases; d. critical day, e. typical weekday, f. typical weekend.;CAP bank operation for three cases; g. critical day, g. typical weekday, i. typical weekend.	89
FIGURE 3.7: CVR factor for CVR with and without LS.	89
FIGURE 4.1: Conceptual framework of WSN for ADMS.	92
FIGURE 4.2: One-line distribution system schematic (a). W/o fault; (b). W fault.	98
FIGURE 4.3: Modified DFS (MDFS) algorithm for fault location.	102
FIGURE 4.4: Modified distribution feeder for fault analysis.	108
FIGURE 4.5: Identified faulty zones for voltage profile comparison.	109
FIGURE 4.6: Error for buses in (a). Zone 1; (b). Zone 2; (c). Zone 3 (d).combination of buses in different zones; Error for fictitious root buses in (e). Zone 1; (f). Zone 2; (g). Zone 3. (h) combination of fictitious root buses in different zones.	111
FIGURE 4.7: Combined error of sets of fictitious buses using MC simulation.	112
FIGURE 5.1: Hierarchical control and assessment of CVR deployment.	114

LIST OF TABLES

TABLE 1.1: Experimented DR programs by the utilities.	8
TABLE 2.1: Normal distribution parameters for CVRoff voltage shape.	33
TABLE 2.2: Performance comparison in two stages for both load models.	38
TABLE 2.3: ZIP coefficients with customer class.	42
TABLE 2.4: Distribution of Winter Voltage Profile.	50
TABLE 2.5: Load and loss analysis for different sub-cases.	69
TABLE 3.1: Total load consumption cost and DRP selection for each customer.	90
TABLE 4.1: RT at the sensor buses.	109
TABLE 4.2: Set of fictitious root buses.	110

CHAPTER 1: INTRODUCTION

In the past, utilities had very negligible visibility over their distribution feeders. Recently, measurement devices, such as smart meters, current and voltage sensors, synchro phasors or micro phasor measurement unit (μ -pmu) as well as high-speed communication have become available to increase visibility. In parallel to the technical advancement in measurement and communication, massive amounts of distributed energy resources (DERs) are being deployed in distribution feeders. As a consequence, today's distribution management systems (DMS) and outage management systems (OMS) have limited functionality in dealing with DERs, let alone leveraging the benefits of DERs and feeder measurement devices have to offer. As part of ongoing grid modernization efforts at utilities, these systems are being replaced with an advanced distribution management system (ADMS). ADMS is an integrated system that combines the applications those were previously part of a DMS and an OMS with a distributed energy resources management system [1]. According to the department of energy, ADMS is a software platform that should have the real-time estimation, and optimization framework for the following applications: conservation voltage reduction (CVR), Fault location, isolation, and service restoration (FLISR), and demand response (DR) [2]. Apart from these applications, ADMS can also be a part of Distribution System Operator's (DSO) decision support system based on economic dispatch, optimal power flow (OPF), and/or intelligent algorithms considering different constraints.

An ADMS platform is designed to improve efficiency, affordability, reliability, and resiliency concerns in the presence of DER. The ADMS platform coordinates with both utility and customer level DERs, loads, and field devices through available

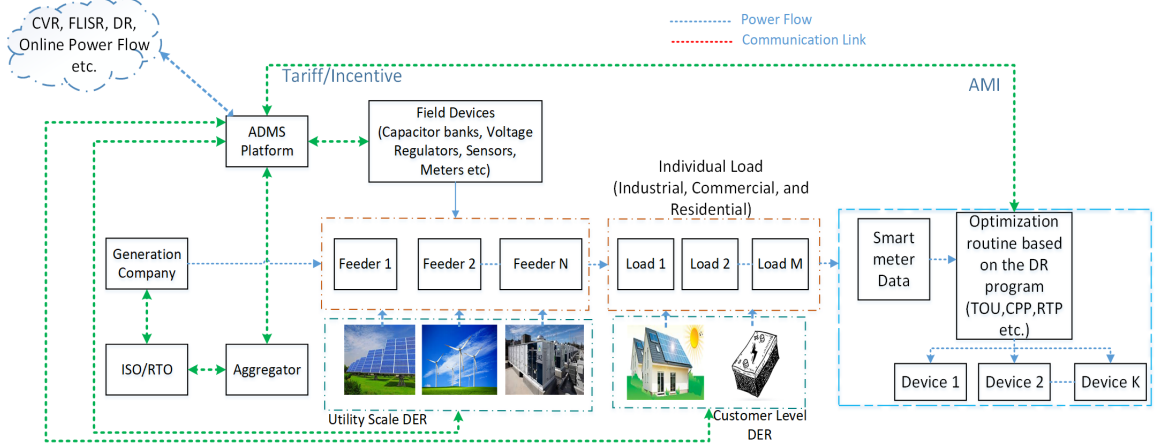


Figure 1.1: ADMS platform for envisioned distribution system.

communication schemes for better integration and service. This management also helps to balance the generation and distribution along with the implication of desired functionalities as shown in Fig.1.1. However, depending on the specific situation at each utility, the constraints can vary. This dissertation discusses newly defined critical challenges for the major ADMS applications listed above and provides solution for those.

1.1 Conservation Voltage Reduction (CVR)

1.1.1 Implementation of CVR

Conservation voltage reduction (CVR) is a volt-var control technique in the modern smart grid for reducing the load consumption or long-term energy consumption. The implementation of CVR relies on a simple technique that voltage sensitive loads will consume less energy with a reduction in operational voltage. Moreover, while reducing the load, line losses also get reduced during the deployment of CVR. However, the constraint is to maintain the voltage in the lower ANSI band (0.95-1.0 $p.u.$) at the customer premises. Therefore, multi-objective formulation of CVR can be presented as:

$$\text{Min} \sum_i P_{i,t}^{\text{Load}} + \sum_s P_{s,t}^{\text{Loss}} \quad (1.1)$$

$$\textit{where } V_{min} \leq V_i \leq V_{max} \quad (1.2)$$

$i, s \in \mathbb{Z}$ refer the nodes and sections in the feeder, respectively. Since voltage, V is the primary control variable, traditional voltage control devices such as capacitor banks or step voltage regulators play a vital role in CVR deployment. Their placement can be made based on the level of voltage reduction and minimum investment capital of the utility [3]. However, these devices are limited in number in the entire distribution feeder. Thus, the increasing number of DERs can be used to control the voltage. DERs integrated with conventional inverters are not able to control the voltage. Depending on the uncertainty of renewable energy-based DERs, node voltages might go beyond the upper or lower limits. Therefore, smart inverters with various voltage control algorithms have been proposed in the literature [4],[5].

1.1.2 Assessment of CVR

Since the deployment of CVR mainly depends on load to voltage sensitivity (LTV), therefore, precise measurement and estimation of load consumption and voltage profile is the primary affair on the assessment of CVR. As yet, several assessment methodologies are found in the literature to estimate these factors which can be categorized as follows[6]: comparison-based [7], synthesis-based [8], regression-based [9], and simulation-based [10]. Comparison-based methods need two sets of feeders with similar configuration and topology- one is referred as the control group, and the other is denoted as the treatment group. CVR is deployed in treatment group and comparison is conducted with the control group to measure energy savings. In some cases, energy savings is retrieved by comparing the same feeders on two different days with similar weather and load patterns: one with CVR deployment and the other without CVR deployment. In these cases, control and treatment groups are treated as the same. Synthesis-based methods sum up the individual characteristics as a function of voltage for different types of loads or customer classes. This type of study is con-

ducted in laboratory testing for individual devices, such as [11]. However, it does not consider the stochastic behavior of loads or time-varying characteristics. Regression-based methods linearize the load behavior depending on voltage and other associated coefficients [12]. Simulation-based methods compare the energy consumption for the same feeder with and without voltage reduction by real circuit type simulation.

1.1.3 Challenges in CVR deployment

CVR is already a well-established technique for utilities to minimize the energy consumption and reduce the peak loading condition. However, there are still some challenges left for deploying and quantifying CVR as a energy efficiency measure, which can be achieved using the ADMS platform:

- i. Evaluating the effectiveness of CVR deployment is the most crucial thing. In other words, the correct estimation of energy savings is important for both technical and economic evaluation to provide the proof of concept. Incorrect estimation of energy savings can lead to wrong revenue calculation out of CVR deployment investment. The afore-mentioned methodologies have some limitations. For example, usage of comparison-based methods need two similar feeders with the same topology or configuration or two different days with similar loading and weather pattern which is difficult to find in reality. Synthesis based methods do not consider the stochasticity in the load profile. For regression and simulation-based methods, selection of the accurate load model, parameter identification of the associated load model, and voltage profile estimation of CVR off time during the CVR deployment period are of utmost importance. In [12] and [13], time varying parameter identification for exponential and ZIP load model is shown using recursive least square (RLS) and robust RLS methods, respectively. However, there is no certain comparison of the load models to figure out which load model works with maximum precision to estimate energy

savings using CVR factor(CVRF). The CVRF can be represented as below:

$$CVRF = \frac{\frac{P_o - P}{P_o}}{\frac{V_o - V}{V_o}} \quad (1.3)$$

where P and P_o define the CVR on and off time load consumption, respectively. Similarly, V and V_o denote the CVR on and off time operating voltages. P_o and V_o are fictitious terminologies since they need to be estimated when CVR is on. If accurate V_o is estimated with statistical analysis of the voltage variation during CVR off time and the correct load model is selected with associated estimated parameters, the CVRF can be calculated effectively with minimum error. Since the ADMS is the center of gathering all the data from substation to smart meters, historical data can be utilized to find the actual representation of voltage and load profile both during CVR on and off time.

- ii. Deploying CVR improves the overall voltage profile of the feeder if the load is mixed. A mixed load can be described as ZIP load where a reasonable mix of constant P, Q, Z, and I are present rather than the presence of only P and Q components as the majority percentage. If the loads are mostly constant P, Q, and the operational voltage is reduced at the substation, CVR does not reduce the load consumption significantly. Therefore, almost similar amount of current flows towards the load which eventually increases the difference in voltage drop throughout the feeder comparing CVR on and off time. On the other hand, for ZIP loads, the consumption gets reduced along with voltage reduction. Thus, the current flow also gets reduced which leads to loss reduction and improves the voltage profile, as presented in Fig.1.2. The theoretical framework for CVR can be described by quantifying voltage sensitivity factor (VSF) as:

$$VSF_{i,j} = \frac{\sum_i \frac{V_{o,i} - V_i}{V_{o,i}}}{K \sum_j \frac{P_{o,j} - P_j}{P_{o,j}}} \quad (1.4)$$

where $i, j \in \mathbb{Z}$ refer to the number of load and source buses, respectively and K denotes the number of total load buses. P and P_o represent CVR on and off time instantaneous load consumptions. In (1.4) numerator and denominator presents the change in average voltage profile and real power injection from the sources, respectively. VSF is higher if the change in average voltage profile is higher and the change in load consumption is lower, and vice versa. Thus, based on the VSF, a utility company can draw conclusions about load characteristics, and prospective success of CVR deployment over time using the ADMS platform. This study will provide more insights on load characteristics by quantifying VSF and CVRF using both exponential and ZIP model in a time-varying manner with the consideration of stochasticity. Comparison of load models are also extensively discussed in this dissertation.

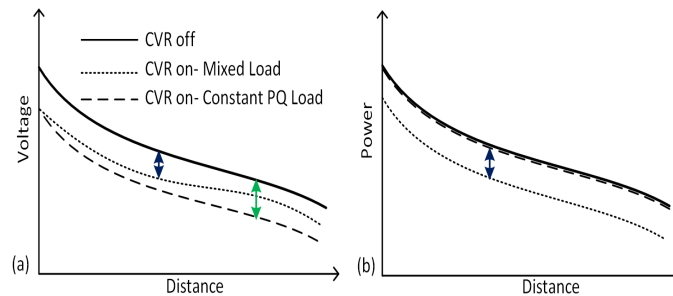


Figure 1.2: CVR deployment with different load types; a. Voltage difference, b. Power difference.

- iii. More often, utilities need to analyze a feeder in details to run CVR and rank the benefits with time depending on various factors. ADMS based online power flow (OLPF) can be utilized to assess the benefits depending on several factors. Along with the afore-mentioned factors, loss factor(LF) can also be integrated in the time-varying analysis. In such kind of analysis, stochasticity of load shape and DERs generation should be included. This study discusses about the ranking of benefits of CVR deployment.
- iv. With the advent of smart inverter technologies, implementation of CVR might receive additional benefits to flatten the voltage profile. However, to achieve this

a centralized ADMS controller is needed which can optimize and co-ordinate the operation of distributed smart inverters with other voltage regulating devices, such as, step voltage regulators (SVR) and capacitor banks. This study discusses the coordination of all the devices during CVR deployment.

1.2 Demand Response

1.2.1 Implementation of DR

Demand response (DR) refers to the management of end-user loads in response to the signals from the utility or operator for modifying the demand over time. The signal can be based on price or reliability indices during peak loading condition. Enhanced two-way communication using AMI between utilities and customers is making DR efforts much easier. The primary goals of DR implementation are achieving energy efficiency, and ensuring reliability and safety during system stress. The concept of DR is to alter or shift the load from one time to another with the cooperation of the customers evoked by utilities using some set of constraints. The modern DR concept is incorporated with distributed energy resources (DERs) and energy storage systems (ESSs) [15],[16]. The entire idea can be portrayed as below:

$$P_{TL,t}^n = \sum_L (P_{L,s}^o - P_{L,t}^s - P_{L,t}^c) - \sum_x (P_{x,t}) + \sum_y (P_{y,t}^c - P_{y,t}^d) \quad (1.5)$$

where $\forall L \in \text{Loads}$, $x \in \text{DERs}$, $y \in \text{ESSs}$, and $\sum_L \sum_t P_{L,t}^s = 0$. P_{TL}^n and P_L^o refer to the accumulated net and original consumption for each individual load, respectively. P_x , P_y^d , and P_y^c denote the production from DERs, discharging, and charging state of ESSs, respectively. P_L^s and P_L^c denote the shifted and curtailed load, respectively. Subscript t defines time of the implementation. As yet, DR programs have been analyzed and optimized based on three categories [17]: control mechanisms, price or incentive based motivations, and decision based operations. Control mechanisms have a communication structure between customers and the utility either with or without

peer to peer networking among the customers. The price or incentive based category is followed by the process that establishes a tariff for different time periods of the day or incentive payments to consume less energy when the market has high electricity price or grid reliability is threatened. Decision based operations are mainly task scheduling or energy management to activate or deactivate the load. They all have a direct or indirect relationship to price. Pricing is dependent on several schemes such as time of use (TOU), critical peak pricing (CPP), real time pricing (RTP), peak rebate time (PRT) etc. embedded with other categories [18]. On the other hand, incentive based programs are operated by giving rights to utilities to control or curtail the load for participating customers when there are contingencies or emergencies on the basis of some pre-defined values. Several incentive-based schemes have been utilized so far such as, capacity market planning (CMP), emergency demand response program (EDRP) etc. where participating customers receive incentives and non-participating customers may be penalized. Table 1.1 demonstrates some pilot DR programs [19]:

Table 1.1: Experimented DR programs by the utilities.

Utility	DR program
APU	PTR
PG&E, SCE, SDG&E	CPP,TOU
Xcel Energy	CPP,TOU
Gulf Power	CPP
Idaho Power Company	TOU
Commonwealth Edison	RTP
Ameren	TOU, CPP
GPU	TOU, CPP
PSE&G	CPP, TOU
Hydro Ottawa	RTP
BPA,PGE,PUD, Pacific Corp	TOU, CPP

PTR: peak time rebate, CPP: critical peak pricing, TOU: time of use, RTP: real time pricing.

1.2.2 Challenges in DR program

Using the schemes described above, DR programs can be optimized based on the following objective functions: minimization of electricity cost, minimization of total power consumption, maximization of social welfare, and maximizing reliability during peak loading condition [18]. Some research studies included multi-objective functions by appending the aforementioned function(s). A wide range of algorithms are also deployed to achieve these objectives. However, there are still many challenges remaining that need to be solved for better picturization of DR programs, which are explained below:

- i. Table 1.1 depicts a number of DR plans experimented by utilities. However, all these plans were induced separately. In the open market, to attract more customers and change their load behavior pattern with maximum comfortability, all available options need to be provided. Therefore, if there are n number of customers and p number of schemes, each customer should have the flexibility to choose any scheme which is the most suitable for them. Similarly, the utility should be able to observe n^p instances to find the maximum beneficial DR programs that can reduce customer billing and increase the reliability. Moreover, customers should have the preference to switch from one plan to another scheme utilizing a day-ahead program. For such cases, the ADMS platform can play a role to manage every device within a load using direct load control, or customers can let the utility know their preference of load shifting for energy management. Consequently, ADMS can guide the customers about which DR plan to choose for minimizing the consumption cost. This plan preference method will create a win-win situation for both utility and customers.
- ii. In an ADMS platform, combined CVR and DR framework can be modelled for higher energy efficiency and maximum reliability. In addition to DR signals,

smart inverter functionalities with distributed control and traditional voltage control devices, such as capacitor bank and SVR throughout the feeder can be used to control the voltage in the lowest possible service range for reducing stress during peak loading conditions, resulting in better energy management. Recent research has demonstrated that CVR is well suitable for thermostatic loads as well[20]. Therefore, in direct load control (DLC) type DR, thermostatic loads do not necessarily have to be subjected to control, which can provide maximum comfort to customers.

- iii. Due to geo-spatial difference, each DER can demonstrate a different sort of uncertainty. The ADMS platform should be capable of implementing such probabilistic features for accurate pricing and control of DERs.

A combined CVR and DR framework with the guidance of choosing the appropriate DR plan for each customer is proposed in this dissertation. Stochasticity in load consumption and DER injection is considered while developing the framework.

1.3 Fault location, isolation, and service restoration (FLISR)

1.3.1 Implementation of FLISR

Fault location, isolation, and service restoration (FLISR) is a significant application of ADMS. Isolation and service restoration basically depends on faster and accurate identification of the fault location. Therefore, faster fault location can improve system average interruption duration index (SAIDI) and the system average interruption frequency index (SAIFI) [21]. Most of the fault location approaches for distribution systems, discussed in the literature, are based on impedance based method [22]. Recent developments in smart meter technology have brought a new dimension to fault-location strategy using voltage sag analysis [23]. Moreover, information from different sources, such as fault indicators (FID), and fault terminal unit (FTU) installed in switches have also been used to identify the fault location in

medium-voltage (MV) and low-voltage (LV) distribution systems [24]. After identifying the location of the fault, switches surrounding the faults may be opened to isolate the faulted section. Service restoration procedures are created based on available resources downstream to fault. Normally opened tie switches can be closed to utilize the neighboring feeders or nearby DERs to feed the unfaulted sections and isolated loads downstream to fault. Local microgrids can also be formed to serve the critical loads using available DERs.

1.3.2 Challenges in FLISR

Using the methodologies mentioned above, the implementation of FLISR is possible. However, there are many exceptional cases which might create uncertainties and may lead to failure of the FLISR procedure. A summary of those challenges, which need to be addressed in the ADMS platform is discussed below:

- i. Most of the current fault location schemes are based on impedance calculations from the faulted data stored at the substation meter. Subsequently, this impedance is matched with the actual impedance collected from the feeder data to estimate the length from the substation to the fault. However, this might yield to wrong estimation of the locations of the fault by identifying un-faulted section(s) on the feeder based on the impedance calculations. Un-faulted section(s) basically lead to an identical distance as the faulted section from the substation to the fault. Therefore, distributed data sources are needed throughout the feeder. Smart meters provide data of the load locations only, and these are mostly placed on the LV system. Thus, the MV system often remains unobserved. FIDs and FTUs can be utilized throughout the feeder as [24]. However, installing these devices at every node/section might be expensive for the utility company. Therefore, optimal allocation of low-cost sensors is essential for increasing the FLISR performance and decreasing investment cost. Such low-cost sensors are reported in [25], [26]. Alternatingly, ADMS functions

can rely on a distribution system state estimators (DSSE) to reduce the sensor deployment cost that (a) identifies topological errors and (b) calculates the states at unobserved nodes.

- ii. Synchronous data collection is the primary step for achieving maximum accuracy for FLISR. Data from the measurement devices are needed periodically or only when an anomaly happens. Otherwise, massive amounts of data can overwhelm the data mining algorithm(s), while increasing the cost of storing and transmitting the data, and reducing the life-time of sensors due to continuous operation. Therefore, a real-time platform is needed to ping sensors to collect and store data only when a fault happens.
- iii. Voltage sag based analysis can create discrepancies due to the bi-directional power flow complexities created by DERs depending on the penetration level, location of the fault, fault resistance, heterogenous line conductors, and lengths on different segments. Therefore, pattern recognition or knowledge based rules might not always be useful due to identical measurement. For simultaneous faults, voltage sag based analysis might create more difficulties to identify the location(s) due to the same reason. Thus, ADMS based online power flow (OLPF) can be used to distinguish the difference.

In this dissertation, a fault location scheme for ADMS based FLISR program is proposed. Installed voltage and current sensors data throughout the feeder are utilized to pin-point the faulty section(s). The proposed scheme considers a graph theory based method to identify zones which are infected simultaneously. After identifying the zones, analysis of voltage profile is conducted to reveal the actual faulty section(s).

CHAPTER 2: Assessment and Implementation of Conservation Voltage Reduction

2.1 Comparison of Load Models for Assessing CVR deployment

2.1.1 Overview

An increased awareness of environmental impact is created by the steady load growth which leads to the general desire of energy efficiency for the utility companies. To achieve the goal of energy efficiency utility companies are forced to focus on conservation voltage reduction (CVR). CVR is a volt-var control (VVC) technique in a smart-grid environment to minimize load consumption and system losses (i.e., line loss and transformer loss) following a reduction in the source voltage [27]. As yet, two different methodologies are used for CVR deployment. These are: (1) Adjust the end of line voltage using load tap changer (LTC) to the desired set point. The X and R settings of the LTC can be set in such a way to fix the desired voltage; (2) Unlike the first method, narrow adjustments of the LTC can be executed from the SCADA for adaptive voltage control by retrieving data from the line voltage monitor. Recent technological developments have made it much simpler using the communication capabilities of SCADA and field devices [28].

For assessment, CVR relies on a process that voltage sensitive loads will consume less energy while keeping the voltage in the lower band of acceptable range. As per American National Standards Institute (ANSI) C84.1, voltages at the customer end must be within 1 ± 0.05 p.u. [29]. Therefore, for CVR deployment, voltage throughout the feeder must stay within 0.95-1.0 p.u. or 114 V-120 V. In case of an emergency, the boundary can be maintained in the lower 10% of the nominal voltage. CVR can be deployed for both peak demand reduction and long-term energy reduction on short

and long-term basis, respectively. Many utilities are attracted by the economic and operational advantage of CVR to reduce the energy demand and carbon emission while generating electricity. This also helps consumers in decreasing their utility bill. Thus, several utility companies, such as Bonneville Power Administration (BPA), BC Hydro, Southern California Edison (SCE), Northeast Utilities (NU), Hydro Quebec (HQ), and Dominion Virginia Power have demonstrated the performance of CVR on their feeders and found that they can reduce 0.3% to 1% load consumption per 1% voltage drop [6]. PNNL also described in one of their report that if CVR is deployed in all the distribution feeders throughout the USA, it can save around 3.04% of annual energy consumption [30]. The CVR factor (CVRF) is the primary index to measure the performance of CVR deployment or energy savings as represented in (1.3). Higher CVRF corresponds to higher energy savings. This factor is represented as the change in load reduction ($\% \Delta P$) in accordance to the voltage reduction ($\% \Delta V$):

$$CVRF = \frac{\% \Delta P}{\% \Delta V} \quad (2.1)$$

Moreover, deployment of CVR relieves congestion in the distribution feeder since it reduces the load consumption and eventually improves the overall voltage profile. For voltage sensitive loads, the consumption gets reduced with a reduction in voltage in contrast to constant PQ load. Thus, the current flow also gets reduced which leads to an improved overall voltage profile through the reduction in line loss[31]. Improvement of voltage profile is measured by the voltage sensitivity factor (VSF), presented below:

$$VSF_{i,k} = \frac{\sum_k \Delta V_k}{K \sum_i \Delta P_i} \quad (2.2)$$

where $i, k \in \mathbb{Z}$ denote the source and load buses, respectively and K is the total number of load buses. The higher the VSF, the weaker the system is and vice versa. In recent days, CVR is being implemented in feeders which have integrated moderate

to high penetration of distributed energy resources (DER) [32]. Since the CVRF is impacted by the voltage profile, it impacts the VSF as well. Irrespective of the presence of DER, precise estimation of CVRF and VSF is necessary to retrieve the accurate energy savings and voltage margin, respectively, within the constraint of voltage boundary, due to the variation of load behavior. Quantification of these factors is a challenging issue. Exact estimation of the factors provides an in-depth knowledge about a feeder for CVR deployment.

Thus far, four assessment methodologies can be utilized, those are found in the literature, to estimate these factors: comparison-based [33], [7], synthesis-based [8], regression-based [9], and simulation-based [10],[32]. Comparison based method compares two different feeders with the same configuration, topologies, load types, and load size: one with voltage reduction and another without voltage reduction. Comparison based method also analyzes the difference on consumption in the same feeder and time interval on two different days having similar weather conditions with and without voltage reduction, respectively. In reality, it is very difficult to find two feeders with similar condition or two different days with similar weather and load pattern. Synthesis based method aggregates the characteristics of different types of loads or different customer classes as a function of voltage. This can be performed either in circuit level or in laboratory test for any individual appliance[11]. However, it does not consider the stochastic behavior of loads. Regression based method linearizes the load behaviors depending on voltage and other associated coefficients [12]. Simulation based method compares the same feeder by simulating with and without voltage reduction [32]. However, the latter two methods need a proper selection of load model, the associated load parameters and/or the estimated CVRoff period voltage profile of source(s) during the CVRon period. In this analysis, CVRon period refers to the time interval(s) during the day when CVR is deployed, and CVRoff period denotes the time interval(s) during the CVRon period if CVR was not deployed.

There are several static load models in the literature [34]. Out of these, ZIP and exponential models are widely discussed. These models are used for various voltage reduction studies which are explained in the next section. However, their performances have not been compared for voltage reduction. Since the parameters of each load model capture different behaviors, it is expected each model will demonstrate different results. Therefore, it is required to compare their performances and find the most suitable load model for the CVR study. This study extensively compares the aforementioned load models in a time varying manner by estimating CVRF and VSF using (1) and (2) since they demonstrate variability from time to time. Moreover, stochasticity in load variation is also considered while demonstrating the comparison of load models. To do so, the parameters of each model also need to be estimated accurately at each instant because standard models use fixed coefficients over time, which can lead to inaccurate estimation of the factors. Due to load-to-voltage (LTV) sensitivity, there are interdependencies between these parameters and voltage profile of the feeder. Alternatingly, the voltage profile is impacted by the variation of load, and vice versa, at different times of the day. Moreover, to estimate CVRF and VSF, the CVRoff period voltage profile is also needed. In [12], a Euclidean distance-based method is used to find the voltage set point of CVRoff time along with load consumption. However, the authors assumed a constant operational voltage of 1.0 *p.u.* during the CVRoff time which is not always true. Utilities operate above 1.0 *p.u.* voltage for long feeders to maintain the lower ANSI band at the load ends which will be shown in the Section 2.1.4. This study performs a probabilistic analysis of historical voltage profile to retrieve time-varying CVRoff operational voltage, which is shown in the section 2.1.4. The major contributions of this analysis are pointed out below:

- i. Parameter identification or estimation of the load models are done using regression-based methods by employing two different sets of dual-stage adaptive filters. One consists of a Recursive Least Square (RLS) and a Constrained Recursive

Least Square (CRLS) filter. The other set is comprised of a Kalman Filter (KF) and an equality-constrained Kalman Filter (CKF). The advantages of a dual-stage filter over a single-stage filter are described in section III. The filters also consider stochasticity in the estimation process.

- ii. A comparison of time-varying ZIP (TZIP) and exponential (TEXP) models are provided to estimate the CVRF and the VSF using the identified load parameters.
- iii. Apart from load models, the line impedance, and the presence of capacitor banks and voltage regulators also impact CVR deployment. Therefore, the estimations are needed to validate on the original distribution feeder from where the measurements are acquired. This is significant since circuit type simulation can prove the accuracy of estimation in a realistic manner by inducing the effects of all voltage control devices. Therefore, in this study, simulation-based method is used to validate the estimated factors. To that end, a 22.86 kV real distribution feeder, consisted of 2268 nodes, is utilized. OpenDSS is chosen for the simulation due to its flexibility in interfacing with other tools and to receive external data as attribution. However, the feeder data was received from the utility in a CYMEDIST format. Thus, the feeder is converted in OpenDSS [35] from CYMEDIST [36] using a conversion tool. The design of the tool, conversion process, and performance are explained in section 2.1.4.

The entire study helps the utility to gain an in-depth knowledge about a feeder for CVR deployment with correct load model selection. The rest of the analysis is presented as below: section 2.1.1 describes the details of load modeling and importance of comparing models for CVR assessment. Section 2.1.3 represents the procedure and significance of dual-stage filter design. Section 2.1.4 discusses the estimation of the factors. Section 2.1.5 analyzes the simulation results. Section 2.1.6 summarizes the

analysis with major findings.

2.1.2 Load Modeling

2.1.2.1 Static load models

CVR has different impacts on residential, commercial, and industrial type loads because of their composition. In addition, not all loads are suitable for CVR implementation, such as water heaters [37]. Some other thermostatic loads work effectively under the CVR scheme, i.e., refrigerators and air-conditioners [38]. Thus, it depends on the nature (resistive, inductive or capacitive) and type of the load. However, many utilities, when estimating energy savings, do not consider the load types and combinations of load characteristics of their customers. Instead, they measure the total amount of demand, and operating voltage at the substation at CVR on time and use a fixed CVR factor over the time [39]. In [12], the exponential load model is used to estimate the CVR factor after retrieving the load parameters. The ZIP load model is used to observe the reduction in load consumption in [28]. In their previous experiments, the authors of [11] had tested several appliances of different load types to observe their P-V and Q-V relationships along with associated parameters [32]. None of the appliances showed a typical biasness to a constant power load. Each load including thermostatic loads demonstrated variability with voltage level based on the composition of constant impedance (Z_p), constant current (I_p), and constant power (P_p) percentage. If any of the coefficients of a load is negative, it can emit power as well. The Pacific Northwest National Laboratory (PNNL) have used the ZIP load model to show the voltage dependency of loads [30]. Exponential and ZIP load models are presented below, respectively [12],[27]:

$$P_{exp} = P_o \left(\frac{V}{V_o} \right)^a \quad (2.3)$$

$$P_{ZIP} = P_o \left[Z_P \left(\frac{V}{V_o} \right)^2 + I_P \left(\frac{V}{V_o} \right) + P_P \right] \quad (2.4)$$

$$\text{where } Z_P + I_P + P_P = 1 \quad (2.5)$$

In (2.3) and (2.4) P_o and V_o are the nominal power and voltage, respectively. In the exponential model, load to voltage (LTV) sensitivity depends on the exponential factor (a) and in the ZIP model, constant impedance (Z_p), constant current (I_p), and constant power (P_p) coefficients create the dependency. Both the above-mentioned load models are static in behavior and represent the active power. However, similar models can be found for reactive power. This study only deals with real CVRF and corresponding VSF. The theoretical foundation of this study can be used for reactive power as well.

2.1.2.2 Time-varying load models

Although a majority of the literature targets static load models, the coefficients will vary with time due to the change in voltage profile and load factors. In addition, as mentioned earlier, the load factor also changes in different seasons depending on the weather or human behavior. Moreover, in some subsequent time instants in the same day, extreme change in load behavior may be observed due to switching of large individual loads. For instance, the set of loads which are switched on at time t might not remain on at time $t + n$ or a different set of loads might be turned on altogether. Therefore, it is important to study the load models that vary with time and how each model demonstrates a different behavior with the change of load factor. In order to do that, a time-varying models should be adopted to observe the load behavior. Time-variability in an exponential load model (TEXP) is seen in [12]:

$$P_{exp}(t) = P_o(t) \left(\frac{V(t)}{V_o} \right)^{a(t)} \quad (2.6)$$

Similarly, TZIP model can be defined as [40]:

$$P_{ZIP}(t) = P_o(t) \left[Z_P(t) \left(\frac{V(t)}{V_o} \right)^2 + I_P(t) \left(\frac{V(t)}{V_o} \right) + P_P(t) \right] \quad (2.7)$$

$$\text{where } Z_p(t) + I_p(t) + P_p(t) = 1 \quad (2.8)$$

In the above models, due to the variation in consumption a , Z_p , I_p , and P_p will also be time-varying parameters. As a result, CVRF and VSF will also show stochastic behavior. Since, advanced metering infrastructure (AMI) is not employed at every customer end yet, the total consumption of the entire feeder is measured at the substation end. This study will estimate all the parameters based on the data retrieved from substation meter. Therefore, this study will help to find a suitable composite load model. This study only deals with CVRF and the corresponding VSF using active power measurements since CVR is mainly deployed for active power reduction. However, the theoretical foundation of this study can be used for reactive power as well.

2.1.3 Dual-Stage Filtering

The two load models described in the previous section are of different physical representations. Both are non-linear by nature. However, both representations can be linearized to present as a multiple linear regression formulation with two and three explanatory variables for exponential and ZIP models, respectively. Therefore, the formulated structure can be presented as:

$$W_m = \varphi_m^T \omega_m \quad (2.9)$$

Where $m \in \mathbb{Z}$ considering total M number of measurement data. Assuming $V_0 = 1.0$ p.u., (2.6) can be modified as: $W_m = \ln P_{exp}(t_m)$, $\varphi_m = [1 \quad \ln V(t_m)]^T$, and $\omega_m = [\ln P_o(t_m) \quad a(t_m)]^T$. Similarly, (2.7) can be represented as $\omega_m = [Z_p(t_m) \quad I_p(t_m) \quad P_p(t_m)]^T$, $\varphi_m = [V(t_m)^2 \quad V(t_m) \quad 1]$, and $W_m = \frac{P_{ZIP}(t_m)}{P_o(t_m)}$. In the above formulation, ω_m represents parameters to be identified for m^{th} sample, and W_m and φ_m are the measured vectors. In both the above representations, $P_o(t_m)$ refers to the nominal power at the nominal voltage. In exponential model, it behaves as an independent

variable, whereas in ZIP model, it is part of a dependent variable. Therefore, it is not possible to estimate $P_o(t_m)$ separately in the ZIP load model. On the other hand, assuming $P_0(t_m) = 1.0 \text{ p.u.}$ is not justifiable since operational voltage might not be nominal voltage at any or every time instant. Thus, a dual-stage filtering is needed where the first stage filtering is used to estimate all the unknowns, first stage filtering is used to estimate the nominal power along with the exponential factor, $a(t_m)$ using the exponential model and is rendered to the second stage in the ZIP model for estimating $Z_P(t_m)$, $I_P(t_m)$, and $P_P(t_m)$. Since the measurement for both models are the same, $P_0(t_m)$ denotes the same numeric value. Moreover, the second stage filtering is bounded with a constraint associated with the ZIP load. This study utilizes two different dual-stage filtering process to identify the proper load model: (a). RLS-CRLS combined filter, and (b). KF-CKF combined filter.

2.1.3.1 RLS-CRLS combined filter

The least squares method is widely used in many areas of signal processing, control, communication, etc. for real time state estimation [41]. The load models formulated in eq (2.9) can be presented as a least square problem to find the unknown parameters $\hat{\omega}_m$ in such a way that the error between the measured and the estimated output at any time instant m is minimized. The formulation is presented below:

$$\hat{\omega}_m = \arg \min_{\omega_m} f(W_m - \varphi_m^T \omega_m) \quad (2.10)$$

Where $f(\omega_m)$ refers to the objective function. The function is formulated based on the error measurement ε_m :

$$\varepsilon_m^2 = (W_m - \hat{W}_m)^2 \quad (2.11)$$

where $\hat{W}_m = \varphi_m^T \hat{\omega}_m$. However, the recursive least square (RLS) method can be adopted to take advantage of the updated information in the derived time-varying load models. The RLS is a widely used adaptive filter in the application of parameter

identification. It has been used in [12] to identify the exponential load model parameters, which is adopted in the first stage of RLS-CRLS combined filter. Therefore, the objective function is modified as below:

$$\hat{\omega}_m = \arg \min_{\omega_m} \sum_{k=0}^m \lambda^{m-k} f(W_m - \varphi_m^T \omega_m) \quad (2.12)$$

Where λ is the forgetting factor. The letter is a scalar value, between 0^+ to 1, which holds the number of previous measurements to retain in memory for error minimization. In general, a high forgetting factor (0.95-1.0) is utilized if the measurements vary smoothly with time. However, abrupt deviations may be detected which needs only recent measurement for best estimation of the parameters. In this study, λ is considered to be a variable forgetting factor, so that sudden deviation in load consumption can be tracked. λ can be updated at each instant as:

$$\lambda_{m+1} = [\lambda_m - \mu \Delta_m^\lambda]_{\lambda_{min}}^{\lambda_{max}} \quad (2.13)$$

Where $\Delta_m^\lambda = \frac{\partial E\{\varepsilon_m^2\}}{\partial \lambda}$ and μ is the time-step; λ_{max} and λ_{min} represent the boundary of the forgetting factor with maximum and minimum values. In this dissertation, $\lambda_{max}=0.995$ and $\lambda_{min}=0.485$ are used. A detailed derivation of the forgetting factor can be found in [42].

$\hat{\omega}_m$ is the estimated coefficient vector which also relies on the estimation of the previous sample $\hat{\omega}_{m-1}$, and can be written as [43]:

$$\hat{\omega}_m = \hat{\omega}_{m-1} + K_m(W_m - \hat{W}_m) \quad (2.14)$$

Where K_m is the gain which determines how much the previous error affects the

current update of the coefficient estimation.

$$K_m = \frac{L_{m-1}\varphi_m}{\lambda + \varphi_m^T L_{m-1} \varphi_m} \quad (2.15)$$

$$L_m = \frac{1}{\lambda} [L_{m-1} - K_m \varphi_m^T L_{m-1}] \quad (2.16)$$

Here L_m is the covariance matrix of the desired output. Since, it remains unknown until the second sample, a high covariance matrix is assumed for initialization, suggested in [44]. In the second stage for ZIP coefficients identification, the constraint is introduced which redefines (2.14):

$$\hat{\omega}_m = \hat{\omega}_{m-1} + \frac{K_m}{H} (W_m - \hat{W}_m) \quad (2.17)$$

$$\text{where } H = \sum_{j=1}^3 \hat{\omega}_m[j] \quad (2.18)$$

The constraint defined in (2.17) guarantees to provide the $Z_P(t_m)$, $I_P(t_m)$, and $P_P(t_m)$ as percentages of total power. In this analysis, the filter is addressed as a dual-stage RLS.

2.1.3.2 KF-CKF combined filter

The Kalman filter (KF) is defined as a state estimator with Gaussian noise used in dynamic linear system identification. Kalman filter is also known for minimum variance. Some different modifications are done on Kalman filter to estimate the state, such as the extended Kalman filter (EKF), and the unscented Kalman filter (UKF) [45]. The UKF is utilized for load modeling identification in [46]. In this dual-stage filter, first, an unconstrained KF is used for exponential model parameter identification in the first stage with single step prediction to address the stochasticity. A similar type of KF is used for PV generation forecasting in [47]. Next, in the second stage filter, a linear constraint is projected for ZIP model parameter identification.

Throughout the study, this filter is addressed as a dual-stage KF. This combined filter is designed based on the theoretical foundation of [45], [48], and [49]. The unconstrained Kalman filter based on the load models is stated below:

$$\omega_{m+1} = A_m \omega_m + u_m \quad (2.19)$$

$$W_m = \varphi_m^T \omega_m + v_m \quad (2.20)$$

Where ω_m is the current state, W_m is the current measured output, u_m and v_m are the zero-mean process noise and measurement noise with covariance C and D , respectively. A_m and φ_m represent the state transition and measurement matrices. Since this is time varying design of KF, A_m needs to be updated periodically and approximate tuning of A_m can lead to better estimation. A_m can be derived by testing the response to the initial condition as:

$$\dot{\omega} = F\omega \quad (2.21)$$

where F is an identity matrix since $Z_P(t_m)$, $I_P(t_m)$, and $P_P(t_m)$ are not dependent on each other. However, their numerical quantity can be changed over the time by maintaining the constraint (2.8). Therefore, to illustrate the change in the time domain, the following representation can be used:

$$\omega_{t+\Delta t} = \mathcal{L}^{-1}[(sI - F)^{-1}] \omega_{t=0} \quad (2.22)$$

Similarly, comparing the state from m to $m+1$ with $t = 0$ to $t + \Delta t$ and $\omega_{m+1} = A_m \omega_m$ with (2.22), it can be written as:

$$A_m = \mathcal{L}^{-1}[(sI - F)^{-1}] \quad (2.23)$$

Process noise refers to how much the state is deviated from m to $m+1$ by a random signal with constant spectral density. This can be stated as:

$$u_m = I[E(Z_p(t_m)) \ E(I_p(t_m)) \ E(P_p(t_m))] \quad (2.24)$$

where $E(\cdot)$ represents expected value of the state vector element. The co-variance of two subsequent measurements can be presented as:

$$J_m^- = A_m J_{m-1}^+ A_m^T + C \quad (2.25)$$

$$K_G = J_m^- \varphi_m (\varphi_m^T J_m^- \varphi_m + D) \quad (2.26)$$

$$\hat{\omega}_m^- = A_m \omega_{m-1}^+ \quad (2.27)$$

$$\hat{\omega}_m^+ = \hat{\omega}_m^- + K_G (W_m - \varphi_m^T \hat{\omega}_m^-) \quad (2.28)$$

$$J_m = (I - K_G \varphi_m^T) P_m^- \quad (2.29)$$

where K_G is the Kalman gain and I is the identity matrix; $\hat{\omega}_m^-$ is the priori estimate of ω_m up to, and including the measurement $m-1$; $\hat{\omega}_m^+$ is the posteriori estimation of ω_m up to, and including the measurement m ; J_m^- is the covariance matrix of the priori estimation error of $\omega_m - \hat{\omega}_m^-$, and J_m^+ is the covariance matrix of the posteriori estimation error of $\omega_m - \hat{\omega}_m^+$. The filter is initialized using:

$$\hat{\omega}_o^+ = E(\omega_o) \quad (2.30)$$

$$J_o^+ = E[(\omega_o - \hat{\omega}_o^+)(\omega_o - \hat{\omega}_o^+)^T] \quad (2.31)$$

Where $E(\cdot)$ is the expected value that represents the initial covariance matrix. The equality constraint of (2.8) can be fitted in different ways, i.e., model reduction, perfect measurements, estimation projection etc., [49],[51]. In this study, the perfect

measurement method is adopted to process the constraint since it can be considered with zero measurement noise. The constraint can be formulated as below:

$$X\omega_m = Y \quad (2.32)$$

Where X is a $m \times n$ matrix and $m < n$, which can be augmented in (2.20) with perfect measurement state as below:

$$\begin{bmatrix} W_m \\ Y \end{bmatrix} = \begin{bmatrix} \varphi_m^T \\ X \end{bmatrix} \omega_m + \begin{bmatrix} v_m \\ 0 \end{bmatrix} \quad (2.33)$$

Yet, the state equation (2.19) remains unchanged. Therefore, (2.19) and (2.20) are used in the first stage and (2.19) and (2.33) are utilized for the second stage.

2.1.4 Factor Estimation

This section defines two sets of formulations based on the measurement and estimation for both load models to retrieve the CVRF and VSF. The proposed dual-stage filtering method only requires active load and voltage data at the substation during the CVRon period. However, this filtering approach can be deployed for a feeder where every load is connected with a smart meter. In this study, real data from the substation is used due to missing smart meter at all the load ends.

2.1.4.1 CVR Factor (CVRF) Estimation

CVRon and CVRoff load $\hat{P}_{CVRon}(t)$ and $\hat{P}_{CVRoff}(t)$ can be estimated during the same period by using identified parameters of the exponential load model as follows:

$$\hat{P}_{CVRon,TEXP}(t) = \hat{P}_o(t)[V_{CVRon}(t)]^{\hat{a}(t)} \quad (2.34)$$

$$\hat{P}_{CVRon,TEXP}(t) = \hat{P}_o(t)[V_{CVRoff}(t)]^{\hat{a}(t)} \quad (2.35)$$

Similarly, for the ZIP load model:

$$\hat{P}_{CVRon,TZIP}(t) = \hat{P}_0(t)[\hat{Z}_P(t)V_{CVRon}(t)^2 + \hat{I}_P(t)V_{CVRon}(t) + \hat{P}_P(t)] \quad (2.36)$$

$$\hat{P}_{CVRoff,TZIP}(t) = \hat{P}_0(t)[\hat{Z}_P(t)V_{CVRoff}(t)^2 + \hat{I}_P(t)V_{CVRoff}(t) + \hat{P}_P(t)] \quad (2.37)$$

$\hat{P}_{CVRon}(t)$ can also be retrieved from the last iteration of each sample as the best approximation. From (2.1), we can derive:

$$CVRF = \frac{\frac{P_{CVRoff} - P_{CVRon}}{P_{CVRoff}}}{\frac{V_{CVRoff} - V_{CVRon}}{V_{CVRoff}}} \quad (2.38)$$

Therefore, the estimated CVRF is presented as:

$$\widehat{CVRF}_{TExp}(t) = \frac{1 - \left[\frac{V_{CVRon}(t)}{V_{CVRoff}(t)} \right]^{\hat{a}(t)}}{1 - \frac{V_{CVRon}(t)}{V_{CVRoff}(t)}} \quad (2.39)$$

$$\widehat{CVRF}_{TZIP}(t) = \frac{1 - \frac{\hat{Z}_P(t)V_{CVRon}(t)^2 + \hat{I}_P(t)V_{CVRon}(t) + \hat{P}_P(t)}{\hat{Z}_P(t)V_{CVRoff}(t)^2 + \hat{I}_P(t)V_{CVRoff}(t) + \hat{P}_P(t)}}{1 - \frac{V_{CVRon}(t)}{V_{CVRoff}(t)}} \quad (2.40)$$

Similarly, using the measured $P_{CVRon}(t)$ and $V_{CVRon}(t)$ from the substation meter, the CVRF can be calculated and compared with the CVRF estimated above. Using direct measurement data, CVR factors can be calculated as:

$$CVRF_{TExp}(t) = \frac{1 - \frac{P_{CVRon}(t)}{\hat{P}_{CVRoff,exp}(t)}}{1 - \frac{V_{CVRon}(t)}{V_{CVRoff}(t)}} \quad (2.41)$$

$$CVRF_{TZIP}(t) = \frac{1 - \frac{P_{CVRon}(t)}{\hat{P}_{CVRoff,ZIP}(t)}}{1 - \frac{V_{CVRon}(t)}{V_{CVRoff}(t)}} \quad (2.42)$$

In this study, $V_{CVRoff}(t)$ is estimated using the cumulative density function (CDF) of the neighboring days voltage profile in the same interval as the CVR deployment period instead of assuming it is constant. In [12] V_{CVRoff} is assumed 1.0 p.u.. to find the most reasonable time. However, it is not true always since some feeders have

higher length which are operated in the upper band of ANSI range. The probabilistic analysis of $V_{CVRoff}(t)$ is shown in the latter section. After retrieving both sets of factors, they can be compared to observe which load model identification matches closely based on the difference on measurement and estimation. Fig. 2.1 depicts the dual-stage filtering for CVRF and VSF estimation.

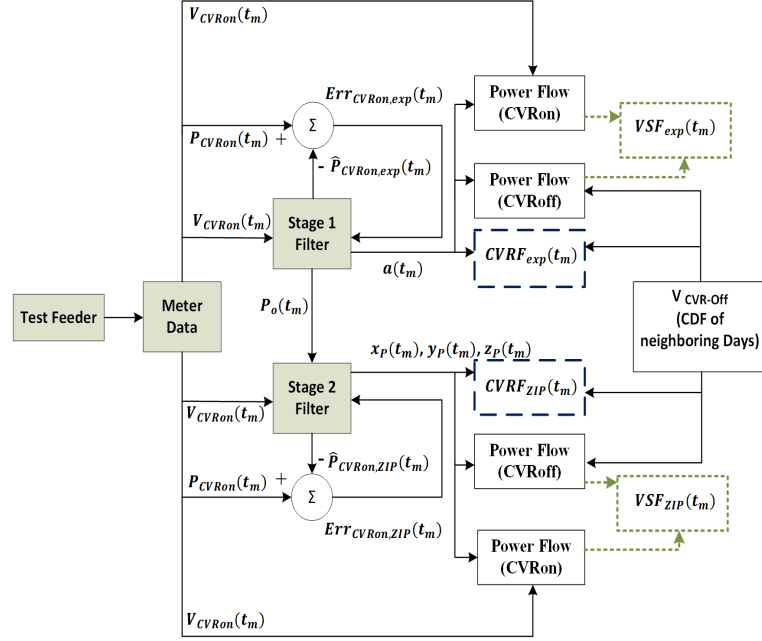


Figure 2.1: Dual-stage filtering for CVRF and VSF estimation.

2.1.4.2 Voltage Sensitivity Factor (VSF) Estimation

Similar to CVRF, VSF estimation can be elaborated from (2.2):

$$VSF_{i,k}(t) = \frac{\frac{1}{K} \sum_{i,k} \frac{V_{CVRoff,k}(t) - V_{CVRon,k}(t)}{V_{CVRoff,k}(t)}}{\sum_i \frac{P_{CVRoff,i}(t) - P_{CVRon,i}(t)}{P_{CVRoff,i}(t)}} \quad (2.43)$$

From (2.43), it is clear that if a feeder has multiple sources, i.e. renewable energy based distributed energy resources, or other generators, perturb and observe methodology can be used to calculate the voltage sensitivity using (2.44) and (2.45). Therefore,

estimated VSF is presented as:

$$\widehat{VSF}_{TExp}(t) = \frac{\frac{1}{K} \sum_k [1 - \frac{V_{CVRon,k}(t)}{V_{CVRoFF,k}(t)}]}{\sum_{i=1}^N N - [\frac{V_{CVRon,i}(t)}{V_{CVRoFF,i}(t)}] \hat{a}(t)} \quad (2.44)$$

$$\widehat{VSF}_{TZIP}(t) = \frac{\frac{1}{K} \sum_k [1 - \frac{V_{CVRon,k}(t)}{V_{CVRoFF,k}(t)}]}{\sum_{i=1}^N N - \frac{\hat{Z}_{P,i}(t)V_{CVRon,i}(t)^2 + \hat{I}_{P,i}(t)V_{CVRon,i}(t) + \hat{P}_{P,i}(t)}{\hat{Z}_{P,i}(t)V_{CVRoFF,i}(t)^2 + \hat{I}_{P,i}(t)V_{CVRoFF,i}(t) + \hat{P}_{P,i}(t)}} \quad (2.45)$$

where K and N represent the total number of load and source buses. From the measurement, VSF can be calculated as:

$$VSF_{TExp}(t) = \frac{\frac{1}{K} \sum_k [1 - \frac{V_{CVRon,k}(t)}{V_{CVRoFF,k}(t)}]}{\sum_{i=1}^N N - \frac{P_{CVRon,i}(t)}{\hat{P}_{CVRoFF,exp}(t)}} \quad (2.46)$$

$$VSF_{TZIP}(t) = \frac{\frac{1}{K} \sum_k [1 - \frac{V_{CVRon,k}(t)}{V_{CVRoFF,k}(t)}]}{\sum_{i=1}^N N - \frac{P_{CVRon,i}(t)}{\hat{P}_{CVRoFF,ZIP}(t)}} \quad (2.47)$$

2.1.5 Simulation and Results

In this section, real measurement data from a 22.86 kV distribution feeder, provided by Duke Energy Progress, is utilized to estimate the CVRF and the VSF using the proposed dual-stage filtering method, explained in the previous sections. One years' data from 2015 is collected to test the proposed methodology from the meter placed at the feeder-head. One-minute interval data of P, Q, I, & V were available from the meter. After visiting the datasets, it was found that CVR was deployed on 23 days. In all the cases, a short term CVR was deployed. Among those 23 days, the data for February 7th was selected since it demonstrates some stochasticity with respect to load behavior. To validate the estimation of CVRF and VSF, the OpenDSS platform is used. OpenDSS provides the flexibility to use component object model (COM) interface to be integrated with other platforms like MATLAB, VBA, Python, C# etc. This additional benefit aids to retrieve data for analysis and implant the

estimation on the DSS files driven from the above-mentioned platforms. However, the circuit model, provided by the utility was developed in CYMEDIST, and therefore, it had to be converted to OpenDSS scripts using a conversion tool. The conversion tool also validates the circuit models in both platforms.

2.1.5.1 CYMEDIST to OpenDSS Conversion

CYMEDIST models are generally retrieved as self-contained extensive mark-up language (XML) format. This XML files can be sub-divided into several ASCII files, such as equipment, network, and load. The conversion tool reads the ASCII files, creates structure of power delivery elements (PDE), power conversion elements (PCE), controls, meters, and the line models. Later, these structures are formatted as DSS files. Fig. 2.2 provides a block diagram of the entire feeder conversion and estimation/validation process. Both softwares can retrieve power and current flow

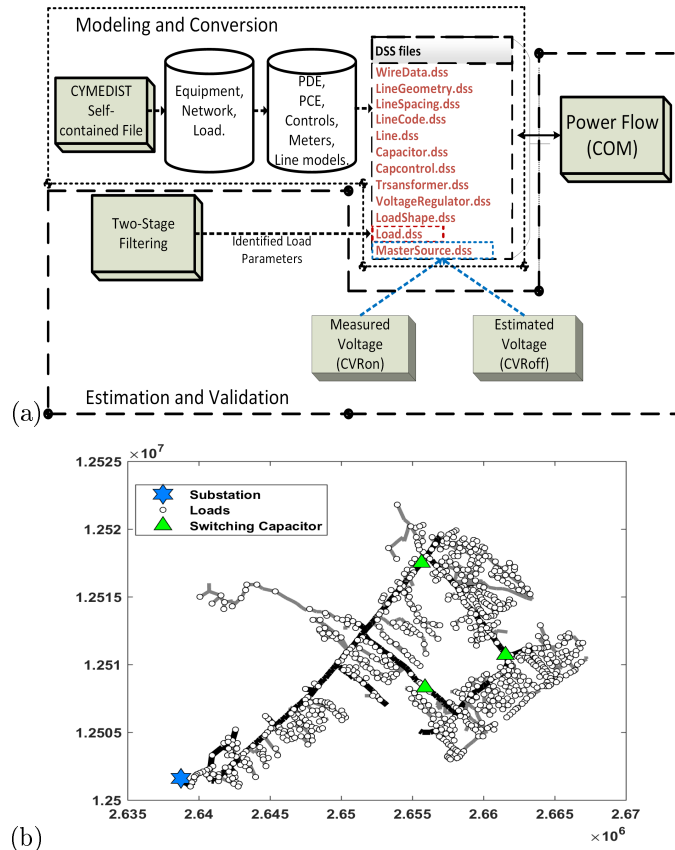


Figure 2.2: (a).Schematic diagram of the simulation. (b).Converted feeder

through each bus. Figs.2.3 (a) and (b) show the bus current and power respectively versus distance along the feeder. It provides the validation of the model conversion by matching power flow and short circuit current of the feeder in both software. Histogram data, shown in Figs.2.3 (c) and (d), are also provided to show the deviation in both software. Results demonstrate that around 95% buses possess accurate data, meaning near exact modeling.

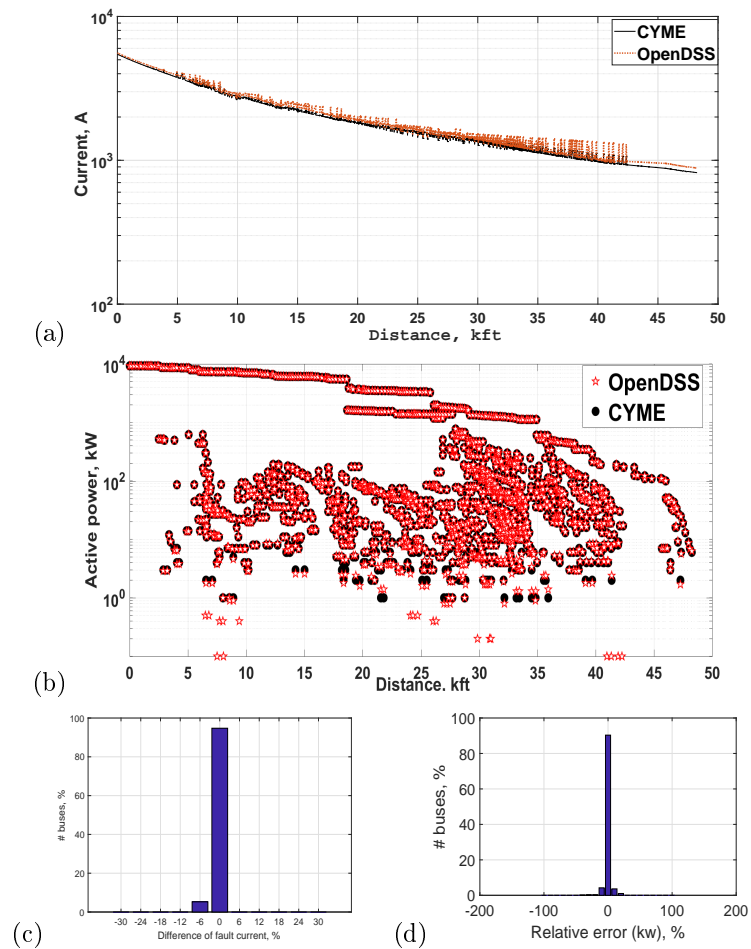


Figure 2.3: CYME vs OpenDSS (a). Short circuit (b). Power Flow (c). Short-circuit histogram (d). Power flow histogram.

2.1.5.2 CVRoff Voltage Shape

To estimate $V_{CVRoff}(t_m)$, during CVR deployment period the voltage data shapes of the neighboring days of CVR deployment day and time were included to see the distribution fit. Fig.5. shows the phase A voltage levels of six preceding days leading

up to February 7th. CVR is deployed from 6:36 AM and 8:31 AM on February 7th. It

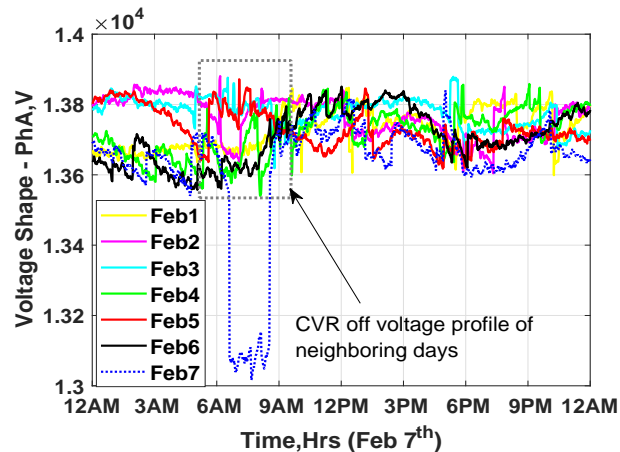


Figure 2.4: Phase A voltage profile of a February week.

is clearly visible from Fig.2.4 that, in neighboring CVRoff days within the same time span of CVR deployment day, the voltage band lies between 13.6 to 13.85kV (1.03 to 1.05 *p.u.*). The cumulative distribution function (CDF) of CVRoff days is provided in Fig. 2.5 which distinctly exhibits the fact that the CVRoff voltage profile follows a normal distribution. Therefore, time-varying nature of CVRoff operational voltage can be represented as:

$$V_{CVRoff}(t_m) = \mathcal{N}(\mu_{V,CVRoff}, \sigma_{V,CVRoff}^2) \quad (2.48)$$

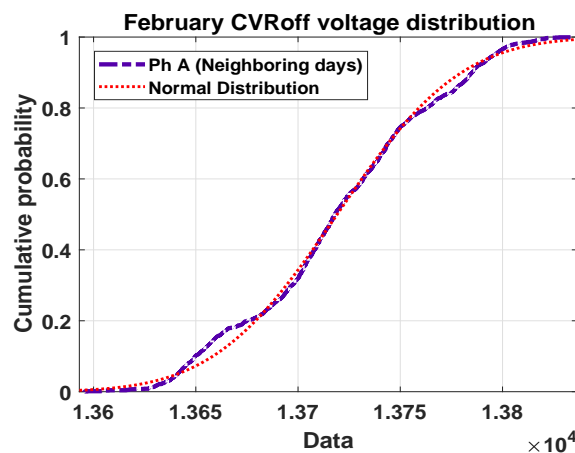


Figure 2.5: Phase A CVRoff voltage distribution for a February week.

Table 2.1 provides the distribution parameters of all three phases. Since CVRF is calculated for the entire substation irrespective of the phases, a weighted mean and variance are needed to calculate using the data from Table I to find the combined CVRoff voltage at every time instant using (48), as shown below:

$$\mu_{V,CVRoff} = \beta_A \mu_A + \beta_B \mu_B + \beta_C \mu_C \quad (2.49)$$

$$\sigma_{V,CVRoff}^2 = \beta_A^2 \sigma_A^2 + \beta_B^2 \sigma_B^2 + \beta_C^2 \sigma_C^2 \quad (2.50)$$

Where β_A , β_B , and β_C are the weights for each phase and represent the ratio of the base load of each phase to the total load. Therefore, by considering the unbalanced nature of the distribution system, the phase which has a higher load profile will receive a relatively higher voltage set point at any individual instant.

Table 2.1: Normal distribution parameters for CVRoff voltage shape.

Day	Parameters	Phase A,V	Phase B,V	Phase C,V
February 7 th	Mean, μ	13717.45	13738.39	13697.33
	Variance, σ^2	3278.91	2788.94	2444.47

2.1.5.3 Estimation error of factors

This section deals with the estimated CVRF and VSF. The estimation is done based on the methodology elaborated in sections III and IV. The entire estimation process is run for for the same dataset with both dual-stage filters to demonstate the accuracy of the load models and their associated parameter identification. Figs.2.6,2.7, and 2.8 depict the CVRF and VSF using the estimated TEXP and TZIP model parmeters and measured load profile of February 7th.

In this case, a total 116 measurements were taken at one-minute intervals and CVRF and VSF are calculated for each instant. Fig.2.6 (a) and Fig.2.7(a) represent the CVRF in the first stage (TEXP) using RLS and KF filters of dual-stage RLS and dual-stage KF, respectively. Similarly, Fig.2.6 (b) and Fig.2.7(b) depict the CVRF

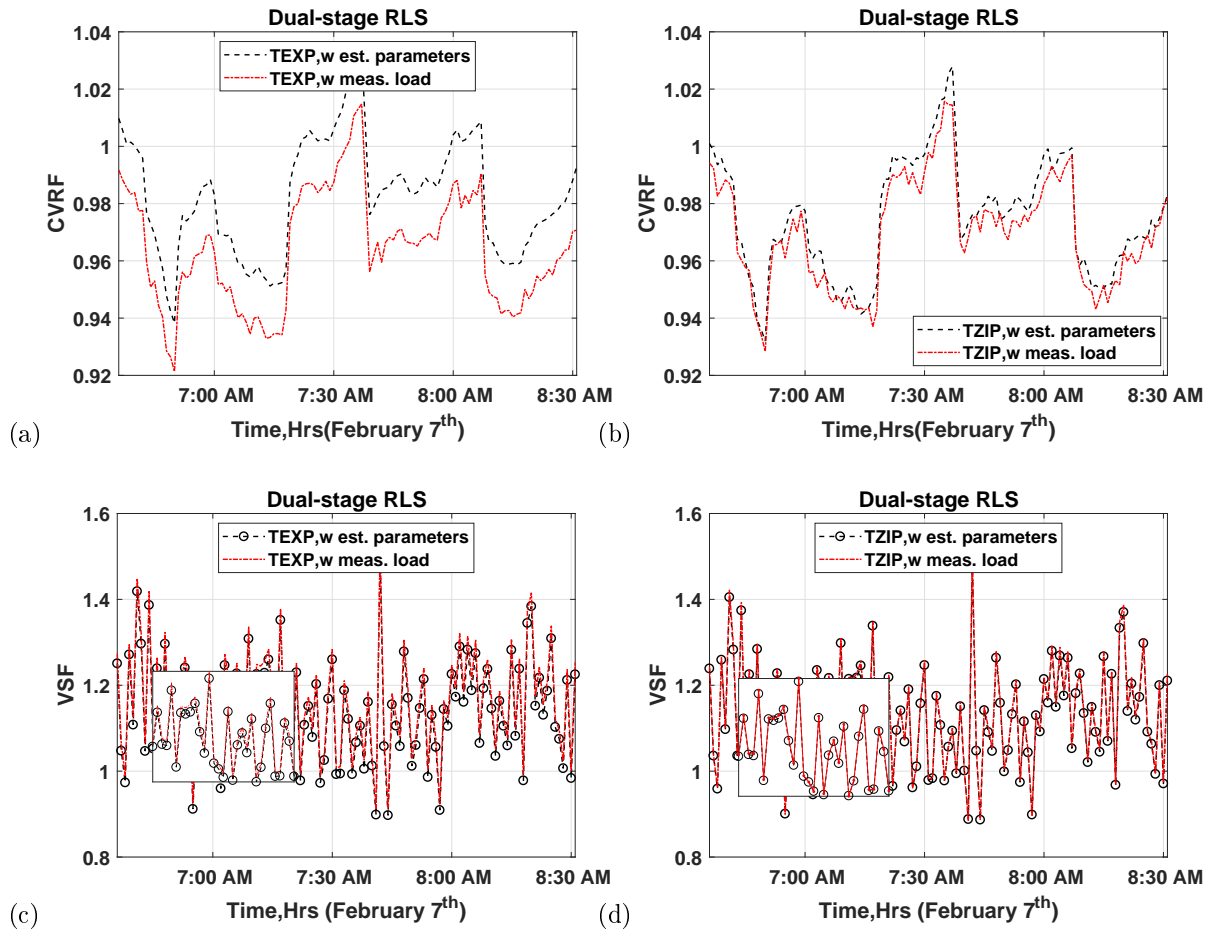


Figure 2.6: Usage of dual-stage RLS (a) CVRF in first stage (TEXP), (b) CVRF in second stage (TZIP), (c) VSF in first stage (TEXP), (d) VSF in second stage (TZIP).

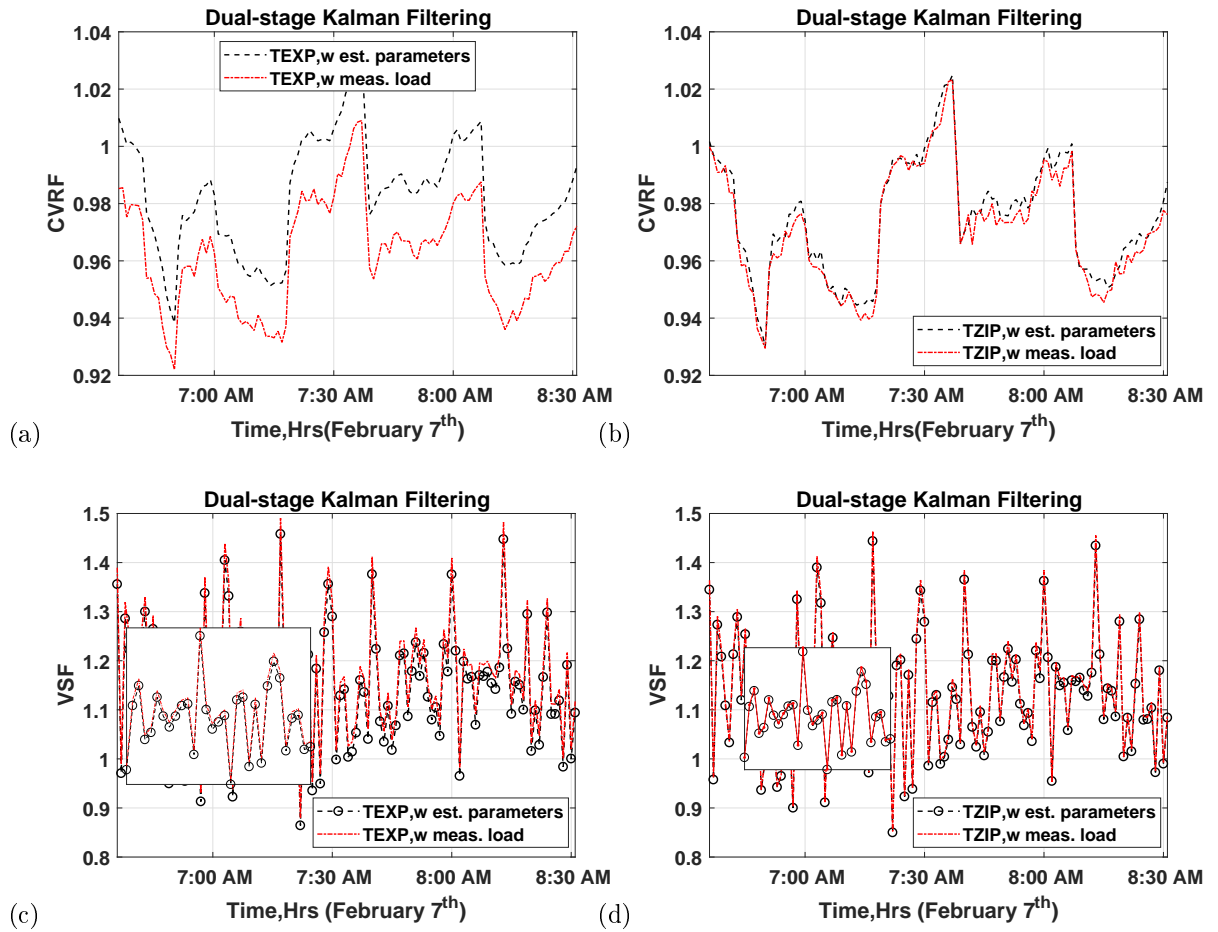


Figure 2.7: Usage of dual-stage KF (a) CVRF in first stage (TEXP), (b) CVRF in second stage (TZIP), (c) VSF first stage (TEXP), (d) VSF in second stage (TZIP).

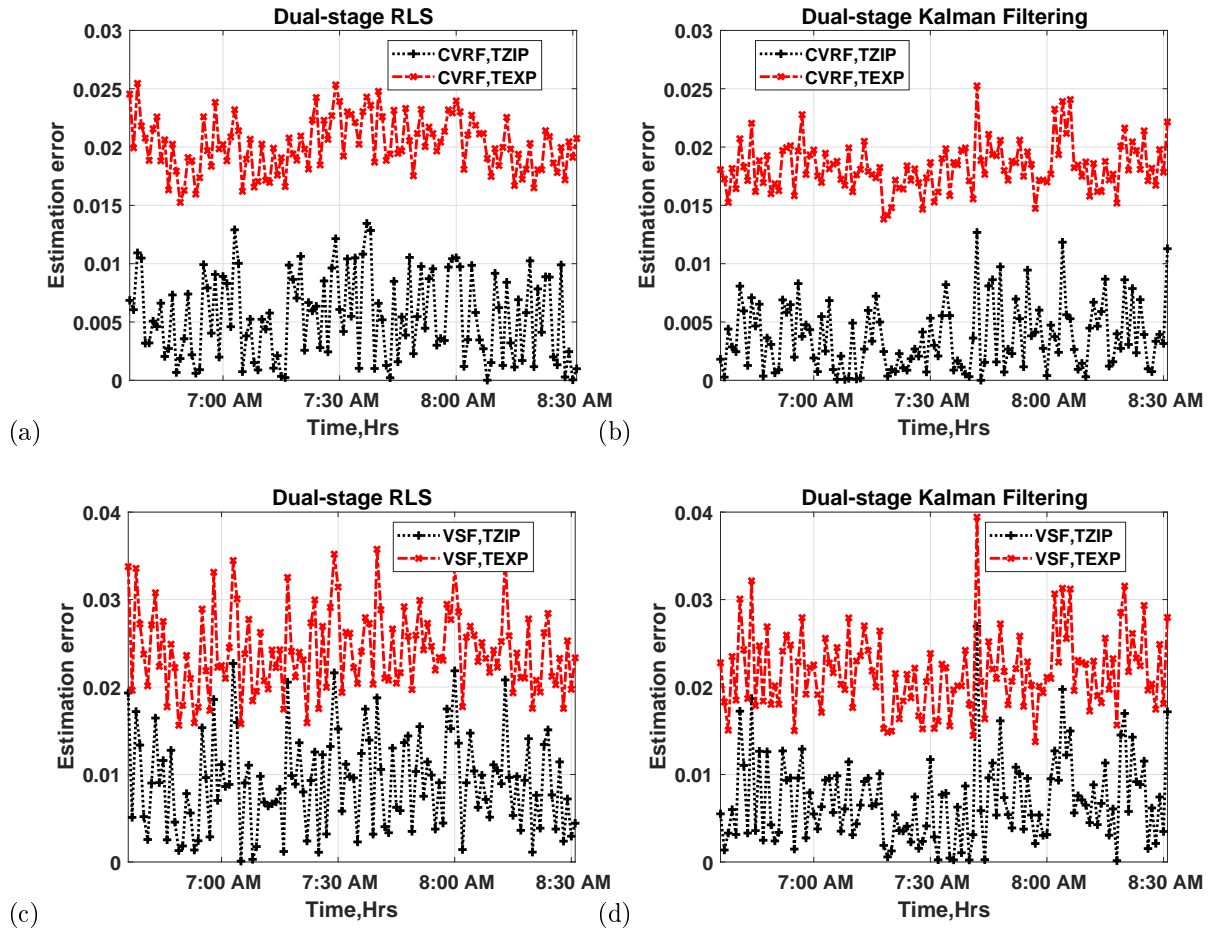


Figure 2.8: Estimation error for CVRF (a) using dual-stage RLS, (b) using dual-stage KF; Estimation error for VSF (c) using dual-stage RLS, (d) using dual-stage KF.

in the second stage (TZIP) using CRLS and CKF filters of dual-stage RLS and dual-stage KF, respectively. Consequently, VSF is shown in Figs.2.6 (c),(d), and 2.7 (c), and (d) using both filters in both stages. Out of the 116 measurements, some sudden load deviations were observed around 7:10 AM and 7:35 AM which are shown in Fig. 2.9 in the validation part. However, a significant estimation error is not seen using the methodologies due to use of variable forgetting factor and single-step prediction in dual-stage RLS and dual-stage KF, respectively. Fig.2.8 (a) and (b) depict the estimation error of CVRF for both stages using dual-stage RLS and dual-stage KF, respectively. It is evident that the second stage (TZIP) exhibits a lower estimation error for both CVRF and VSF. For TZIP, the error margin is minimal, whereas, the TEXP error margin is close to 2.5% for CVRF and nearly 4% for VSF in some of the worst cases.

2.1.5.4 Validation of the proposed model

To validate the above assertion, the entire feeder is simulated under CVR condition using the calculated CVR factors, shown in the previous subsection. The purpose of this extended simulation is to observe the alignment of the simulated load profiles with the measured load profiles in the real circuit where all control devices are active. The respective calculated CVRF using the identified parameters of both models of both filters are projected in the OpenDSS simulation to retrieve the total active power consumption during CVR deployment periods. Fig. 2.9(a) presents the comparison case of measured CVR on load consumption with simulated CVR on load consumption. For clear visibility, two different slots of the figure are zoomed in and represented in Fig. 2.9(b) and (c). Fig. 2.9(b) shows a sudden deviation from 13.6 kW to 12.1 kW between 7:08 AM and 7:09 AM. However, the simulated TZIP model using the second stage filters of both dual-stage RLS and dual-stage KF reflect proximity to the measured profile. Other zoomed in part, in Fig. 2.9(c), reflects relatively smoother load profile deviation and also portrays the effectiveness of the TZIP model.

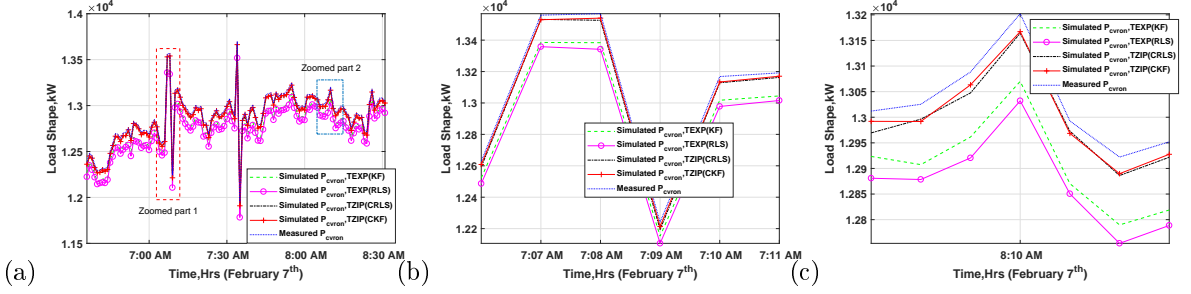


Figure 2.9: (a) Measured and simulated active power on February 7th ; (b) Zoomed part 1 of Fig. 2.9(a); (c) Zoomed part 2 of Fig. 2.9(a).

The proposed methodology is also compared for both load models in two stages in terms of the relative percentage error (RPE), mean absolute percentage error (MAPE), and normalized mean square error (NMSE). The definitions of these terminologies can be found in [52]. All the performance indices presented in Table 2.2 indicate that the second stage filtering for TZIP model works better. Moreover, if the performance of filters is considered, the KF-CKF combined filter exhibits the highest accuracy with minimum REP (0.3651%), MAPE (0.3073%), and NMSE (0.0304).

Table 2.2: Performance comparison in two stages for both load models.

Time	Stage (filter, model)	REP (%)	MAPE (%)	NMSE
Feb 7 th	1 st stage (RLS, TEXP)	0.6538	0.4783	0.2563
	2 nd stage (CRLS, TZIP)	0.3741	0.3161	0.0319
	1 st stage (KF, TEXP)	0.6297	0.4476	0.2313
	2 nd stage (CKF, TZIP)	0.3651	0.3073	0.0304

2.1.6 Summary

A time-varying comparison of exponential and ZIP load models was conducted in this study to identify the most suitable load model for CVR assessment. A dual-stage adaptive filtering approach is proposed utilizing both TEXP and TZIP models. The first stage filter is used to identify the exponential factor and the nominal power associated with the exponential load model, which is then used in the second stage to identify the ZIP coefficients. A separate filter for the ZIP load model is unable to find

the nominal power due to the dependency of nominal power and actual consumption based on the voltage profile. Thus, the usage of nominal power from the first stage to the second stage makes the formulation much more accurate for the identification of ZIP coefficients. Two different dual-stage filters were designed for proper identification of load parameters/coefficients. The filters are able to handle the stochasticity if sudden load variation is reported. In addition, a historical analysis of voltage profile is performed statistically which eliminates the assumption that during the CVRoff time, the source voltage regulator set point is around 1.0 *p.u.* The proposed method will help the utilities to estimate the CVRf and VSF using the dual-stage filter by obtaining ZIP coefficients in a time-varying manner. Lastly, the time varying comparison is validated in a real circuit type simulation, with all the active control elements of a distribution feeder, which makes the study more valuable.

2.2 Time-Varying Stochastic and Analytical Assessment of CVR

2.2.1 Overview

In recent days, CVR has drawn an immense attention due to the state-mandated energy efficiency requirements. Moreover, due to a paradigm shift in utility operations, the concept of CVR is receiving substantial interest along with other smart-grid technologies. For example, CVR is being executed in utility feeders where DERs are integrated [32]. DERs provide added advantage by serving the loads locally which eventually reduces line losses. In addition, smart inverter-interfaced DERs can control the voltage in the desired range by applying special droop curves. However, due to the stochastic nature of renewable energy-based DERs and load profiles, penetration from the sources may vary from time to time which impacts energy savings, loss reduction, and voltage sensitivity. CVR can be implemented on short and long term basis. Fig.2.10 depicts an example of long and short term CVR implementation based on the energy savings. Even though long term CVR shows the evidence of higher en-

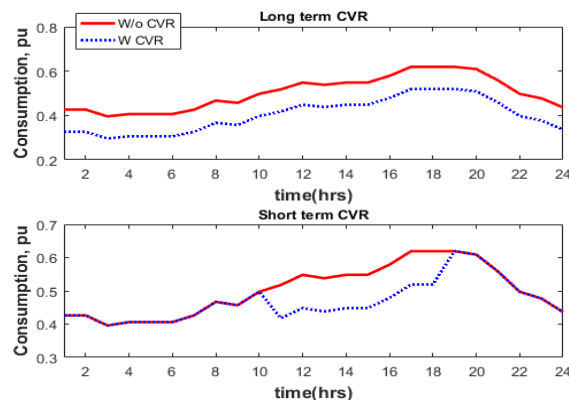


Figure 2.10: Long term CVR vs short term CVR.

ergy savings, in practice, it does not reduce much energy as a total due to various thermostatic loads in the system. Thermostatic loads, i.e. water heater, HVAC etc. need to run much longer to reach the desired operation during CVR-on time than the regular operation time [53]. Therefore, in general, utilities deploy CVR on a short-

term basis. Nevertheless, long term CVR analysis yields information about the circuit that can help determine the suitable times for CVR deployment since utilities can predict the operation of different appliances on the feeder based on the circuit load characteristics. Apart from the energy savings benefits measured by the CVR factor and loss factor, the voltage sensitivity factor also provides an in-depth knowledge to the utility about an individual circuit type to prioritize for CVR implementation at different times and balance the CVR-on and regular operation.

This study analyzes the CVR factor (CVRF), the loss factor (LF), and the voltage sensitivity factor (VSF) at different time steps by creating uncertainty with load profile and PV-based DERs using normal and beta distribution, respectively. In addition, the CVR-off operational voltage at the CVR-on time is retrieved using the historical probabilistic analysis. This helps to estimate the factors properly. The benefits of CVR are weighted using the Analytical Hierarchical Process (AHP) for day long CVR implementation so that the utility can determine the proper time for CVR implementation for obtaining the maximum benefits with associated voltage reduction. A real utility feeder and CVR-off voltage profile is utilized for simulation. The remainder of the study is organized as follows: Section 2.2.1 describes the detailed modeling of the system along with DERs, Section 2.2.2 introduces the uncertainty modeling, Section 2.2.3 describes AHP for the analysis, Section 2.2.4 demonstrates the simulation and analysis, and Section 2.2.5 concludes the study with major outcomes and suggests further research.

2.2.2 Distribution System Modeling

2.2.2.1 Load Modeling

Power flow and voltage profile of the system rely on the types of load, such as: residential, commercial, and industrial types. Depending on the nature of loads:

resistive, inductive, and capacitive behavior voltage profile is impacted in different ways. Therefore, accuracy of operation of a distribution system precisely depends on the load modeling. As mentioned earlier, utilities do not consider these characteristics when delivering power, to analyze voltage profile voltage sensitive loads should be considered. In the previous analysis, it is established that ZIP load model is more suitable and accurate for CVR study. Thus, in this study ZIP model is utilized. In addition to ZIP model of real power, defined earlier, reactive power is also considered as below:

$$Q_{ZIP} = Q_o \left[Z_Q \left(\frac{V}{V_o} \right)^2 + I_Q \left(\frac{V}{V_o} \right) + P_Q \right] \quad (2.51)$$

$$\text{where } Z_Q + I_Q + P_Q = 1 \quad (2.52)$$

where Q_o is the nominal reactive power and $Z_Q, I_Q,$ and P_Q are the coefficients for constant impedance, constant current, and constant power coefficients for reactive power. Different appliances and equipment for different class of loads have been tested in distribution feeder in [11] to observe their P-V and Q-V relationships. Since this study requires load to voltage sensitivity, the experimental coefficients of [11] are taken, provided as below:

Table 2.3: ZIP coefficients with customer class.

Customer	Sub-class	Z_P	I_P	P_P	Z_Q	I_Q	P_Q
Residential	A	0.96	-1.17	1.21	6.28	-10.16	4.88
	B	1.18	-1.64	1.47	8.29	-13.67	6.38
Small Commercial	Restaurant	0.69	0.04	.27	1.82	-2.24	1.43
Commercial	Laundry	0.77	-0.84	1.07	8.09	-13.65	6.56
Large Commercial	School	0.40	-0.41	1.01	4.43	-7.98	4.56
Commercial	Hotel	0.76	-0.52	0.76	6.92	-11.75	5.83
Industrial	School	1.21	-1.61	1.41	4.35	-7.08	3.72

2.2.2.2 PV Modeling

In this study, PV modeling is dependent on the state variables and look up table. The state variables are: Irradiance, panel kW, derating factor based on temperature, and efficiency of the inverter. Panel kW is the total active power output of the panel. Derating factor, and efficiency are read from a look up table [54].

$$PV\ output = P_{mpp} \times Irradiance \times Dfactor \times Efficiency \quad (2.53)$$

where P_{mpp} is provided as a panel temperature of 25°C and irradiance is provided from the predicted model which will be discussed in the next section. The look up table is presented in Fig. 2.11.

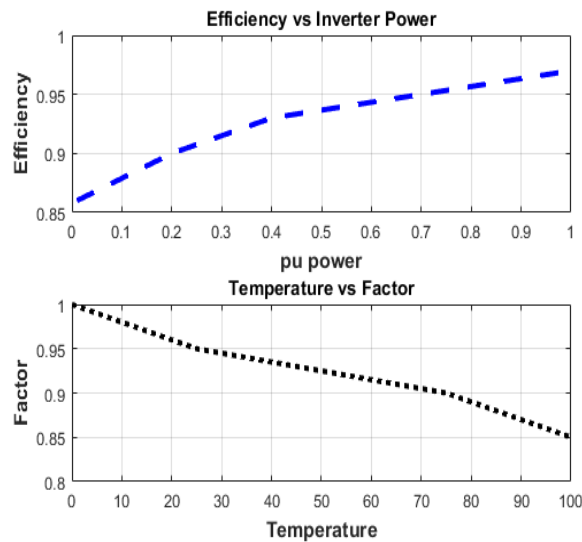


Figure 2.11: Efficiency vs Power and Derating factor vs Temperature relationship.

In addition, adaptive voltage set point can be used by utilizing dynamic Q-V droop curve which helps to adjust the voltage over time. The droop curve can be modified with a moving dead band from fixed 0.98-1.0 p.u. for voltage rising and falling set point over smart inverter working group (SIWG) presented curve [55], represented in Fig.2.12. The dynamic curve is used to fix the voltage to the desired ANSI lower range by monitoring the local voltage- reactive power absorption (inductive vars) can

be called upon if the voltage starts to exceed a predetermined upper level (defined by the volt-var curve). On the other hand, if the voltage at the terminals of the PV system is lower than nominal voltage, for instance, due to a reduction in active power output from PV or LTC set up, reactive power can be delivered to the corresponding bus (capacitive vars) to boost the voltage back to desired levels.

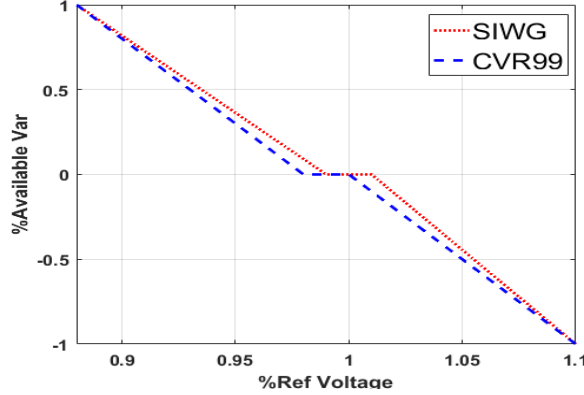


Figure 2.12: Modified dynamic volt-var curve.

2.2.2.3 Voltage Regulator Settings

CVR is deployed by means of voltage regulators with LTC. For accurate CVR arrangements and getting maximum economic benefits, proper regulator settings are needed. Correct setting properties may be seen in [56]. Three key quantities need to be updated when a change occurs in the regulated voltage: the voltage transformer ratio (PT ratio), rated current of the transformer, and compensators R/X settings, which are shown below:

$$PT_{ratio}(t) = \frac{V_{TL-N}}{V_{reg}(t)} \quad (2.54)$$

where V_{TL-N} is rated transformer line to neutral voltage and $V_{reg}(t)$ is the desired regulated voltage at any time instant.

$$I_{rated} = \frac{KVA_T}{\sqrt{3}V_{TL-N}(t)} \quad (2.55)$$

where KVA_T is transformer KVA rating. Also,

$$R(t) + jX(t) = (R_L + jX_L) \frac{I_{rated}}{PT_{ratio}(t)} \quad (2.56)$$

where $R_L + jX_L$ is the equivalent line impedance between the regulator and the load center. Per the settings, the typical voltage regulator has 32 steps. However, for CVR deployment, voltage will be in the lower range of the bands. Thus, it will have a maximum of 16 steps.

$$\begin{cases} a_T(t) = 1 - .00625 \times TAP^{abc} \\ a_T(t) = 1 + .00625 \times TAP^{abc} \end{cases} \quad (2.57)$$

2.2.3 Uncertainty Modeling

To estimate the CVRF, LF, and VSF under stochastic conditions, uncertainty is considered for load profile and solar irradiance. These represent the anomaly in the customer usage pattern and weather conditions.

2.2.3.1 Load Uncertainty Modeling

Load forecast error can be defined by the Probability density function (PDF) of the forecasted load of the system. It is clear from several literatures that normal distribution works better for creating uncertainty in load modeling [14],[57]. Fig.2.13 shows a typical discretization of the PDF of the load forecast error. This study adopts a similar procedure using the distribution function divided in several intervals with a mean in the center. Each interval defines the width of error with standard deviation (σ).

2.2.3.2 PV Irradiance Uncertainty Modeling

Power generation from a PV module depends on three parameters: solar irradiance, ambient temperature, and the module characteristics. Among these, solar

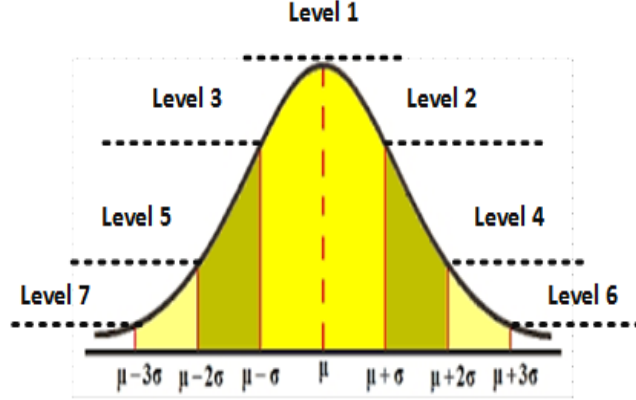


Figure 2.13: Typical discretization of the PDF of load forecast error.

irradiance exhibits the highest amount of uncertainty. Similar to modeling load uncertainty, we use beta distribution to model the irradiance uncertainty due to its appropriateness [14]. Beta distribution has a mean μ , which is the current irradiance prediction, Ird_{norm} in a time horizon and a standard deviation σ , which is a function of the mean. Both variables depend on two corresponding parameters: u and v . The occurrence k of any prediction $Ird_{norm}(t)$ can be modelled as follows:

$$F_{Ird_{norm}(t)}(k) = k^{u-1}(1-k)^{v-1} \quad (2.58)$$

The relationship of u and v with mean and variance for each time instant of the prediction interval are presented below:

$$Mean, \mu(t) = Ird_{norm}(t) \frac{I_{pred}(t)}{I_{max}} = \frac{u(t)}{u(t) + v(t)}, \quad (2.59)$$

$$Variance, \sigma^2(t) = \frac{u(t)v(t)}{[u(t) + v(t)]^2[u(t) + v(t) + 1]} \quad (2.60)$$

The relationship between mean and the variance of the beta function can be presented for each instant as:

$$\sigma(t) = .2Ird_{norm}(t) + 0.21 \quad (2.61)$$

(2.59)-(2.61) can be used to find the value of u and v to create the uncertainty using (2.58).

2.2.4 Analytical Approach

In this study, the analytical approach for CVR deployment analysis takes on three measurements: CVRF, LF, and VSF. Mathematical elaboration of CVRF and VSF is provided earlier. Similar to those, LF can be presented as:

$$LF = \frac{\Delta P_{loss}}{\sum_i \Delta P_i(t)} \quad (2.62)$$

Elaborately,

$$LF = \frac{\frac{P_{CV\text{Roff},loss} - P_{CV\text{Ron},loss}}{P_{CV\text{Roff},loss}}}{\sum_i \frac{P_{CV\text{Roff},i} - P_{CV\text{Roff},i}}{P_{CV\text{Roff},i}}} \quad (2.63)$$

Since CVRF is the primary index of load reduction measurement, by keeping it constant and making alternative pairs with the other two factors, AHP can be utilized to find the benefits of CVR deployment. AHP is a decision-making methodology using multiple criteria [31],[58]. AHP is applied to find a suitable substation for CVR implementation in [31]. However, the authors considered a lumped load for different feeders while transferring power from transmission system which does not truly identify the end user loads due to different characteristics mentioned earlier. Moreover, LF and VSF will not be reflected accurately due to the same reason. Considering these issues, AHP is modelled in a feeder to identify the suitable timing for short-term CVR deployment in an ascending order. Afterwards, weights of the benefits can be ranked in an ascending order for different time intervals. Every time interval is compared with all the other intervals in the AHP process. Hence, a utility can have flexibility in choosing the alternatives before CVR implementation. Steps of the AHP are mentioned below, while Fig.2.14 exhibits the AHP method for this work:

- i. Set up the hierarchical model which includes goal (H1), criteria (H2), and alternatives (H3).
- ii. Produce a judgement matrix for each criterion in the pairs. The judgement matrix resembles the relative importance of each criterion for all the alternatives. The formulation of the judgement matrix is presented below:

$$j_c = \begin{bmatrix} \frac{w_1}{w_1} & \dots & \frac{w_1}{w_T} \\ \vdots & \ddots & \vdots \\ \frac{w_T}{w_1} & \dots & \frac{w_T}{w_T} \end{bmatrix} \quad (2.64)$$

where w_i/w_j symbolizes the importance of i^{th} alternatives compared to j^{th} alternatives time interval of criterion c for this study. Intensity scale can be used to find the relative importance [58].

- iii. Calculate eigenvector, $WF_c = [WF_{c,1}, WF_{c,2}, \dots, WF_{c,T}]^T$ of the judgement matrix J_c associated with the maximum eigenvalue to find the weight factor for each time instant compared with others.
- iv. Rank the benefits of each time intervals with unified weight factor by summing up the criteria of each pair.

$$UWF_T = \sum_c WF_{c,T} \quad (2.65)$$

2.2.5 Simulation and Results

Similar to the previous study, the feeder is modeled in OpenDSS and simulated using an interface with Matlab. A day-long load shape and a solar irradiance shape of 5 minutes interval are used from a winter day to create the uncertainty in load modeling and solar irradiance. In addition, CVR-off nominal operation voltage data of two

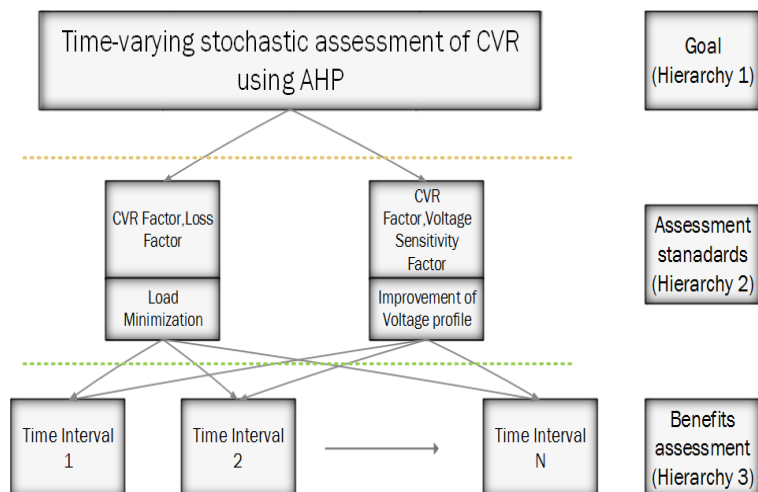


Figure 2.14: Hierarchy of time alternatives of AHP.

winter months: January and February, retrieved from the meter, are used to determine the probability distribution of CVR-off voltage at the CVR on day. Simulation and analysis is conducted using the methodology shown in Fig. 2.15.

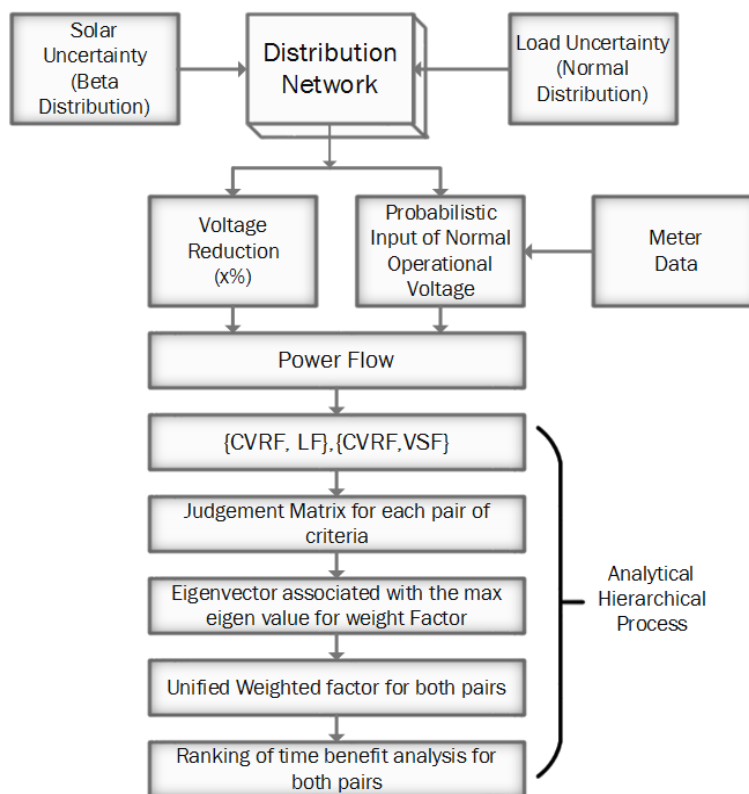


Figure 2.15: Ranking strategy for CVR deployment benefits.

Table 2.4: Distribution of Winter Voltage Profile.

Phase	A	B	C
Mean, $\mu(p.u.)$	1.028	1.031	1.027
Variance, $\sigma^2(p.u.)$	$1.834e^{-4}$	$1.939e^{-4}$	$1.665e^{-4}$

The probability distributions of phase A is depicted in Fig. 2.16. From the figure, it can be easily assumed that the CVR-off operational voltage follows the normal or lognormal distribution very closely. Hence, either distribution can be used to run the power flow for normal operations. For this study, a normal distribution is used to identify the CVR-off voltage during CVR-on day. Table 2.4 provides the parameters for simulation based on the historical data. Two cases are simulated: (Case 1) 1% VR with 30% penetration; (Case 2) 2% VR with 30% penetration. Percentage of penetration resembles the number of loads associated with customer types installed with PV, i.e. 30% residential, industrial, and commercial customers have PV installed in their systems. The PV installed at the load locations can serve a maximum of 50% of the load.

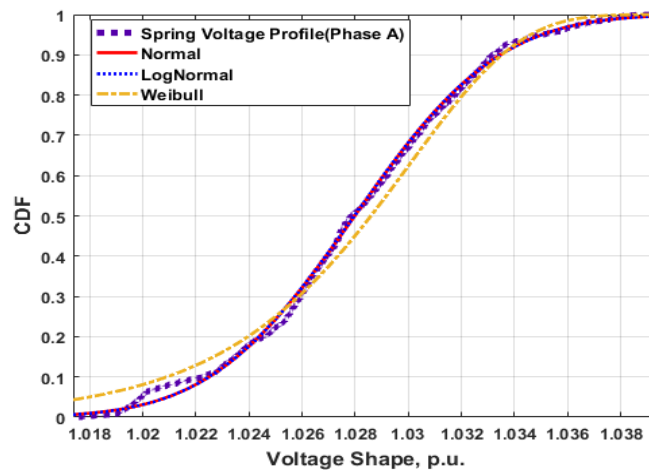


Figure 2.16: CDF of CVRoff voltage profile for winter.

2.2.5.1 Voltage Profile Margin

For both cases, the average voltage profile of the secondary system is depicted in Fig.2.17. The figures confirm that the voltage profile always remains at or above

0.95 pu throughout the feeder. During the evening time, near about 18th-21st hour

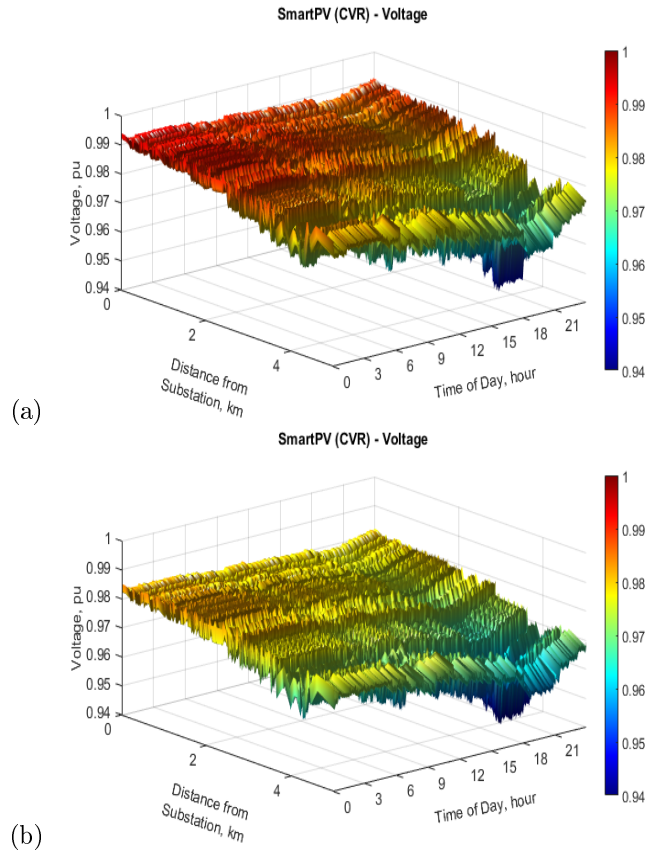


Figure 2.17: Average secondary system voltage profile: (a). Case 1. (b). Case 2.

(6 PM-9 PM), the voltages turn lower near the end of the feeder due to increase in demand and no PV generation. Thus, up to 2% voltage reduction is performed for this feeder.

2.2.5.2 Weight Factors

The cases described above are simulated to estimate the factors at each time instant over other instants to check the mutual benefits using the eigenvectors of the judgement matrix, which is depicted in Fig.2.18. In both cases, it is evident that the LF is proportional to the CVRF. For instance, when the CVRF is high, LF also becomes high in between 12 AM-6 AM, and with lower CVRF, LF becomes low as well in between 6 PM-9 PM. However, in between 6 AM-5 PM at some instants the LF becomes even higher than the CVRF during the day time when PV is able to produce

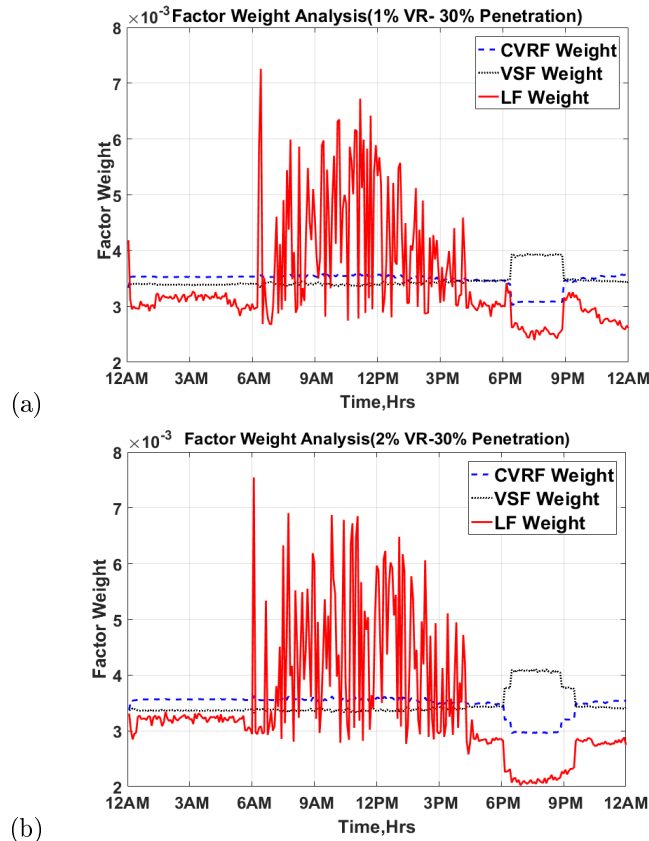


Figure 2.18: Factor Weights: (a). Case 1. (b). Case 2.

power since the locations of the PV systems are distributed, which can partially meet the demands and the substation does not need to carry the total power to the loads. On the other hand, VSF is inversely proportional to the CVRF. A higher CVRF represents lower VSF, and vice versa. Therefore, higher amounts of load reduction reduces the stress on the system. The scenario gets more clear during the evening time, between 6 PM to 9 PM. In that interval, load reduction is lower than during other intervals due to higher demand. A higher VSF indicates that the stress needs to be reduced as much as possible by maintaining the voltage within constraints.

2.2.5.3 Unified Weight Factors

Unified weight factors (UWF) for two different pairs of the factors are shown in this section, presented in Fig. 2.19 and Fig. 2.20, using box plots so that it can be visible more clearly how the performance justifies CVR deployment at different times

of the day.

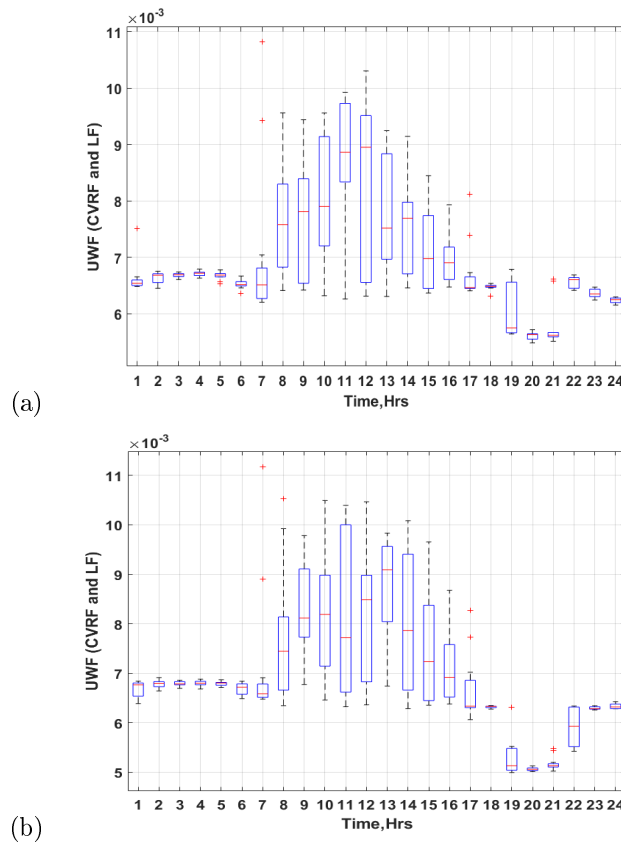


Figure 2.19: UWF for case 1 a. CVRF and LF. b. CVRF and VSF.

The box plots are the statistical data for each hour with a defined mean, maximum, and minimum UWF for the pairs. The pair of CVRF and LF shows better performance in the day time (7AM - 5PM) than the pair of CVRF and VSF. On the contrary, CVRF and VSF pair exhibits better performance at night time (5PM - 7AM). Thus, the utility can decide on the priority of short-term CVR deployment by measuring the benefits of each hour over others. A priority can be set based on higher energy savings or higher stress relief.

2.2.6 Summary

This study describes a method to identify the most beneficial times for CVR deployment under uncertain conditions. This analysis provides utilities with an in-depth knowledge about a feeder for CVR deployment at different times of the day with

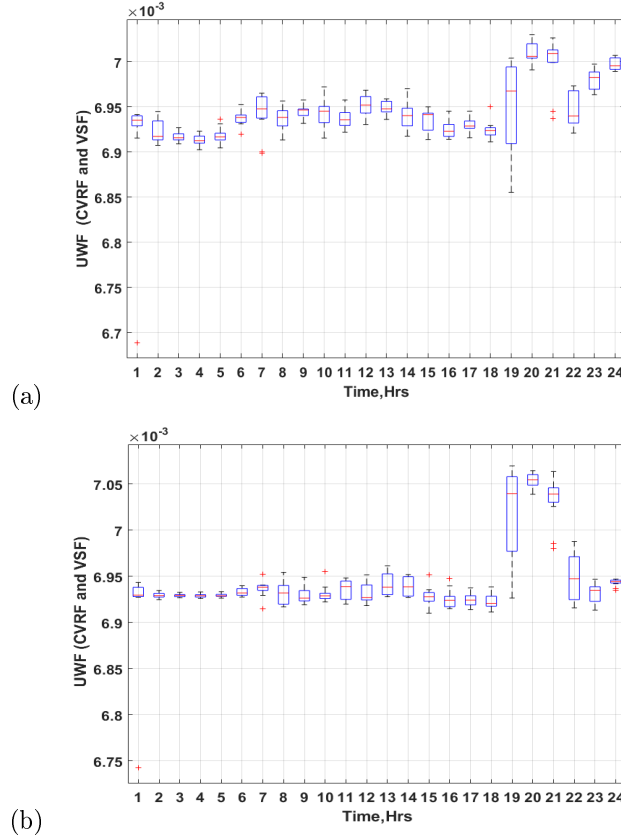


Figure 2.20: UWF for case 1 a. CVRF and LF. b. CVRF and VSF.

different factors associated with it, while keeping the voltage limit within the required band. Moreover, probabilistic CVR-off voltage profile determination provides more accuracy to estimate the factors. Further research can be made on this topic to compare different analysis methods, such as Game Theory, Cost-Benefit analysis, or Multi-Voting system etc. by integrating the electricity price of the markets and demand response techniques at different instants.

2.3 Effective CVR planning with Smart DERs

Nomenclature

$P_{i,t}, Q_{i,t}$ Active, reactive power through node i at time t .

$P_{n,t}, Q_{n,t}$ Active, reactive power through section n at time t .

$p_{i,t}^b, q_{i,t}^b$ Active, reactive base load at node i at time t .

p_i^b, q_i^b, S_i^b Active, reactive, and apparent assigned load at node i .

r_n, x_n Resistance, reactance of section n .

$P_{n,t}^{loss}$ Real power loss at section n at time t .

$Q_{n,t}^{loss}$ Reactive power loss at section n at time t .

$V_{i,t}$ Voltage at node i at time t .

$q_{i,t}^{cap}$ Reactive power supplied from capacitor bank at node i at time t .

$P_{i,t}^{PV}, Q_{i,t}^{PV}$ Active, reactive power injected/absorbed from/to DG at node i at time t .

S_i^{PV} Size of DG at node i .

$V_{s,t}$ Voltage set point at substation at time t .

$P_{s,t}, Q_{s,t}$ Source provided active, reactive power at time t .

PN_{max} Maximum penetration of DGs based on the load size.

Pm_{pp} Maximum active power injection.

Pf_{pv}, Pf_L PV, Load power factor.

$Lf_{i,t}$ Load factor at Node i at time t .

$V_{n,l,t}$ Voltage of the l^{th} terminal of section n at time t .

V_0 Nominal voltage of the system.

A_m Switching status of cap bank where $m \in \{1, 2, \dots, N\}$.

V_{tap} Number of tap change at node i at time t .

$Tap_{i,t}$ Number of tap change at node i at time t .

n Section index $\in \{1, 2, \dots, S\}$.

t Time index $\in \{1, 2, \dots, T\}$.

i Node index $\in \{1, 2, \dots, N\}$.

l Section terminal $\in \{1, 2\}$.

j Number of downstream nodes to any node $\in \{1, 2, \dots, X\}$.

2.3.1 Overview

CVR effectiveness always relies on the level of voltage reduction at the substation and is constrained by the requirement of maintaining the lower service boundary throughout the feeder. Wherever the voltage magnitudes stray below or above the ANSI band, it will diminish the CVR property. To retain this property capacitor placement is formulated as a multi-objective problem to maintain the voltage along with active power loss reduction with minimum capital investment using Genetic Algorithm (GA) in [3].

In recent days, integration of distributed energy resources (DERs) is increased in the distribution grid. Specially, PV based DERs are being integrated at many customer locations (i.e., rooftop solar) essentially in a random manner. Therefore, with an increased/high penetration on distribution feeders, DER impacts the voltage profile along with energy efficiency and system dependability by locally controlling the generation of active and reactive power based on the inverter rating and type. DER incorporated system is studied using different objectives, such as voltage improvement, loss reduction, and economic considerations[59],[60]. However, all of them considered the active power injection from the DERs. CVR implementation in a DER integrated feeder has great potential for load consumption and line loss reduction by using the reactive power (Var) control capability of smart inverters to conserve the voltage[4]. Co-ordination of smart inverters independently with the existing network voltage controller can help to achieve a higher CVR factor [6]. Conventional inverters are not able to provide reactive power control capability. Thus, based on the penetration at a certain node, voltage might violate both upper and lower bound. This study presents a method to maintain the voltage bound property, if CVR is deployed, by co-ordinating the smart inverter interfaced DERs with the existing network infrastructure such as capacitor banks and step voltage regulator (SVR). The entire process is done by estimating the appropriate source voltage in such a point which

can maintain the whole feeder voltage within the range of ANSI band. In this study, some large load locations (large commercial and/or industrial loads) are chosen randomly for DER placement since large scale DERs can control the local and adjacent node voltage to achieve deeper CVR benefits by injecting/absorbing reactive power. However, This method can be tested with any network that have DERs at random locations to know what would be the appropriate source voltage setting for CVR deployment in any particular time. This way utilities might also know the percentage of voltage reduction for any circuit. This methodology can also be tested in conventional DER based circuits. Nevertheless, it might not give desired result compared to smart inverter interfaced DER based circuits.

The remainder of the study is organized as follows: Section 2.3.1 presents the motivation of using smart inverters which is beneficial for CVR deployment, Section 2.3.2 introduces a mixed integer nonlinear programming (MINLP) formulation to estimate the possible deeper source voltage setting for CVR deployment where smart inverter settings are properly replicated with existing network infrastructure. Section 2.3.3 validates the concept using the IEEE 37 bus test system and compares the result with existing conventional inverters. Section 2.3.4 concludes the study discussing the major outcomes and further works.

2.3.2 Var Control Using Smart Inverter

In the future grid, a large number of solar power plants will likely be integrated in the distribution system. While planning for operation, this will create a number of issues for distribution service operators (DSOs) to deal with -such as resource adequacy, voltage rise at the injection point, low voltage ride through for short circuit studies or protection coordination in bidirectional power flow.

High penetration of PV causes the voltage to increase locally which can create an impact on nearby customers because of violating the service range of voltage (nominal \pm 5%). On the other hand, deploying CVR results in voltage reduction as

opposed to the voltage rise due to the high penetration of DER. The purpose of CVR in a DER integrated system is twofold: a) serving the loads locally which can reduce the line loss with less power travelling through the line towards the load locations, and b) reducing the load consumption and providing stress relief during high loading time by applying low source voltage. Due to highly unbalanced nature of distribution systems voltage drops much below than the source voltage at the loading points. Smart inverters are capable of giving that support of voltage control to raise or lower by injecting or absorbing reactive power during the intermittency/absence and high penetration of active power, respectively[61]. In case of CVR, it can follow special droop curves for reactive power adjustments to achieve possible deeper voltage reduction and maintain the range in the whole feeder depending on available resource. Such need based reactive power adjustments are incorporated in the formulation, which will be evident in next section. Smart inverters can also be counted as a complementary to capacitor banks for nearby reactive load support along with voltage control. Moreover, in a typical distribution feeder cap banks are not deployed densely whereas DERs can be placed distributively throughout the feeder which can create impact in neighboring node voltages.

2.3.3 Formulation Methodology

This section presents the widely used distribution system load flow model and proposes a formulation to achieve a deeper voltage reduction by integrating CVR and smart inverter interfaced DERs (smart PVs).

2.3.3.1 Distribution System Modeling

Considering the conceptual system diagram,depicted in Fig.2.22, it is assumed that the distribution system consisted of N number of nodes and S number of sections. To demonstrate the complex power flows in each of the nodes, DistFlow equations are used [62]:

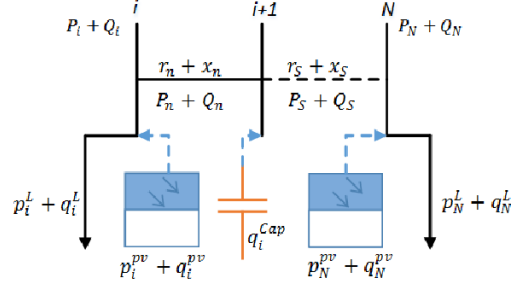


Figure 2.21: Conceptual system diagram.

$$P_{i+1} = P_i - r_n \frac{P_n^2 + Q_n^2}{V_i^2} - p_i^L + p_i^{DG} \quad (2.66)$$

$$Q_{i+1} = Q_i - x_n \frac{P_n^2 + Q_n^2}{V_i^2} - q_i^L + q_i^{DG} + q_i^{Cap} \quad (2.67)$$

$$V_{i+1}^2 = V_i^2 - 2(r_n P_n + x_n Q_n) + \frac{P_n^2 + Q_n^2}{V_i^2} (r_n^2 + x_n^2) \quad (2.68)$$

The DER units, which are subjected to uncertainties, generate the active power of amount p_i^{DER} and reactive power of q_i^{DER} at bus i . In addition, the reactive power injectors or var compensation devices, e.g., capacitor banks generate reactive power q_i^{Cap} . Active and reactive power flow through each node considering the loss, load consumption, and DER production is described in (2.65) and (2.66). In this study, DistFlow equations are implemented in a radial test feeder. The simulation environment is created in a mathematical modeling platform as a time series manner which creates a large number of optimization instances depending on the number of time stamps. Therefore, eq (2.67) is linearized to alleviate computational burden which describes the voltage drop. These are detailed in the next subsection.

2.3.3.2 Problem Formulation

As mentioned earlier, the prime objective of CVR is to reduce the load consumption. To achieve this objective, the voltage needs to be reduced at the substation while maintaining the lower service range throughout the feeder which eventually reduces

line losses. Line losses are also reduced by using local support from the DERs. In this study, a multi-objective problem is formulated, presented in (1.1), which optimizes both load and line loss reduction. ZIP load model is used to quantify the load to voltage (LTV) sensitivities due to its appropriateness. The problem formulation is detailed as below:

$$\text{Minimize } \sum_i p_{i,t}^L + \sum_n P_{n,t}^{loss} \quad (2.69)$$

subject to

$$p_{i,t}^L = p_{i,t}^b [Z_i^p (\frac{V_{i,t}}{V_0})^2 + I_i^p (\frac{V_{i,t}}{V_0}) + P_i^p] \quad (2.70)$$

$$q_{i,t}^L = q_{i,t}^b [Z_i^q (\frac{V_{i,t}}{V_0})^2 + I_i^q (\frac{V_{i,t}}{V_0}) + P_i^q] \quad (2.71)$$

$$Z_{i,t}^p + I_{i,t}^p + P_{i,t}^p = 1 \quad (2.72)$$

$$Z_{i,t}^q + I_{i,t}^q + P_{i,t}^q = 1 \quad (2.73)$$

$$S_{i,t}^b = S_i^b Lf_{i,t} \quad (2.74)$$

$$p_{i,t}^b = S_{i,t}^b P f_L \quad (2.75)$$

$$q_{i,t}^b = \sqrt{(S_{i,t}^b)^2 - (p_{i,t}^b)^2} \quad (2.76)$$

$$P_{n,t}^{loss} = \frac{P_{n,t}^2 + Q_{n,t}^2}{V_{n,t}^2} r_n \quad (2.77)$$

$$Q_{n,t}^{loss} = \frac{P_{n,t}^2 + Q_{n,t}^2}{V_{n,t}^2} x_n \quad (2.78)$$

$$\sum_{j=1}^X P_{i+j,t} = P_{i,t} - p_{i,t}^L + P_{i,t}^{PV} - \sum_n P_{n,t}^{loss} \quad (2.79)$$

$$P_{s,t} = \sum_i p_{i,t}^L - \sum_i p_{i,t}^{PV} + \sum_n P_{n,t}^{loss} \quad (2.80)$$

$$\sum_{j=1}^X Q_{i+j,t} = Q_{n,t} - q_{i,t}^L + q_{i,t}^{PV} + q_{i,t}^{cap} - \sum_n Q_{n,t}^{loss} \quad (2.81)$$

$$Q_{s,t} = \sum_i q_{i,t}^L - \sum_i q_{i,t}^{PV} - \sum_i q_{i,t}^{cap} + \sum_n Q_{n,t}^{loss} \quad (2.82)$$

$$q_{i,t}^{cap} = \sum_m A_m Q^{cap} \quad (2.83)$$

$$S_i^{PV} = PN_{max} S_i^b \quad (2.84)$$

$$Pmpp_i^{PV} = S_i^{PV} P f_{pv} \quad (2.85)$$

$$P_{i,t}^{PV} = Pmpp_i^{PV} Ird_t (F_T T_t + C_T) \quad (2.86)$$

$$0 \leq P_{i,t}^{PV} \leq Pmpp_i^{PV} \quad (2.87)$$

$$|q_{i,t}^{PV}| \leq \sqrt{(S_i^{PV})^2 - (Pmpp_i^{PV})^2} \quad (2.88)$$

$$V_{i+1,t} = V_{i,t} - \frac{r_n P_{n,t} + x_n Q_{n,t}}{V_{i,t}^2} \quad (2.89)$$

$$V_{s,t} - V_{i,t} \leq tolerance \quad (2.90)$$

$$V_{i,t}^{new} = V_{i,t}^{old} + V_{tap} Tap_{i,t} \quad (2.91)$$

$$Tap_{min} \leq Tap_{i,t} \leq Tap_{max} \quad (2.92)$$

$$V_{cvr,min} \leq V_{i,t} \leq V_{cvr,max} \quad (2.93)$$

$$V_{cvr,min} \leq V_{s,t} \leq V_{cvr,max} \quad (2.94)$$

In the above formulation, (2.69) is the objective function which minimizes the sum of loads and line losses, measured by the same unit. Eqs (2.70)-(2.94) describe the constraints for the formulated problem. Eqs (2.70) and (2.71) are the ZIP load models for active and reactive load, respectively which depend on the LTV parameters $Z^p, I^p, P^p, Z^q, I^q,$ and P^q are specified in Table 2.3. Eqs (2.72) and (2.73) are conditions for the ZIP load model which are also satisfied by the provided data in Table 2.3. In eqs (2.74)-(2.76), load behavior depending on load factor and power factor is shown. The Power factor is considered to be 0.95 lagging for all the loads throughout the

simulation. Active and reactive power loss are represented by (2.77) and (2.78). Eqs (2.79) -(2.82) represent the power balance relationship of generation and demand for both active and reactive power. All the downstream nodes connected to any upstream node in the network are considered in (2.79) and (2.81). In the power balance relationship equations source is providing based on the production from DERs. Switching operation of capacitor bank is shown in eq (2.83). DER rating is portrayed in (2.84). In this study, panels are rated to penetrate at a maximum 30% of the apparent load of the individual location where DERs are placed. Active power injection is represented by (2.85). Ambient temperature and factors related to the panel output is also taken into considerations to make the formulation much realistic in (2.86). Temperature dependent factor (F_T) and constant (C_T) are calculated from the linear dependency of panel output and ambient temperature given in [63]. Eqs (2.87) and (2.88) show the active and reactive power control based on the DER rating. Eq (2.89) provides a voltage drop relation between consecutive nodes. Eq (2.90) states the maximum voltage difference between the source node and all other nodes in the feeder. Since CVR is deployed in the lower service range, the tolerance is given 0.05 pu. It was relaxed to some extent in the result section when it is compared with the conventional inverters. Eq (2.91) renders the operation of voltage regulator. Eq (2.92) bounds the tap operation of regulator based on the maximum and minimum tap range. Eq (2.93) is the lower service range for CVR deployment in the whole feeder, which is known as voltage constraint. At the end, eq (2.94) gives flexibility to the source to operate in lower service range at individual time periods.

2.3.4 Results and Analysis

This section presents the results of simulation. The IEEE 37 bus test system [64] is used for simulation. Since the loads are being considered as voltage dependent, the system is modified with an assigned load sub-class based on load size, mentioned in the previous subsection. Moreover, in the modified system four solar inverter based

DERs are placed at buses 701,722,728, and 737 because they contain the highest loads in the system. Modified system is shown in Fig.2.22.

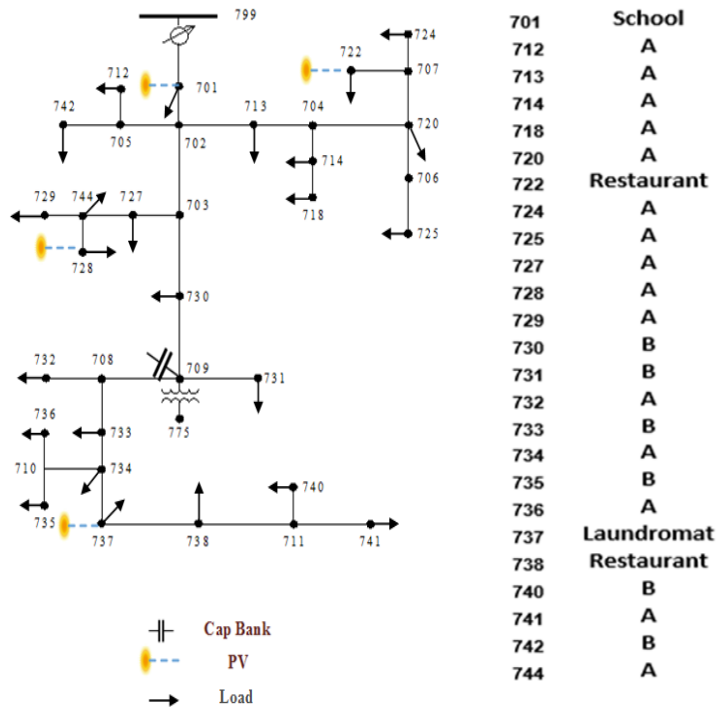


Figure 2.22: Modified IEEE 37 bus test system.

A 200 kVar capacitor bank is also integrated at bus 709 since the average voltage goes below 1 *p.u.* (distance $\approx 10^4$ ft) in a normal operating condition (1.04 *p.u.*) before CVR deployment, as presented in Fig.2.23.

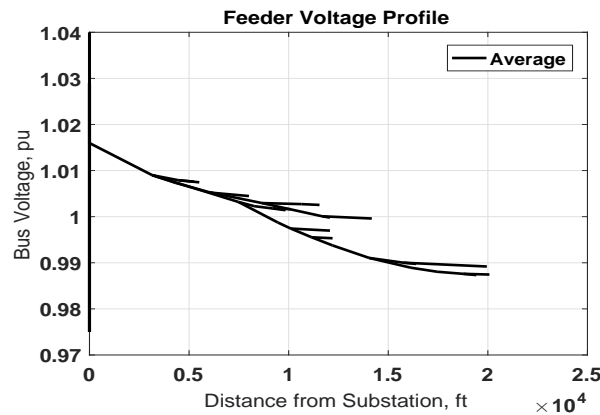


Figure 2.23: Average voltage profile of the system (Operating voltage=1.04 *p.u.*).

The simulation was run on two cases: a) CVR with smart PV (Smart inverter iter-

faced DER) b) CVR with conventional PV (Conventional inverter interfaced DER). For both of the cases a maximum of 30% PV penetration is considered and 0.95 power factor considered in the smart PV case for reactive power allocation from the inverter. Different sets of load shapes [65], temperature data and solar irradiance [66] are used for summer and winter season which are depicted in Fig.2.24. These data represent a typical summer and a winter day. Using the data set, the MINLP formulation presented in Section III is coded in A Mathematical Programming Language (AMPL), and solved via BARON, an MINLP solver [67]. Solution iteration is provided at the end of this section in comparative analysis for the two cases mentioned above.

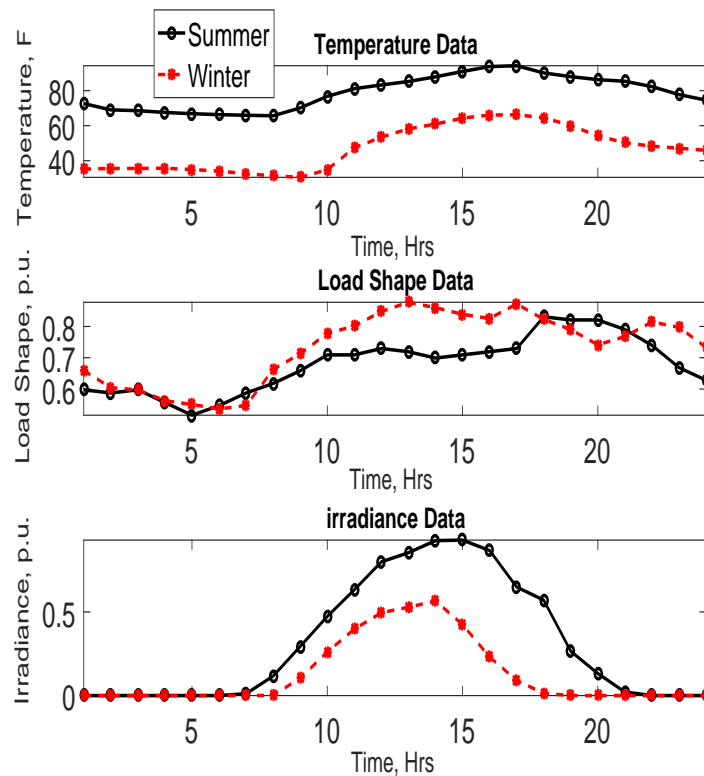


Figure 2.24: a. Time vs Temp b. Time vs Load Shape c. Time vs Irradiance.

2.3.4.1 Case 1: CVR with smart PV

According to the formulation source voltage is decided at each time instant to meet the constraints and keep the voltage as low as possible. Fig.2.25 shows the source voltage in the presence of smart PVs. Fig.2.26 provides the voltage profile throughout

the feeder which reflects at no time instant any part of the feeder violates the voltage bound. Since the smart PVs can provide reactive power support which can raise the voltage at different locations of the feeder, if needed, source is able to keep low voltage for deeper CVR deployment. Fig.2.27 exhibits the active and reactive power generation from the PVs. At the PV locations, generated active power can support the loads partially which cannot increase the voltage to a high extent at the injection points. Thus, reactive power injection is provided during the whole simulation period to support the local and nearby loads in addition to uphold the voltage or reduction in voltage drop.

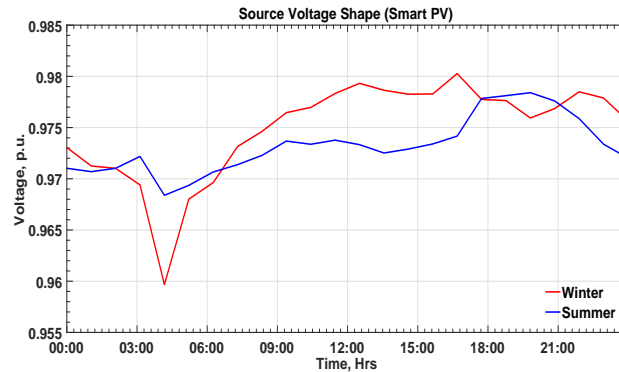


Figure 2.25: Source voltage shape (Smart PV).

Fig.2.28 demonstrates the voltage profile at the inverter interconnections and Fig.2.29 shows the inverter characteristics for reactive power injection in accordance with the voltage profile. It seems that due to the constant lower voltage profile at the inverter ends, reactive power maintains to inject near to the maximum availability. This resembles that inverters follow the typical droop curves independently.

2.3.4.2 Case 2: CVR with Conventional PV

Similarly, the same experiment is conducted using conventional PVs. In this case, source voltage is kept higher than the previous case at all times since it does not have any other distributed device except the existing capacitor bank and LTC. The scenario is depicted in Fig.2.30. Despite of keeping the source voltage above 0.98 pu

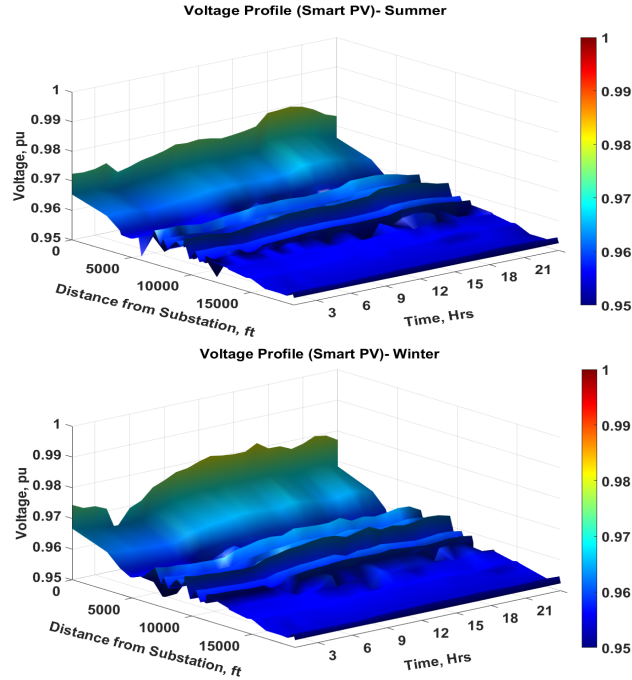


Figure 2.26: Feeder voltage profile (smart PV) a. Summer b. Winter.

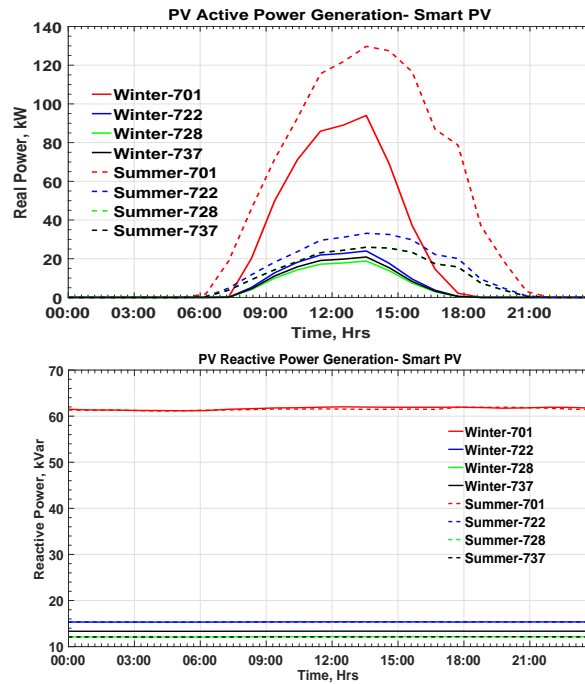


Figure 2.27: Smart PV generation a. active Power b. reactive Power.

most of the time, high voltage drop could not satisfy the constraint to keep the voltage within the range. Because in this case, except the existing network equipment no PVs are able to supply reactive power. Therefore, the voltage constraint is relaxed to 0.93

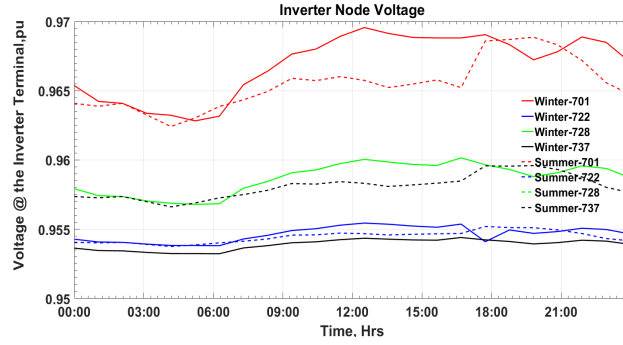


Figure 2.28: Node voltage at interconnection points.

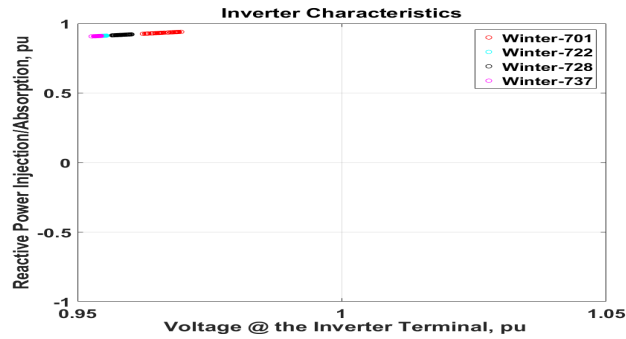


Figure 2.29: Inverter droop settings.

pu in the lower bound. Fig.2.31 shows the voltage profile throughout the feeder for conventional PV case which denies the voltage constraint property of CVR at some time instants. Fig.2.32 demonstrates the active power generation of conventional PVs which is not significantly higher than the smart PV case.

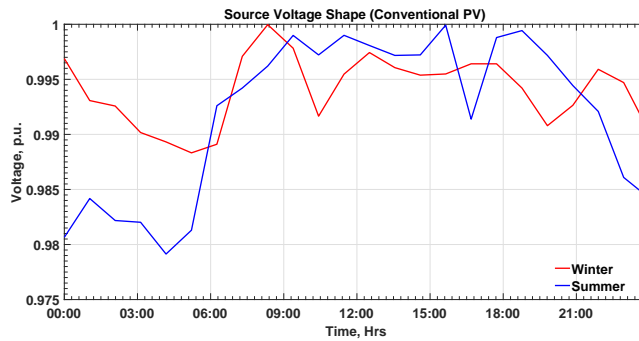


Figure 2.30: Source voltage shape (Conventional PV).

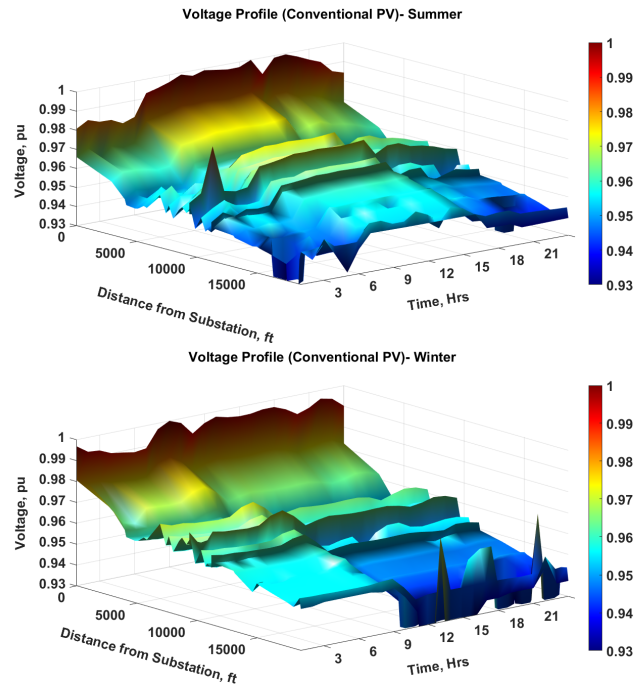


Figure 2.31: Feeder voltage profile (Conventional PV) a. Summer b. Winter.

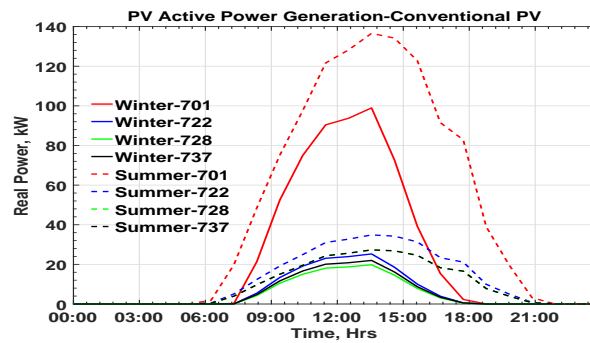


Figure 2.32: Conventional PV active power generation.

2.3.4.3 Comparative analysis

In this subsection a comparative analysis is provided for the cases simulated above. The analysis provided in Table 2.5 demonstrates that smart PVs give additional reduction in load consumption and line loss than the conventional PVs along with satisfying the voltage constraint.

Table 2.5: Load and loss analysis for different sub-cases.

Sub-cases	Load(MWh)	Loss(MWh)	# of iter.
Winter(Smart PV)	43.59	1.27	968
Summer(Smart PV)	40.11	1.05	892
Winter(Conventional PV)	44.01	1.77	1476
Summer(Conventional PV)	40.72	1.33	1383

2.3.5 Summary

This study presented a deterministic MINLP formulation for CVR effectiveness under the presence of smart PVs. The formulation describes a planning methodology for estimating the source voltage for precise CVR deployment as deep as possible in accordance to the existing network infrastructure. An illustrative analysis of cases displays effective performance of smart inverters in load and line loss reduction by controlling the voltage in a radial network autonomously compared to the conventional inverters. This helps to deploy deeper CVR throughout the feeder. The concept is well-proved to maintain required voltage boundary even at the end of the feeder. More investigation can be conducted using stochastic formulation of the system considering loading and irradiance as uncertain variables.

CHAPTER 3: Integrated CVR and Demand Response Framework for Distribution System

Nomenclature

Sets and indices

Γ_M Set of nodes with index $i \in \mathbb{Z}$.

Γ_S Set of sections $(i, j) \in \mathbb{Z} \times \mathbb{Z}$.

Γ_R Set of sections with SVR $(i, j) \in \mathbb{Z} \times \mathbb{Z}$.

$\Gamma_{DER} \subset \Gamma_M$ Set of nodes with DER interconnections.

$\Gamma_L \subset \Gamma_M$ set of load nodes.

$\Gamma_{CAP} \subset \Gamma_M$ set of nodes with capacitor banks.

T Set of Time $t \in \mathbb{Z}$.

S Set of scenarios $s, s' \in \mathbb{Z}$.

sub Index of substation node.

Parameters

$r_{i,j}/x_{i,j}$ Line resistance/reactance between nodes i and j .

Z_t^p/Z_t^q constant impedance coefficient for active/reactive power at time t .

I_t^p/I_t^q constant current coefficient for active/reactive power at time t .

P_t^p/P_t^q constant power coefficient for active/reactive power at time t .

α_i Customer defined boundary for load shifting at node i .

$C_{tou,t}$ Price for time of use (TOU) plan at time t .

$C_{cpp,t}$ Price for critical peak pricing (CPP) plan at time t .

$C_{ptr,t}$ Price for peak time rebate (PTR) plan at time t .

CT carbon taxation price.

E_{esd}/E_{esc} Discharging/ Charging rate of the BESS.

V_{max}/V_{min} Max/min voltage limit for any node.

tap_{max}/tap_{min} Max/min tap settings for Step voltage regulators (SVR).

V_{tap} Voltage change for each tap.

V_{nm} Nominal operational voltage.

S_i^{PV}/S_i^{ES} Inverter size of PV/BESS at node i .

H Time for BESS to reach at maximum SOC.

$Ird_{i,t}^n$ Solar irradiation in node i at time t in scenario n .

$Temp_t$ Ambient temperature at time t .

m Slope of reference temperature and derating factor set points.

q_c Size of each unit of capacitor bank.

a_{max}/a_{min} Max/min number of unit for capacitor bank.

V_{TL} Tolerance limit of voltage boundary.

$P_{i,t}^b/Q_{i,t}^b$ Base active/reactive power for each node i at time t .

PF_l Power factor for load.

PF_{pv} Power factor for load.

BP_t Net price of electricity at time t .

lf_t^n Load factor at time t in scenario n .

PT_{bg}/PT_{end} Beginning/Ending of peak time.

Variables

$P_{i,t}^L/Q_{i,t}^L$ Active/reactive load at node i at time t after load shifting.

$S_{i,t}^{sh}$ Shifted apparent load at node i at time t .

$P_{i,t}^{sh}/Q_{i,t}^{sh}$ Shifted active/reactive load at node i at time t .

$P_{i,t}^{cvr}/Q_{i,t}^{cvr}$ Active/reactive load after deploying CVR at node i at time t .

$P_{i,t}^c/Q_{i,t}^c$ Active/reactive load curtailment by deploying CVR at node i at time t .

$P_{i,t}^{cl}/Q_{i,t}^{cl}$ Consumed active/reactive load at node i at time t .

$P_{i,t}^{PV}/Q_{i,t}^{PV}$ Active/reactive PV injection/absorption at node i at time t .

$P_{i,t}^{ES,d}/Q_{i,t}^{ES,d}$ Active BESS discharging/charging at node i at time t .

$V_{i,t}$ Voltage magnitude($p.u.$) at node i at time t .

$SOC_{i,t}^{ES}$ State of charge of BESS at node i at time t .

$NP_{i,t}$ Net price of electricity at node i at time t .

$K_{tou,i}/K_{cpp,i}$ Decision for using TOU/ CPP plan at node i .

$K_{ptr,i}$ Decision for using PTR plan at node i .

$R_{i,t}$ Total peak time rebate at node i at time t .

$L_{i,j,t}^p/L_{i,j,t}^q$ Total active/reactive power flow between nodes i and j at time t .

$I_{i,j,t}$ Current flow between nodes i and j at time t .

$L_{i,j,t}^{Loss,p}/L_{i,j,t}^{Loss,q}$ Total active/reactive power loss between node i and j at time t .

$L_{sub,t}^p/L_{sub,t}^q$ Total active/reactive power delivered from substation at time t .

$TAP_{i,t}$ Tap switching at node i at time t .

$a_{x,t}$ Switched on capacitor banks at time t .

D_t Derating factor at time t .

ρ_n/ρ_s Probability of n/s scenarios.

3.1 Overview

The primary aim of energy efficiency techniques discussed in the introduction is to preserve the energy consumption and to ensure the reliability by maintaining the network security constraints whenever the system is at risk [68], [69]. There has been a considerable amount of studies done for each of these techniques, separately. Several papers have studied VVO/CVR with DG integration [70]-[73]. Reference [70] discusses a VVO approach using model predictive control (MPC) for optimal dispatch of on-load tap changer (OLTC) and capacitor banks (CB). They also consider an exponential load model to represent load to voltage (LTV) sensitivity and uncertainty in DER injection and load consumption. Reference [71] discusses a multi-stage VVO by coordinating OLTC and step voltage regulators (SVR) throughout the distribution feeder. Their study considers high penetration of DERs and ZIP load model to represent the LTV. Reference [72] reports on optimal reactive power injection from different DERs to minimize the number of tap operations of SVRs. A combined scheme of centralized and local control for VVO is presented in [73] to minimize line losses while integrating induction machine-based DERs. Likewise, several DR programs have been studied with the integration of DERs [16],[74]-[77]. Reference [74]

discusses the coordination of the DERs throughout the feeder to minimize the operating cost of virtual power players using particle swarm optimization (PSO) in the presence of DR programs. They consider a deterministic mixed integer non-linear program (MINLP) where DERs are utilized as energy exporter. Another MINLP for energy hub operation is presented in [75] to minimize the total cost of demand when stochasticity is present in load and pricing. They also consider the integration of energy storages in their model. In reference [76], a mixed integer linear programming (MILP) based energy management system for DR is studied to reduce the operational and maintenance cost of DERs. Their model demonstrated stochasticity of wind power, load consumption, and real time pricing. A MINLP based two-stage optimal DR program is discussed in [16] for each load-type (e.g. residential, commercial, industrial), separately, with the integration of energy storages. Their model considers stochasticity in the load profile. In [77], a MILP based study is conducted for DR in an industrial load to coordinate the grid and DERs for scheduling the load shift to minimize the energy cost.

All the above reported studies discussed the implementation of either CVR/VVO or DR separately, in the presence of different types of DERs. However, to establish the integrity of ADMS, the available techniques should be implemented together in the same step, since doing so may lead to the maximum energy efficiency. With this guiding principle, this study proposes a MINLP based integrated CVR and DR framework for ADMS. Based on the forecasted base load, ADMS should be able to schedule the load shifting amount according to the input of each customer to maintain the network constraints in terms of reliability with cost minimization. In addition, CVR can be deployed after the potential load shifting to minimize the load consumption as a curtailment function as shown in Fig.3.1. Therefore, customers are not required to conduct additional curtailment that would compromise their comfortability.

Contributions of this study can be summarized as:

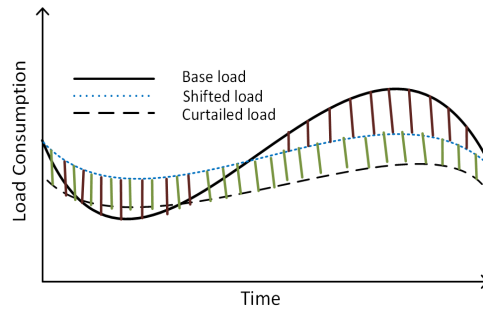


Figure 3.1: Load consumption with integrated CVR and DR.

- i. An MINLP-based integrated CVR and load shifting (LS)-based DR program is proposed within the confinement of network constraints and applicable to operations of any DSO. In addition, time-varying LTV is considered in this model using the ZIP coefficients.
- ii. As shown in Table 1.1, some utilities have experimented with multiple DR plans. However, all these plans were started separately. In the open market, utility companies would benefit from offering a pool of plans so that the participation from the customer increases. Our proposed model utilizes different DR plans and offers the most suitable plan to each customer to maximize their participation and minimize the consumption cost. The model also demonstrates the inclination of customers to multiple and different DR plans due to the variation of LS for each customer. This also leads to the flattening of voltage profile with the distribution of load from peak time to any other periods of the day.
- iii. Two different types of DERs: PV and Battery energy storage system (BESS) are interconnected in different locations of the feeder. Moreover, stochasticity in PV generation and load consumption is considered by creating different scenarios to validate the proposed model. The proposed optimization framework can be depicted as an energy management tool within the distribution feeder.

The rest of the chapter is organized as below: section 3.1 presents the problem for-

mulation where some derivation is inherited from chapter 2; section 3.2 discusses the procedure of scenario generation and reduction; section 3.3 analyzes the numerical results; and section 3.4 summarizes the major findings of this chapter.

3.2 Problem Formulation

This section provides the mathematical foundation of the integrated CVR and DR framework. Detailed modeling is used to represent distribution feeder line flow, load behavior, active and reactive power injection/absorption from DERs. A load consumption cost analysis is also done, which is based on different DR plans. The following subsections presents the objective function, and the equality and inequality constraints related to the model.

3.2.1 Objective Function

The objective function of this model is to minimize the expected cost of purchasing electricity by reducing load consumption, as stated below:

$$\text{Min } \mathbb{E}[X_{i,t}] \quad (3.1)$$

$$\text{Where } X_{i,t} = \sum_i \sum_t [P_{i,t}^{cl} (NP_{i,t} + CT) - R_{i,t}], \forall i \in \Gamma_L, t \in T \quad (3.2)$$

To reduce the cost, the consumption of load is minimized in two different stages. At first, load shifting is imposed on the forecasted base load. Next, during the consumption phase, CVR is deployed to reduce the consumption. The consumption cost depends on the selected DR plan, carbon taxation, if present, and the rebate from peak periods.

3.2.2 Load Modeling

Load modeling is the most significant component of both CVR and DR and for the integrated framework, it will remain the same. As stated earlier, firstly, the load shifting function will work with the cooperation of customers. Functions related to

load shifting are presented below:

$$P_{i,t}^b = \mathcal{N}(lf_t, \sigma_i^L) P_i^b, \quad Q_{i,t}^b = P_{i,t}^b \sqrt{\frac{1}{pf_t^2} - 1} \quad (3.3)$$

$$P_{i,t}^L = P_{i,t}^b - P_{i,t}^{sh}, \quad Q_{i,t}^L = Q_{i,t}^b - Q_{i,t}^{sh} \quad (3.4)$$

$$|S_{i,t}^{sh}| \leq \alpha_i \sqrt{(P_{i,t}^b)^2 + (Q_{i,t}^b)^2} \quad (3.5)$$

$$P_{i,t}^{sh} = S_{i,t}^{sh} pf_t, \quad Q_{i,t}^{sh} = P_{i,t}^{sh} \sqrt{\frac{1}{pf_t^2} - 1} \quad (3.6)$$

$$\forall i \in \Gamma_L, t \in T$$

The base active and reactive forecasted load for each customer is represented by (3.3). The active base load is retrieved by a common load factor multiplier and a variance using normal distribution and reactive base load is identified using a power factor. The active and reactive loads after the necessary shifting is presented in (3.4). The load shifting can be bounded by the customers as presented in (3.5). In this study, customer defined boundary is considered as $\alpha = 0.1$, irrespective of time and customer. However, depending on each customer's input this value can be changed with time. In this day-ahead optimization program, customers can let their service provider know their shifting boundary through AMI[18]. Moreover, any type of shifting cannot ignore the coupled reactive power associated with the apparent power. Therefore, when a customer plan for shifting a load or operation of a device (e.g., dishwasher, washer and dryer, electric vehicle etc.) the associated reactive power also gets shifted along with the active power as presented in (3.6). In addition, the summation of these shifting will always be zero over the time as presented below:

$$\sum_{t \in T} P_{i,t}^s = 0, \quad \sum_{t \in T} Q_{i,t}^s = 0, \quad \forall i \in \Gamma_L \quad (3.7)$$

CVR deployment is conducted after planning the appropriate load shifting. CVR deployment is utilized as a curtailment function and loads are modelled as quadratic ZIP loads because of its higher fidelity in voltage profile analysis, as stated in [40]. Moreover, time-varying ZIP coefficients are utilized from the composite load factor for better accuracy which is discussed in details in chapter 2.

$$P_{i,t}^{cvr} = P_{i,t}^L [Z_t^p w_{i,t} + I_t^p u_{i,t} + P_t^p], \forall P_{i,t}^L \geq P_{i,t}^{cvr} \quad (3.8)$$

$$Q_{i,t}^{cvr} = Q_{i,t}^L [Z_t^q w_{i,t} + I_t^q u_{i,t} + P_t^q], \forall Q_{i,t}^L \geq Q_{i,t}^{cvr} \quad (3.9)$$

$$\forall i \in \Gamma_L, t \in T$$

$$w_{i,t} = (u_{i,t})^2, u_{i,t} = \frac{V_{i,t}}{V_{nm}} \quad (3.10)$$

$$\left(\frac{V_{min}}{V_{nm}} \right)^2 \leq w_{i,t} \leq \left(\frac{V_{max}}{V_{nm}} \right)^2, \forall i \in \Gamma_M, t \in T \quad (3.11)$$

$$\frac{V_{min}}{V_{nm}} \leq u_{i,t} \leq \frac{V_{max}}{V_{nm}}, \forall i \in \Gamma_M, t \in T \quad (3.12)$$

Equations (3.8) and (3.9) represent the active and reactive load models. The quadratic non-linear behavior of the load model is relaxed using second order cone program (SOCP) by introducing new variables in (3.10), as suggested in [4]. Curtailment of load after CVR deployment and the actual consumed load are posed in (3.13)- (3.15).

$$P_{i,t}^C = P_{i,t}^L - P_{i,t}^{cvr}, Q_{i,t}^C = Q_{i,t}^L - Q_{i,t}^{cvr} \quad (3.13)$$

$$P_{i,t}^{cl} = P_{i,t}^{cvr} - P_{i,t}^{PV} - P_{i,t}^{ES,d} + P_{i,t}^{ES,c} \quad (3.14)$$

$$Q_{i,t}^{cl} = Q_{i,t}^{cvr} - Q_{i,t}^{PV} - Q_{i,t}^{CAP} \quad (3.15)$$

$$\forall i \in \Gamma_L, t \in T$$

Equations (3.14) and (3.15) symbolize the actual consumed load from the grid after considering the injected power from the available DERs. In this study, PV and Batter energy storage systems (BESS) are considered as DERs. Detailed modeling of DERs are discussed in a later subsection.

3.2.3 Distribution Feeder Modeling

Consider the distribution feeder, shown in Fig.3.2. Such a radial distribution feeder can be characterized by a directed graph, $G = (N, S)$, which consists of N nodes and S sections. Each section can be represented as $S \in \{(i, j), (j, k_1), (j, k_2), \dots\} \subseteq N \times N$. In the distinct parts of the feeder such adjacent sections can be assumed, as shown in Fig.3.2, to demonstrate the power flow using the Distflow equations [62]. Each section delivers power to the immediate downstream load and connected sections as presented in (3.16) and (3.17). The representation of line losses is provided in (3.18) in terms of the current flow in any section of the feeder. Equation (3.19) represents the flow of current in a relaxed form which does not compromise the optimality. Detailed proof of this relaxation is provided in [4], and [78]. Similarly, power balance relationship at the substation can be extended as shown in (3.20) and (3.21). The substation delivers the active and reactive power demand or actual consumption that is not met by the DERs and total line loss.

$$L_{i,j,t}^p = P_{j,t}^{cl} + L_{i,j,t}^{Loss,p} - \sum_{\{k|(j,k) \in \Gamma_S\}} L_{j,k,t}^p \quad (3.16)$$

$$L_{i,j,t}^q = Q_{j,t}^{cl} + L_{i,j,t}^{Loss,q} - \sum_{\{k|(j,k) \in \Gamma_S\}} L_{j,k,t}^q \quad (3.17)$$

$$L_{i,j,t}^{Loss,p} = I_{i,j,t}^2 r_{i,j}, \quad L_{i,j,t}^{Loss,q} = I_{i,j,t}^2 x_{i,j} \quad (3.18)$$

$$I_{i,j,t}^2 \geq \left[\frac{(L_{i,j,t}^p)^2 + (L_{i,j,t}^q)^2}{v_{i,t}} \right] \quad (3.19)$$

$$L_{sub,t}^p = \sum_{i \in \Gamma_L} P_{i,t}^{cl} + \sum_{(i,j) \in \Gamma_S} L_{i,j,t}^{Loss,p} \quad (3.20)$$

$$L_{sub,t}^q = \sum_{i \in \Gamma_L} Q_{i,t}^{cl} + \sum_{(i,j) \in \Gamma_S} L_{i,j,t}^{Loss,q} \quad (3.21)$$

$$\forall (i,j) \in \Gamma_S, t \in T$$

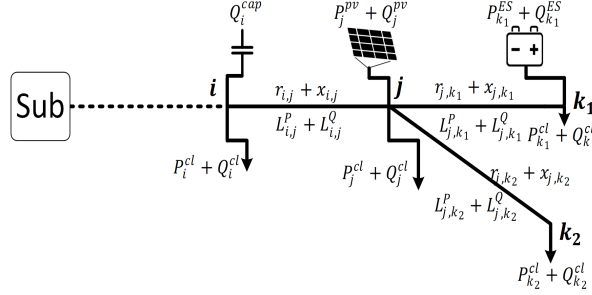


Figure 3.2: Conceptual diagram of radial distribution feeder.

3.2.4 DER Modeling

As stated earlier, only PV and BESS are considered in this study. The PV model considers active and reactive power injections. The active power injection depends on the inverter size, solar irradiance, and derating factor based on the ambient temperature as stated in (3.22). Equation (3.23) describes the linear dependency between ambient temperature and the derating factor[63].

$$P_{i,t}^{PV} = S_i^{PV} Ird_{i,t} D_t PF_{pv}, \forall i \in \Gamma_{DER}, t \in T \quad (3.22)$$

$$D_t = m \times Temp_t, \forall t \in T \quad (3.23)$$

Reactive power injection/absorption from PV inverters are modeled as follows:

$$|Q_{i,t}^{PV}| \leq \sqrt{(S_i^{PV})^2 - (P_{i,t}^{PV})^2}, \forall i \in \Gamma_{DER}, t \in T \quad (3.24)$$

To resolve the non-convex var control problem, (3.24) can be modified by using the following constraints from (3.25)-(3.27), as proposed in [4].

$$S_i^{PV} = \sqrt{(P_{i,t}^{PV})^2 + (Q_{i,t}^{PV})^2} \quad (3.25)$$

$$J_i^{PV} = (S_i^{PV})^2 = (P_{i,t}^{PV})^2 + (Q_{i,t}^{PV})^2 \quad (3.26)$$

$$(\overline{Q}_{i,t}^{PV})^2 = (S_i^{PV})^2 - (P_{i,t}^{PV})^2, |Q_{i,t}^{PV}| \leq \overline{Q}_{i,t}^{PV} \quad (3.27)$$

$$\forall i \in \Gamma_{DER}, t \in T$$

Equations (3.28)-(3.30) represent the formulation for the state of charge (SOC) of the installed BESS. The current SOC of BESS is shown in (3.28) and the limit for SOC is provided in (3.29) based on the duration to reach the maximum charging state. Moreover, it is stated that the SOC at the beginning and the end of the day will be the same. Maximum discharging and charging state is bounded by the inverter rating of BESS in (3.30).

$$SOC_{i,t}^{ES} = SOC_{i,t-1}^{ES} - \frac{P_{i,t}^{ES,d}}{E^{ES,d}} + P_{i,t}^{ES,c} E^{ES,c} \quad (3.28)$$

$$SOC_{i,1}^{ES} = SOC_{i,24}^{ES} = S_i^{ES} H, SOC_{i,t}^{ES} \leq S_i^{ES} H \quad (3.29)$$

$$0 \leq P_{i,t}^{ES,d} \leq S_i^{ES}, 0 \leq P_{i,t}^{ES,c} \leq S_i^{ES} \quad (3.30)$$

$$\forall i \in \Gamma_{DER}, t \in T$$

3.2.5 Capacitor Bank Modeling

Optimal switching of the capacitor bank is significant for controlling the voltage throughout the feeder [3]. The modeling of capacitor bank switching is presented below:

$$Q_{i,t}^{CAP} = \sum_x a_{x,t} q_c, a_{min} \leq a_{x,t} \leq a_{max}, \forall i \in \Gamma_{CAP}, t \in T \quad (3.31)$$

Equation (3.31) in conjunction with (3.15) decide the number of capacitor bank units to switch.

3.2.6 Voltage Control

To achieve deeper CVR deployment and maintain the reliability with load shifting constraints, at any node, holding the voltage profile at the lowest possible range is the highest priority. The voltage drop in any section throughout the distribution feeder can be explained with DistFlow property as:

$$v_{j,t} = v_{i,t} - 2(L_{i,j,t}^p r_{i,j} + L_{i,j,t}^q x_{i,j}) + (r_{i,j}^2 + x_{i,j}^2)I_{i,j,t}^2, \forall (i,j) \in \Gamma_S, t \in T \quad (3.32)$$

$$v_{i,t} = V_{i,t}^2, V_{min}^2 \leq v_{i,t} \leq V_{max}^2, \forall i \in \Gamma_M, t \in T \quad (3.33)$$

Equation (3.33) is used to tackle (3.32) as another relaxed SOCP, similar to (3.11) and (3.12). In addition, the step voltage regulator (SVR), connected at any section of the feeder, controls the immediate downstream node by following the tap settings as portrayed in (3.34) and (3.35). Moreover, OLTC settings at the substation needs to be fixed in such a way that the voltage at any node in the feeder does not extend beyond the tolerance limit as presented in (3.36).

$$V_{j,t} = V_{i,t} + V_{tap}TAP_{j,t}, \forall (i,j) \in \Gamma_R, t \in T \quad (3.34)$$

$$TAP_{min} \leq TAP_{j,t} \leq TAP_{max}, \forall j|(i,j) \in \Gamma_R, t \in T \quad (3.35)$$

$$|V_{sub,t} - V_{i,t}| \leq V_{TL}, \forall sub, i \in \Gamma_M, t \in T \quad (3.36)$$

3.2.7 Electricity Pricing

In the proposed model, three different DR plans are provided and the most suitable plan for each customer is offered. The selection of the plan renders maximum economic benefits for each customer and improves reliability from the utility side since the load is distributed from peak time to other instants based on the pricing schemes.

The electricity pricing model is posed below:

$$NP_{i,t} = BP_t + k_{i,tou}C_{tou,t} + k_{i,cpp}C_{cpp,t} - k_{i,tou}k_{i,cpp}\Delta C_{tou,t} \quad (3.37)$$

$$\Delta C_{tou,t} = \begin{cases} C_{tou,t} & \text{if } PT_{bg} \leq t \leq PT_{end} \\ 0 & \text{Otherwise} \end{cases} \quad (3.38)$$

$$R_{i,t} = \begin{cases} P_{i,t}^{sh} k_{i,ptr} C_{ptr,t} & \text{if } PT_{bg} \leq t \leq PT_{end} \\ 0 & \text{Otherwise} \end{cases} \quad (3.39)$$

$$K_i = k_{i,tou}k_{i,cpp}, K_i \leq k_{i,tou} + k_{i,cpp} - 1 \quad (3.40)$$

$$\forall i \in \Gamma_L, t \in T$$

The net electricity pricing scheme depend on which plan suits each individual customer, as presented in (3.37). If both TOU and CPP can provide minimum cost by maintaining the network constraints, customers are able to participate in both plans. However, in that case, duplicate charge needs to be removed at the peak time [16]. The peak time rebate plan credits for the shifted load for each customer during the peak time which is shown in (3.39). To smoothen the multiplication of two binary variables in (3.37),(3.40) can be utilized to replace the bi-linearity.

3.3 Prediction Uncertainty

The proposed integrated CVR and DR framework includes the hourly load and solar irradiance variation due to several socioeconomic or environmental factors. These variations lead to uncertainty in the day ahead planning. In this section, the process of generating scenarios is discussed by considering uncertainty in prediction error of solar irradiance and load factor. In this dissertation, solar irradiance and load factor prediction error, in respect to PV generation and load consumption, is calculated using beta distribution and normal distribution, respectively[14],[79],[80]. For any

prediction of irradiance in node i at time t , $Ird_{i,t}^{pred}$ beta function can be represented as:

$$f_{Ird_{i,t}^{pred}} = y^{\theta_{i,t}-1}(1-y)^{\lambda_{i,t}-1}, \forall i \in \Gamma_{DER}, t \in T \quad (3.41)$$

The beta function depends on two parameters, $\theta_{i,t}$ and $\lambda_{i,t}$ which can be calculated using the standard deviation of irradiance, $\sigma_{i,t}^{Ird}$ as presented below:

$$\theta_{i,t} = \lambda_{i,t}\xi_{i,t} \quad (3.42)$$

$$\lambda_{i,t} = \left[\frac{\xi_{i,t}}{(\xi_{i,t} + 1)^3(\sigma_{i,t}^{Ird})^2} - \frac{1}{(\xi_{i,t} + 1)} \right] \quad (3.43)$$

$$\xi_{i,t} = \frac{.21 - \sigma_{i,t}^{Ird}}{\sigma_{i,t}^{Ird} - .41} \quad (3.44)$$

$$\sigma_{i,t}^{Ird} = .2Ird_{i,t}^{pred} + .21 \quad (3.45)$$

$$\forall i \in \Gamma_{DER}, t \in T$$

The standard deviation in a beta distribution depends on the value of current prediction as shown in (3.45). If the prediction has higher value, the it will have a higher variance and vice versa. On the other hand, for estimating the load forecasting error, normal distribution is used very frequently with a fixed standard deviation over the time. In this study, 0.02 is employed as standard deviation, σ_s^L , for load forecasting error in each scenario. In addition, for varying each load, separately, σ_i^L is also considered as .02 in (3.3). For the usage of both normal and beta distributions, current prediction is considered as the mean. Since this dissertation is out of scope for prediction of solar irradiance and load consumption, load profile from a typical utility distribution feeder and irradiance data from [66] are used as the predicted value. Similar approach is adopted in [70]. Using the required parameters of probability distributions, as described above, monte-carlo (MC) simulation is conducted to create the required number of scenarios for solar irradiance and load factor. After generating

S scenarios each with a probability of ρ_s , a scenario reduction technique is utilized to reduce it to n scenarios to decrease the computational burden, while keeping a good approximation of the uncertainty. In this dissertation, the fast forward selection (FFS) method is utilized for scenario reduction due to its higher accuracy [81]. Algorithm 3.1 provides the overall procedure of FFS. At first, the algorithm initializes

Algorithm 3.1: Scenario reduction using FFS

- 1 Initialize $c_{ss'}^1 = c(\beta_s, \beta_{s'})$, $s, s' = 1, \dots, S$
 - 2 Initialize $l_{s'}^1 = \sum_{s=1, s \neq s'} \rho_s c_{ss'}^1$, $s' = 1, \dots, S$
 - 3 Initialize $s'_1 \in \arg \min_{s'} l_{s'}^1$, $L^1 = s' \setminus s'_1$
 - for** $i=2:N-n$ **do**

$$c_{ss'}^i = c(\beta_s, \beta_{s'}), \quad s, s' \in L^{i-1}$$

$$l_{s'}^i = \sum_{s \in L^{i-1} \setminus s'} \rho_s c_{ss'}^i, \quad s' \in L^{i-1}$$

$$s'_i \in \arg \min_{s' \in L^{i-1}} l_{s'}^i, \quad L^i = s' \setminus s'_i$$
 - end for**
 - 4 New probability $\rho_n = \rho_s + \sum_{l \in L} \rho_l$
-

the distance, $c_{ss'}$ with a random scenario set as stated in (3.46) and starts filling in the sets of deleted scenarios, L .

$$c(\beta_s, \beta_{s'}) = \max \{1, \|\beta_s - \bar{\beta}\|, \|\beta_{s'} - \bar{\beta}\|\} \|\beta_s - \beta_{s'}\| \quad (3.46)$$

Consequently, it runs the script for $S-n$ steps and fills in the set, L and calculates the new probability, ρ_n for n scenarios. In (3.46), $\bar{\beta}$ is the mean value of scenarios. Each new scenario leads to a $Ird_{i,t}^n$ and lf_t^n for solar irradiance and load factor prediction. Therefore, combining all the scenarios, the new objective function becomes:

$$\text{Min} \sum_n \rho_n \sum_i \sum_t [P_{i,t}^{cl} (NP_{i,t} + CT) - R_{i,t}], \forall i \in \Gamma_L, t \in T \quad (3.47)$$

s.t. (3.3)-(3.40).

3.4 Numerical Analysis

The proposed optimization program is tested in a modified IEEE 37 bus test feeder. Many authors in the past have validated their proposed method on 37 bus test system, such as [82]. The modifications to the feeder are portrayed in Fig.3.3. At some nodes DER installations are comprised of both PV and BESS whereas some nodes only contain BESS. The size of DERs are assigned as half of the loads at the respected locations and allocated as the inverter rating for each associated DER. Power factor for loads, PV inverters, and charging and discharging rate for the ES are attributed as .90. Time for BESS to reach at maximum/minimum SOC in a constant charging/discharging rate is fixed as 4 hours. For the capacitor bank, six units are considered at max with each unit having a size of 25kVar. The base electricity pur-

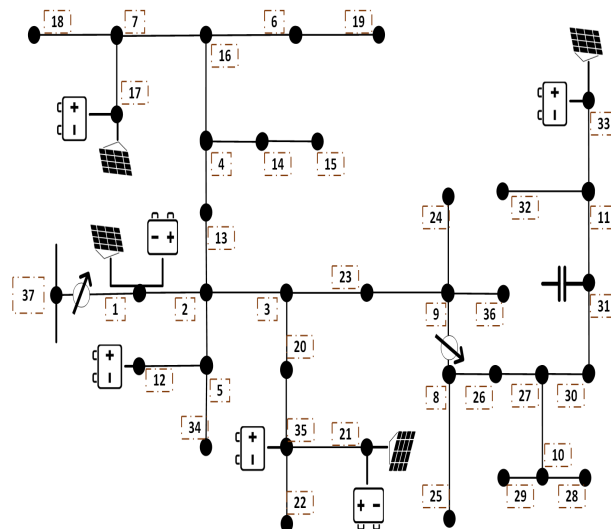


Figure 3.3: Modified IEEE37 bus test system.

chase rate is considered as \$.20/kWh. The price deviation for the DR plans, that have been considered in this study, are depicted Fig.3.4. A similar pricing scheme is also considered in [16]. The complete proposed and sequential steps are mentioned below:

- i. Typical irradiance and load profile are collected as predicted values to create 100 scenarios and reduced to 20 scenarios using the proposed methodology described

in section 3.2.

- ii. ZIP coefficients are retrieved using the dual-stage RLS method from the predicted load factors, described in chapter 2.
- iii. The entire model is coded in AMPL and solved using BARON solver to achieve the global optimality [83], [84]. Simulations are conducted for four different cases to analyze the cost and selection of plan for different customers and shown in Table 3.1. The three cases are: a. No CVR without load shifting (LS); b. CVR without LS. c. CVR with LS. All the cases are analyzed for three different types of days: critical day, typical weekday, and typical weekend. Peak time for the simulation is considered from hour 15 to hour 20 of any given day. A laptop computer with intel core i7 processor and 16 GB RAM is used for the simulation. Step 1 and step 2 are independent of step 3.

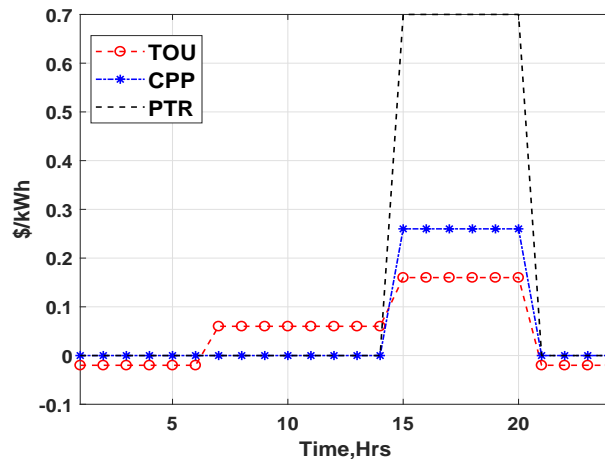


Figure 3.4: Price deviation for three demand response plans.

Fig.3.5 shows the composite load consumption for three cases for all three types of days. The CVR case, when compared with a No CVR case shows reduced consumption due to the reduction in voltage set point at the substation on any day. However, in all the days, it is evident that CVR with LS distributes the consumption from the peak time to other instants in order to cut down

the total consumption cost. Similarly, the mean voltage profile is portrayed in

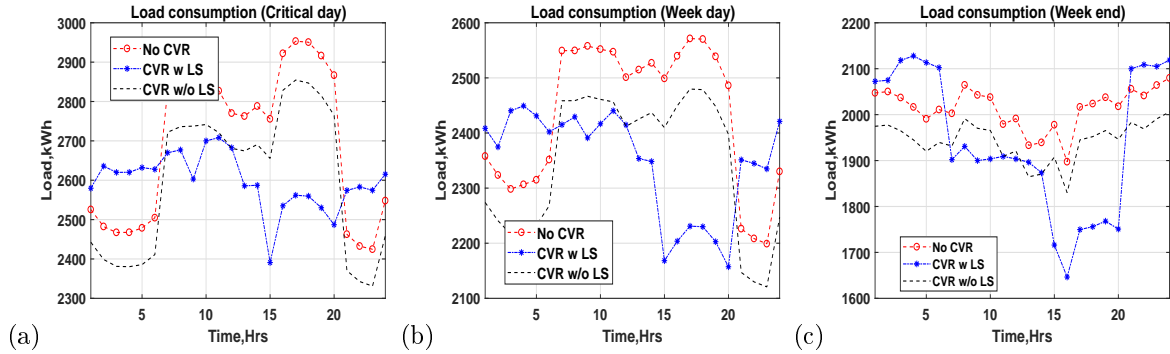


Figure 3.5: Aggregated load consumption for three cases; a. critical day, b. typical weekday, c. typical weekend.

fig.3.6. Both CVR cases reduce the voltage profile considerably within the limits than the No CVR case. However, the CVR with LS property depicts a more flattened voltage profile and reduces the voltage set point at the substation. In addition to the voltage profile, fig.3.6 (d),(e), and (f) depict the tap operation of SVR in between node 8 and 9. Fig. 3.6 (g),(h), and (i) provide the number of switched cap bank units. Since the LS property distributes the load from the peak time and reduces the voltage set point at the substation, it increases the CVR factor a little bit compared to the CVR without any LS case as portrayed in Fig.3.7. Table 3.1 depicts the total consumption cost for three different cases on three different days. The CVR with LS case shows the least consumption cost. In both Case 1 and Case 2, none of the customers are able to receive PTR since there is no load shifting. Moreover, the selection of CPP is also low since there is no additional load pattern change from the customer side. However, with the LS of each customers, as shown in Case 3, the consumption behavior changes drastically. As a result, all customers receive the PTR plan along with increment of selecting CPP.

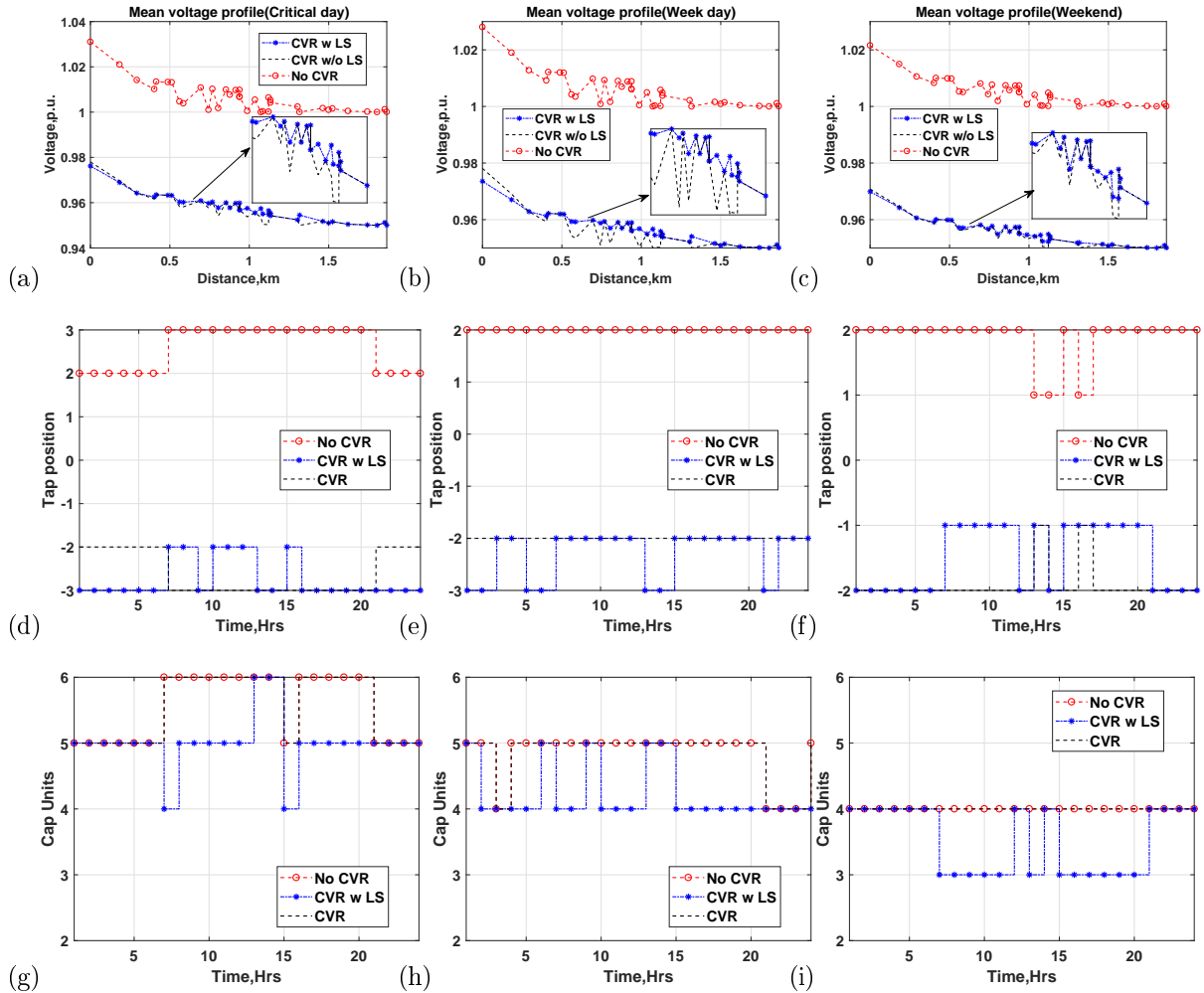


Figure 3.6: Mean voltage profile for three cases; a. critical day, b. typical weekday, c. typical weekend.; SVR operation for three cases; d. critical day, e. typical weekday, f. typical weekend.;CAP bank operation for three cases; g. critical day, g. typical weekday, i. typical weekend.

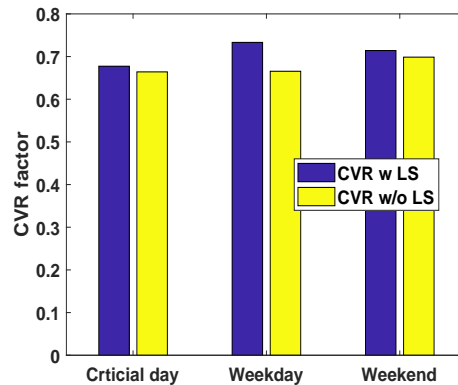


Figure 3.7: CVR factor for CVR with and without LS.

3.5 Summary

This study proposed a MINLP-based integrated CVR and DR framework. The study considers different DR plan for customer participation based on their suit-

Table 3.1: Total load consumption cost and DRP selection for each customer.

Type of Day	Case 1 (No CVR)	Case 2 (CVR w/o LS)	Case 3 (CVR w LS)
Critical Day	Cost: \$18777.86 TOU: All loads, CPP: ϕ , PTR: ϕ	Cost: \$18091.29 TOU{1,13,14,15,16,17,18,19,20,22, 23,24,25,26,27,28,29,30,31,32,33}, CPP:{12,21,35}, PTR: ϕ	Cost: \$16922.73 TOU: {1,14,17,28,31,33}, CPP:{12,13,15,16,18,19,20,21,22,23,24, 25,26,27,29,30,32,34,35}, PTR: All loads
Week day	Cost:\$16807.79 TOU: All loads, CPP:{12,35},PTR: ϕ	Cost: \$16172.98 TOU{1,13,14,15,16,18,19,20,22,23,24,25, 26,27,28,29,30,31,32,33}, CPP:{12,17,21,35}, PTR: ϕ	Cost: \$15150.43 TOU: {1,14,17,22,28,33,35}, CPP: {12,13,15,16,18,19,20,21,23,24,25, 26,27,29,30,31,32,34}, PTR: All loads
Weekend	Cost:\$13561.77 TOU: All loads, CPP:{12,35}, PTR: ϕ	Cost: \$13345.49 TOU: {1, 17,18,30,31,33}, CPP:{12,13,14,16,19,20,21,22,23,24,25, 26,27,28,29,32,34,35}, PTR: ϕ	Cost: \$12212.87 TOU: {1,15,17,20,22,24,30}, CPP:{12,13,14,16,18,19,21,23,25,26, 27,28,29,31,32,33,34,35}, PTR: All loads
**All loads: {1,12,13,14,15,16,17,18,19,20,21,22,23,24,25,26,27,28,29,30,31,32,33,35}			

ability. Stochasticity in load consumption and PV injection was considered within the formulation. The proposed method does not require customers to curtail load from their end. Curtailment is conducted by deploying CVR from the utility side. Therefore, customers are not required to compromise their comfortability. The LS property of DR provides customers the flexibility to shift their load at different time steps, which leads to the distribution of consumption as mentioned, and reduces the consumption cost by selecting the appropriate DR plan. Several SOCP relaxation methods were used to speed up the solution in the day ahead program, which gives flexibility to the service provider to incorporate more scenarios. Global optimality is ensured using BARON. The result shows that the LS property of DR can make the voltage profile flatter when implemented in conjunction with the CVR as compared to the case when deploying CVR only. Thus, it makes the system more reliable, and provides more savings with the lower voltage set point at the substation.

CHAPTER 4: Data-Driven Fault Location Scheme for FLISR Program

4.1 Overview

Power distribution system is a very complex structure with a large number of buses/nodes. As mentioned earlier, operation of distribution system is involved with many uncertainties, such as variation of loads or generation in renewable energy based DER generation due to the weather pattern or human behaviour. Such anomalies can lead to abrupt change in operational scheme. Moreover, massive integration of distributed energy resources (DERs) are on-going in distribution feeders which make the system even more complex with bi-directional power flow. Therefore, to implement the ADMS applications, it is utmost important to create maximum visibility for distribution feeders. With the advent of high speed communication and flexible measurement devices, utilities are taking steps towards grid modernization to make the distribution feeders more observable and controllable. Smart meters are being deployed at the load locations for real-time update about the customer's consumption and power quality issues. Advanced metering infrastructure (AMI) can be used to retrieve the data from smart meters [23]. However, smart meters are placed only at the low voltage (LV) secondary system and the primary system of the feeder remains unobservable. Observability of medium voltage (MV) primary system is important for FLISR since fault might happen anywhere in the feeder. Thus, low cost wireless stick-on voltage and current sensors can be used to monitor at different locations of the feeder in medium voltage (MV) distribution system [25],[26],and [85]. Apart from voltage and current magnitude data these sensors and smart meters can provide phase angles and power factor in real-time manner. For transmitting data, wireless sensors can be integrated with ZigBee® or ZigBee® Pro, depending on the range of signal

transmission. Data from the sensors are sent to a ZigBee® coordinator or data collector which is connected to ADMS through a ZigBee® gateway device (ZGD) such as, GSM module. A link between the ZigBee® network and the IP devices through a gateway allows interoperability and direct binding of the wireless sensor network (WSN) with SCADA. Apart from the cellular network, wi-fi enabled services are also available. Similar type of sensors is being manufactured in today's market, such as lighthouse by Tollgrade and Linewatch by QineitQ [86],[87]. A conceptual framework is presented in Fig.4.1.

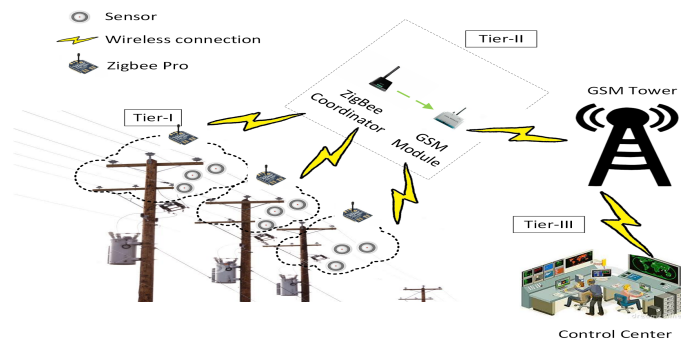


Figure 4.1: Conceptual framework of WSN for ADMS.

For FLISR application, identification of the fault location is the first step since isolation and service restoration depends on that. Reconfiguration of a network becomes easier for the purpose of service restoration and to supply the critical loads if an accurate fault location scheme is integrated in ADMS platform. Moreover, identification of fault location can improve both reliability and resiliency since pinpointing the fault helps the crew members to reach at the location and repair that within a short tenure. This eventually reduces the outage time and minimizes the repair cost, leading to the improvement of reliability indices such as, system average interruption duration index (SAIDI) and the system average interruption frequency index (SAIFI) [21]. Resiliency of a grid refers to the ability of absorbing a low frequency high impact events such as, extreme weather calamity whereas reliability refers to the high frequency low impact events due to regular natural events [88]. This study proposes

a fault location method for ADMS based FLISR program to pinpoint the faulty section(s) using the data from WSN and AMI. A modified graph traverse method depth first search (MDFS) is used to reduce the search space based on a variable called ratio test (RT) to find the faulty section(s) bounded by two sensors. After that, measured voltage profile data during the fault time is compared with ADMS based online power flow data in the reduced search space to identify the faulty section(s). Finally, the robustness of the method is demonstrated using monte-carlo simulation at different times of the day with variable DER penetration, loading, and fault resistance. The proposed method is also able to identify multiple fault locations happening simultaneously at different laterals of the feeder. Advantages of this method are compared with the previous efforts as following:

- i. In the literature, several fault location techniques are discussed on Impedance based methods[22],[23],[89],and[90]. However, some distinct characteristics: only availability of voltage and current measurements at the substation, multiphase laterals, variation of loads, heterogeneous line conductors (Overhead and Underground), variability in fault resistance, and bidirectional power flow because of multiple DERs integration with stochastic penetration level make the task challenging in distribution system [22]. Due to the issues mentioned above, fault locating methods in distribution system can locate different sections with identical distance using conventional impedance based method. The proposed method uses graph theory based approach that does not lead to similar situations.
- ii. Typically, distribution service operators (DSOs) rely on the customer calls to get the area of the outage. However, that does not identify the exact fault location because the protection devices (Recloser, fuse etc.) or intelligent electronic devices (IEDs) disconnect an area where many unfaultry sections are also included [22],[91]. Although some literature discussed fault location scheme by

placing IEDs at every section of the feeder[24], it is not realistic in terms of cost-benefit analysis. Moreover, IEDs are designed to detect a pre-specified fault-current which can impede fault location method if the fault impedance is high. Therefore, this study assumes the placement of low-cost sensors in significant locations and the sensors act as passive devices and provide data to utilize in the algorithm running ADMS control center. The assumption of placing sensors are described in section 4.1.

- iii. Fault location techniques based on traveling wave methods are proposed in several literatures [92],[93]. These methods are efficient in transmission system, as described, due to the structure unlike the distribution system. Travelling wave method needs to estimate the time-of-arrival of propagating waves from fault occurring point to the measurement clock. Distribution system has laterals, sub-laterals, and high number of buses/nodes than transmission system. Thus, it is not possible to place clock in every bus to measure the reflection time to find the exact location. Therefore, low-cost synchronized measurement devices are most suitable for distribution system. In addition, due to the small length of distribution system sections compared to the transmission system and high velocity of the travelling wave, large error can occur which might mislead the fault location scheme.
- iv. In [94], an impedance based method is developed with the presence of DERs and load variation. They used a fault current injection method to calculate the source voltage and ranked them based on the measured and calculated source voltage. This method is iterative by injecting fault current at every bus. Another iterative method is shown in [95] using the voltage matching. However, these iterative methods increase the computation time for feeders with large number of buses. Moreover, calculation of impedance matrix for multiple

faults happening simultaneously will be complex and iterative procedure will be even more complex. In addition, the authors showed results for up to 50Ω of fault resistance. In reality, even higher impedance fault might occur than the demonstrated resistance.

- v. Knowledge based approach such as, artificial neural network (ANN) and learning algorithm based fault location methods are proposed in [96],[97]. However, these methods need a bulk amount training data considering all the possible uncertainties which might not be possible to address always.

The rest of the study is presented as below: section 4.1 describes the details of proposed method, Section 4.2 discusses the Ratio test and use of MDFs for reducing search space, Section 4.3 presents the methodology of voltage profile comparison to identify the faulty section(s), and Section 4.4 analyses the simulation results using a real utility scale distribution feeder. Section 4.5 concludes the study with major findings and further improvement of the method.

4.2 Proposed Fault Location Method

This section presents the proposed fault location method with a few assumptions. The following assumptions are made in case of a fault:

- i. Fault is already detected and classified,
- ii. GPS time stamping is available for all the agents (smart meters and/or sensors),
- iii. Sensors are located at the feeder buses where laterals/sub laterals are coming out,
- iv. Smart meters are deployed at all loading points and sources,
- v. Variability in DER penetration,

- vi. Data retrieval process assume no bad or missing data since this is out of scope for this study. However, there are several algorithms in the literature about imputing the bad or missing data which can be integrated in this FL method [98]-[100].

The entire algorithm is comprised of several steps. The first step is to generate an alarm when a fault occurs for collecting data from sensors and smart meters. Since real-time continuous data collection and transmission needs a lot of bandwidth, this study assumes a event driven method such as [23]- when a fault occurs all the agents are pinged to pull the data and send it to the ADMS control center. After that, MDFS is utilized based on a novel method called ratio test (RT) to reduce the search space and find the faulty zone(s). Details of RT approach and MDFS is discussed in the next section. After reducing the search space, voltage profile data is analyzed in the identified zone(s) to find the faulty section(s). Elaborately, measured voltage profile data is compared with simulated voltage profile of the buses within the identified zone(s). Simulated data is created from the ADMS based online power flow. The entire voltage profile analysis procedure is described in section 4.3. Algorithm 4.1 lists all the steps, sequentially.

4.3 Search Space Reduction

Distribution system modeling is much complicated than transmission system consisting of a high number of buses, laterals, and sub-laterals. To represent the modeling precisely, a system diagram is presented in Fig. 4.2(a), which demonstrates the case of the power flow from one bus to its adjacent bus(es). For a pre-fault condition, power flowing from bus i to all adjacent bus(es) can be represented for per phase analysis as[62]:

$$P_{i,t}^{pf} = \sum_j P_{j,t}^{pf} + \sum_x P_{x,t}^{L,pf} - \sum_y P_{y,t}^{PV,pf} + \sum_k P_{k,t}^{loss,pf} \quad (4.1)$$

Algorithm 4.1: Proposed Fault Location Steps

- 1 In an event of a fault, data is collected from all the agents using an external trigger,
 - 2 Send data to the primary agent (ADMS),
 - 3 Calculate RT (Algorithm 4.2,4.3),
 - 1: **for** 1 : *Number of Sensors* **do**
 - 2: Perform the ratio test (RT)
 - 3: **end for**
 - 4 Utilize modified depth first search (MDFS) to reduce the search space(Algorithm 4.4),
 - 5 Compare the measured and online power flow based voltage profile in the reduced search space to find the error index e_θ (Algorithm 4.5),
 - 6 Identify the root bus(es) of the faulty section(s) based on error index,
 - 7 Create a upstream and downstream bus immediate to root bus(es),
 - 8 Create combinations of all the newly created buses and run an online power flow for every scenario of the combinations,
 - 9 Utilize algorithm 4.5 again among the combinations to find the faulty section.
-

where $i, j \in \mathbb{Z}$ represent the current sensor bus and adjacent/connected sensor bus(es) to i , respectively. $x \in \{\text{load(s) downstream to bus } i\} \setminus \{\text{load(s) downstream to bus } j\}$, $y \in \{\text{DER(s) downstream to bus } i\} \setminus \{\text{DER(s) downstream to bus } j\}$, $k \in \{\text{Section(s) downstream to bus } i\} \setminus \{\text{Section(s) downstream to bus } j\}$ represent the intermediate loads, DERs, and line sections between i and j .

When there is a fault in the same system, demonstrated in Fig.4.2(b), Eq (4.1) can be modified as:

$$P_{i,t}^f = \sum_j P_{j,t}^f + \sum_x P_{x,t}^{L,f} - \sum_y P_{y,t}^{PV,f} + \sum_k P_{k,t}^{TL,f} \quad (4.2)$$

where

$$\sum_k P_{k,t}^{TL,f} = \begin{cases} \sum_k P_{k,t}^{loss,f} + \sum_k P_{k,t}^f, & \text{for faulty sections} \\ \sum_k P_{k,t}^{loss,f}, & \text{for unfaulty sections} \end{cases} \quad (4.3)$$

Eq (4.1) portrays the line loss, $P_{k,t}^{loss,pf}$ during regular operation. On the other hand, (4.2) presents the total loss (TL) during the time of fault which is comprised of line loss, $P_{k,t}^{loss,f}$ and loss dissipated by the fault resistance, $P_{k,t}^f$. Considering the

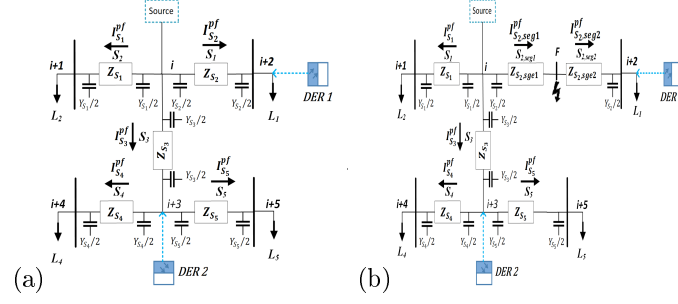


Figure 4.2: One-line distribution system schematic (a). W/o fault; (b). W fault.

assumption in the previous section, sensors are placed in bus i and $i + 3$ in Fig.2, since these buses have laterals coming out. Smart meters are also available in load L_1 to L_5 . Therefore, employing (4.1) is straightforward to retrieve the line loss in case of regular operation. Contrarily, employing (4.2) will provide a combined loss for all the section(s) bounded by two sensors. However, since the fault location(s) are unknown, it is not possible to distinguish the loss. Therefore, the regular operational losses during the time of fault is applied to find the zone(s) of the fault(s). This leads to the formulation of RT. Regular line loss for any individual section(s) are retrieved using online power flow analysis by putting the real-time estimated load shape and DER generation data[1],[101]. Moreover, bi-directional power flow complexity is considered when estimating RT.

4.3.1 Ratio Test

In this study, RT is defined as the ratio of power delivered between two sensor buses or down to a sensor bus, if any downstream sensor bus does not exist, to the actual power delivered to all the intermediate loads, presented as:

$$RT_{node,ph} = \frac{Total\ Power_{i \leftrightarrow j} - Total\ Loss_{i \leftrightarrow j}}{Total\ Load_{i \leftrightarrow j}} \quad (4.4)$$

To demonstrate (4.4), scenarios are represented as case by case basis. In case of a regular operation, such as Fig.4.2 (a), when RT is estimated for bus i and $i + 3$, both buses will end up having $RT = 1$. On the other hand, in case of a fault in the fictitious bus F , depicted in Fig.4.2(b), buses i , $i + 2$, and $i + 3$ will carry the

fault current. Since bi-directional power flow is considered in the presence of DERs, the generation from the main source will increase and generation from other weak sources (DERs) will decrease due to a significant voltage drop when compared to the regular operation at the point of common coupling (PCC). Consequently, losses from the main source to the fault will increase, and all other sections will have smaller losses compared to regular operation. Therefore, attributing the regular loss during the time of fault will demonstrate $RT > 1$ for all the locations of sensor buses from the main source to the fault and $RT \leq 1$ for all other locations of sensor buses. Thus, buses i and $i + 3$ will demonstrate $RT > 1$ and $RT \leq 1$, respectively. While developing algorithms 4.2 and 4.3, below, for the utility feeders, both uni-directional and bi-directional power flow are considered for estimating RT since depending on the location of DERs and their penetration, any sensor can observe power flow in either direction. Algorithm 4.2 describes the procedure of RT when the measurement at the current sensor bus is positive or power is being delivered. Direction of the power flow is calculated from the power factors collected from the sensors following the IEEE standard definitions of measurement [101]. This algorithm first observes the direction of flow at the sensor bus that is attempting to calculate RT and then looks for any existing downstream or intermediate loads. If there are existing loads, then it will look for any existing successor sensor bus(es) to see whether the direction of power flow is positive or negative at those sensor(s).

If the power flow is negative, it implies that both the present and successor sensor bus(es) are feeding the intermediate loads between them, represented in (4.5). If the power flow is positive, two different cases can happen: either the accumulated power of the successor sensor bus(es) is greater or it is less than at the present sensor bus. These cases resemble the different levels of penetration from intermediate DERs, which are presented in (4.6) and (4.7). There are other instances where a sensor is placed at a bus with multiple laterals coming out, and there is no successor sensor

Algorithm 4.2: RT for bi-directional power flow (+ve)

```

1 switch  $P_{i,ph}^f$ 
2 case +ve
3 if exist  $P_{x,ph}^{load}$  then
4   if exist  $P_{j,ph}^f$  then
5     if  $\sum_j P_{j,ph}^f < 0$  then
6       
$$RT_{i,ph}^f = \frac{P_{i,ph}^f + \text{abs}(\sum_j P_{j,ph}^f) + \text{abs}(\sum_y P_{y,ph}^{PV}) - \sum_k P_{k,ph}^{loss}}{\sum_x P_{x,ph}^{load}} \quad (4.5)$$

7     else if  $\sum_j P_{j,ph}^f > 0 \ \&\& \ \sum_j P_{j,ph}^f < P_{i,ph}^f$  then
8       
$$RT_{i,ph}^f = \frac{P_{i,ph}^f - \sum_j P_{j,ph}^f + \text{abs}(\sum_y P_{y,ph}^{PV}) - \sum_k P_{k,ph}^{loss}}{\sum_x P_{x,ph}^{load}} \quad (4.6)$$

9     else
10      
$$RT_{i,ph}^f = \frac{\sum_j P_{j,ph}^f - P_{i,ph}^f - \text{abs}(\sum_y P_{y,ph}^{PV}) - \sum_k P_{k,ph}^{loss}}{\sum_x P_{x,ph}^{load}} \quad (4.7)$$

11   else
12     
$$RT_{i,ph}^f = \frac{P_{i,ph}^f + \text{abs}(\sum_y P_{y,ph}^{PV}) - \sum_k P_{k,ph}^{loss}}{\sum_x P_{x,ph}^{load}} \quad (4.8)$$

13 else
14   
$$RT_{i,ph}^f = \frac{P_{i,ph}^f + \text{abs}(\sum_y P_{y,ph}^{PV}) - \sum_k P_{k,ph}^{loss}}{\sum_j P_{j,ph}^f} \quad (4.9)$$


```

bus, represented in (4.8). Lastly, there are some subsequent sensor buses where no intermediate loads or DERs exist, which is introduced in (4.9). Similarly, algorithm 4.3 portrays the scenarios by employing (4.10)-(4.15) when the direction of power flow is negative at the present sensor bus.

Algorithm 4.3: RT for bi-directional power flow(-ve)

```

1 case -ve
2 if exist  $P_{x,ph}^{load}$  then
3   if exist  $P_{j,ph}^f$  then
4     if  $\sum_j P_{j,ph}^f < 0 \ \&\& \ abs(\sum_j P_{j,ph}^f) < abs(P_{i,ph}^f)$  then
5       
$$RT_{i,ph}^f = \frac{abs(P_{i,ph}^f) - abs(\sum_j P_{j,ph}^f) - abs(\sum_y P_{y,ph}^{PV}) - \sum_k P_{k,ph}^{loss}}{\sum_x P_{x,ph}^{load}} \quad (4.10)$$

6     else if  $\sum_j P_{j,ph}^f < 0 \ \&\& \ abs(\sum_j P_{j,ph}^f) > abs(P_{i,ph}^f)$  then
7       
$$RT_{i,ph}^f = \frac{abs(\sum_j P_{j,ph}^f) - abs(P_{i,ph}^f) + abs(\sum_y P_{y,ph}^{PV}) - \sum_k P_{k,ph}^{loss}}{\sum_x P_{x,ph}^{load}} \quad (4.11)$$

8     else
9       
$$RT_{i,ph}^f = \frac{abs(\sum_y P_{y,ph}^{PV}) - \sum_j P_{j,ph}^f - abs(P_{i,ph}^f) - \sum_k P_{k,ph}^{loss}}{\sum_x P_{x,ph}^{load}} \quad (4.12)$$

10    else
11      
$$RT_{i,ph}^f = \frac{abs(\sum_y P_{y,ph}^{PV}) - abs(P_{i,ph}^f) - \sum_k P_{k,ph}^{loss}}{\sum_x P_{x,ph}^{load}} \quad (4.13)$$

12  else
13    if  $\sum_j P_{j,ph}^f > 0$  then
14      
$$RT_{i,ph}^f = \frac{abs(\sum_y P_{y,ph}^{PV}) - abs(P_{i,ph}^f) - \sum_k P_{k,ph}^{loss}}{\sum_j P_{j,ph}^f} \quad (4.14)$$

15    else
16      
$$RT_{i,ph}^f = \frac{abs(P_{i,ph}^f) - abs(\sum_y P_{y,ph}^{PV}) - \sum_k P_{k,ph}^{loss}}{\sum_j P_{j,ph}^f} \quad (4.15)$$


```

For the next step, RT for all the impacted phases in any sensor bus i can be

accumulated as:

$$RT_i = \frac{\sum_{ph} RT_{i,ph}}{\text{Number of impacted phase}(s)} \quad (4.16)$$

Where ph denotes the impacted phase(s) of the associated sensor bus. This also simplifies the calculation since some sensor buses might not have all the available impacted phases.

4.3.2 Modified depth first search(MDFS)

A distribution system can be characterized by a graph $G = (V, E)$ which consists of vertices and edges. Each vertex V corresponds to the buses i , where $V \in \mathbb{Z}$ and each edge represents E , where $E \in \{i, j\} \subset V \times V$. For this part, we will consider the buses with sensor placement and the edges/sections between sensor buses to identify the search space after calculating RT. A modified version of Depth first search (DFS), a graph traverse algorithm is used to traverse the feeder to find the connected bus(es) with $RT > 1$. DFS is a widely used edge-based algorithm to find the connectivity in a graph with maximum memory efficiency[103]. Fig. 4.3 represents the methodology of modified depth first search (MDFS) for retrieving reduced search space for two faults happening simultaneously with a simple grid architecture using seven sensor buses.

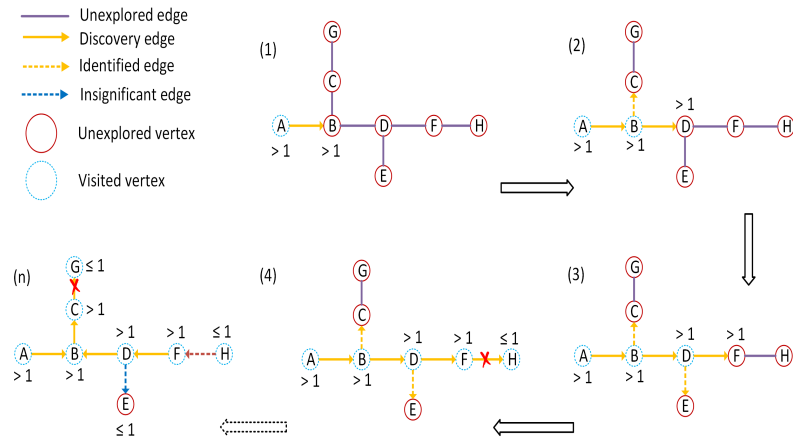


Figure 4.3: Modified DFS (MDFS) algorithm for fault location.

The figure shows that the search process starts with bus A , which is supposed to be the closest sensor bus to the substation, since a majority of the fault current is contributed from the primary or main source. Then, the neighboring bus B is visited

when bus A demonstrates $RT > 1$. Similarly, surpassing bus B , two buses are found to be connected to it. In the algorithm, one path is selected and the other is stored in a stack. Therefore, it randomly chooses the path towards D and stores C in the stack. Similarly, it moves towards F and stores E in the stack, sequentially. Consequently, it travels towards the end of this route and finds H where $RT \leq 1$. Thus, one fault is dissipated somewhere between F and H . Since two faults are detected, another fault lies in any one of the paths towards the stored buses in the stack. According to the organization of stack and methodology of DFS, the search process follows the path towards C . Similar to the previous effort, the fault is located somewhere between C and G . However, there is one more bus, E , stored in the stack. Since both of the detected faults are already located, the unexplored vertex need not to be visited. Thus, the unexplored edge from D to E is denoted as insignificant. In this study, this is the modification to the original DFS search process and it reduces the computation time to traverse the entire feeder if the faults are already located. Algorithm 4.4 presents the entire methodology described above.

4.4 Voltage Profile Analysis

A voltage sag based fault location analysis is conducted in some studies[23],[103]. However, identical sag profiles at multiple locations in the presence of DERs might jeopardize the fault location algorithm [104]. Moreover, voltage sag data collected from the measurement devices may be misleading due to the variation of load in pre-and-post fault time frames. Therefore, this study only deals with during fault measured data and uses the on-line power flow (OLPF) based data from ADMS. The concept of OLPF is presented in [1]. The OLPF is run by utilizing the real-time load. Since real-time load estimation is out of the scope for this dissertation, we use the same data that is used during fault by mimicking with uniform distribution of zero-mean noise and $\pm 1\%$ variation for the purpose of simulation in the OLPF[104]. After identifying the zone(s) using the method described in the previous section,

Algorithm 4.4: MDFS for reduced search space

```

1 Establish  $G=(V,E)$ ,
2 Initialize the closest sensor node to substation as Current sensor node ( $cnode$ ),
3 Find the successor sensor nodes ( $dsnodes$ ) to  $cnode$ ,
4 Enter the no of faults and type of faults, Enter the Ratio Test data( $RTdata$ )
   for all the sensors based on type of faults,
5 Initialize the  $RT_{cnode}$  from  $RTdata$ ,
   while  $any(RT_{cnode}(:)) > 1$  do
     call MDFS;
   end while
 $\widehat{endnode}=cnode$ ;
if  $isempty(stack) == 0$  then
  while  $isempty(stack) == 0$  do
     $\widehat{cnode}=stack(1)$ ;  $\widehat{dsnodes}=\text{successor}(dsnodes)$ 
    while  $any(RT_{cnode}(:)) > 1$  do
      call MDFS;
    end while
     $stack(1)=[]$ ;  $\widehat{endnode}=[\widehat{endnode};\widehat{cnode}]$ ;
  end while
Function  $MDFS(G, dsnodes, RT_{cnode}, RTdata)$ :
  if  $1 < (\text{identified edge} + \text{discovery edge}) \leq \text{no of faults}$  then
    | update  $cnode$  based on the priority and create  $stack$  for rest of the
    | node(s);
  else
    | update  $cnode$  based on discovery edge;
    update  $dsnodes$  based on the  $cnode$ ;
    update  $RT_{cnode}$  for  $cnode$ ;
  return  $\widehat{cnode}, \widehat{stack}, \widehat{dsnodes}, \widehat{RT}_{cnode}$ ;

```

data from the OLPF and measurements within the defined zone(s) are analyzed. In case of multiple faults, since one fault may impact other fault(s) in terms of current contribution depending on the fault resistance, the maximum possible combinations of buses are created among the zone(s). For example, if three zone(s) are identified based on the MDFS and they have 6,7, and 8 buses, $6_{C_1} \times 7_{C_1} \times 8_{C_1}$ simulation scenarios are created for running in the OLPF. Thus, each scenario will have three buses with one bus from each zone. Next, comparison between each OLPF scenario and measured data is done by calculating the error e_θ using the 2-norm of each phase of each bus as presented below:

$$e_{\theta,k} = \sum_k \frac{\|V_{k,m}^{ph,f} - V_{k,s}^{ph,f}\|_2}{\text{Available phase}(s) \text{ in bus } k}, \quad \forall k \in \theta \quad (4.17)$$

where $\theta \in \{1, 2, \dots, P\}$ represents the number of scenarios; k refers to the buses of each θ scenario; m and s denote the measured and simulated data, respectively. The scenario with minimum error will be the set of root buses. For a single fault, the root bus near the fault location will reflect the minimum error. Similarly, for multiple simultaneous faults, the scenario with the minimum error is the set of root buses that are nearest to the faults in the identified individual zones. While calculating the error, voltage difference in the unfaulted phases are also considered for higher precision. To create the simulation scenarios in OLPF, fault resistance, R_f needs to be estimated. Therefore, the approximate fault current, I_F^f is calculated as:

$$I_F^f \approx I_{i,t}^f - \sum_j I_{j,t}^f - \sum_x I_{x,t}^{L,f} + \sum_y I_{y,t}^{pv,f} \quad (4.18)$$

where F is the fictitious faulty bus, such as in Fig. 4.2(b); i and j define only the immediate upstream and downstream sensor bus(es), respectively. Eq (4.18) defines the unidirectional power flow. However, depending on the direction of the current flow, a procedure similar to algorithm 4.2 and 4.3 can be utilized to find the intermediate flow of current through the fault. After retrieving the fault current, fault resistance can be estimated for any L-G or LLL-G type faults using the voltage measurement where the fault is created as:

$$R_f \approx \frac{V_k^{ph,f}}{I_F^f} \quad (4.19)$$

For L-L faults (4.19) can be modified as [105]:

$$R_f \approx \frac{V_{k,m}^{ph1,f} - V_{k,m}^{ph2,f}}{I_F^f} \quad (4.20)$$

Estimation of fault resistance will be most accurate when using the voltage measurement of the bus(es) closest to the fault(s). Therefore, this methodology improves the accuracy while calculating the error. The entire procedure is listed in algorithm 4.5 assuming three faults occurring simultaneously. However, depending on the number of identified faulty zones, the algorithm can be extended to a higher number of scenarios.

Algorithm 4.5: Error calculation for θ scenarios

- 1: **for** $x_1=1$:no of buses in identified zone 1(z_1) **do**
 - 2: estimate \hat{R}_f for bus, $z_1(x_1)$;
 create fault at bus, $z_1(x_1)$;
 - 3: **for** $x_2=1$:no of buses in identified zone 2(z_2) **do**
 - 4: estimate \hat{R}_f for bus, $z_2(x_2)$;
 create fault at bus, $z_2(x_2)$;
 - 5: **for** $x_3=1$:no of buses in identified zone 3(z_3) **do**
 - 6: estimate \hat{R}_f for bus, $z_3(x_3)$;
 create fault at bus, $z_3(x_3)$;
 list the combination of buses in scenario θ ;
 Perform power flow for scenario θ ;
 Record the Voltage, $V_{i,s}^{ph}$ for all the buses in the identified zone(s);
 Calculate e_θ ;
 - 7: **end for**
 - 8: **end for**
 - 9: **end for**
-

After detecting the root buses close to the fault(s) using Algorithm 4.5, the associated faulty section(s) need to be identified. However, faulty section(s) can be the immediately upstream or downstream sections to the root bus(es). Therefore, two new fictitious buses are created in close proximity on both sides of the identified root buses. Consequently, Algorithm 5 can be deployed again among the fictitious buses to create 2^z scenarios where z denotes the number of identified faulted zones. Similar to the aforementioned procedure e_θ is again calculated for the newly created scenarios. Since the new buses are created within the suspected sections, the minimum error will be found with the combination of buses which are closest to the fault and within the faulty section(s).

4.5 Simulation Results

In this section, a real 12.47 kV distribution feeder, provided by Duke Energy Progress, is utilized to estimate the fault location using the proposed method. The one-line diagram of the test feeder is portrayed in Fig.4.4. Wireless sensors and smart meters are placed according to assumptions, mentioned in section 4.1. Five PV based DERs are placed throughout feeder with size of 500, 1800, 500, 1000, and 1200 KVA for DER 1 to DER 5, respectively. During the maximum penetration time, 50% of the loads are supported by DERs. Loads throughout the feeder are modeled as ZIP load so that accurate voltage sensitivity can be retrieved. As demonstrated in the test feeder, four fault locations are determined to create the cases for single and simultaneous fault cases with a combination of different fault types. Simulation is conducted using OpenDSS since it provides the flexibility to use component object model (COM) interface to be integrated with other platforms like MATLAB, VBA, Python, C# etc. At the first place, RT results are acquired when the fault(s) are occurred. Five different cases are discussed during maximum penetration of DER for RT analysis which are demonstrated in Table 3.1. Five cases are designed in such a way that all the type of faults can be demonstrated for single and simultaneously occurring faults. Case 1, 2, and 3 present the cases for three single LG, LL, and LLL faults, respectively. Case 4 and 5 demonstrate the simultaneously occurring fault cases with different fault type combinations.

After retrieving the faulty zone(s), as described in section 4.3, voltage profile comparison is conducted to find the error e_θ for θ scenarios and each individual bus k within the scenario. To illustrate this, case 5 is discussed explicitly in Fig.4.5. where AC, CG, and ABC faults happen at three identified zones: zone 1, 2, and 3, respectively.

The three identified zones have 6,6, and 5 buses which can create maximum 180 scenarios for this case if all the buses have available impacted phases. For instance,

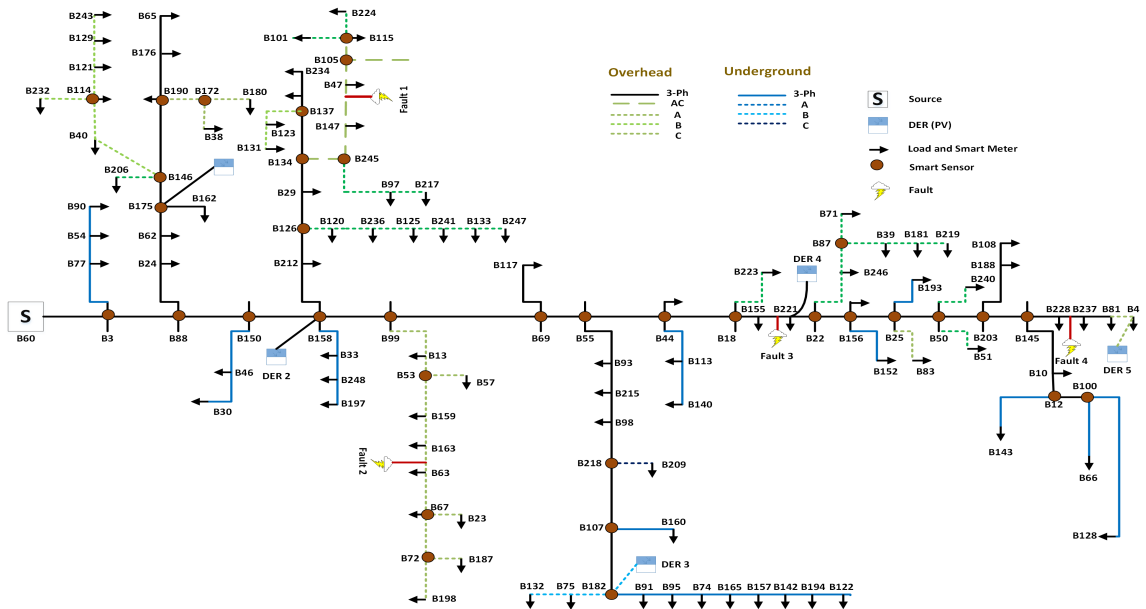


Figure 4.4: Modified distribution feeder for fault analysis.

AC faults are happening at zone 1 and B97 and B217 do not contain phase A. Therefore, only 120 scenarios are possible to create in OLPF. These 120 scenarios will be compared with the measured voltage profile from the sensors and smart meters. After identifying the lowest error from each zone and from the combined sets, root nodes are identified. Fig.4.6 (a), (b), and (c) present the error using (4.16) for each bus in the identified zones. B47, B63, and B221 displays the minimum error. Fig.4.6 (d) visualizes the combined error for the combination of three buses from three zone which also portrays the minimum error for the set of B47, B63, and B221. After that, to determine the faulty sections two fictitious buses are created at upstream and downstream to each root bus with very fractional distance. These are denoted as “u?” and “d?” with the original bus name for upstream and downstream buses, respectively. A combination of fictitious buses created again with a number of scenarios. For case 5, 8 scenarios will be generated since there are 3 faulty zones. All the new scenarios are run into OLPF with the credentials of root buses and the minimum error will be displayed by the buses close to the faults. Since all these are fictitious buses within the assumed faulty sections, the actual faulty sections are identified by the minimum

Table 4.1: RT at the sensor buses.

Sensor Buses	Case 1	Case 2	Case 3	Case 4		Case 5		
	AG \rightarrow 1 Ω	AC \rightarrow 5 Ω	ABC \rightarrow 20 Ω	CG \rightarrow 10 Ω	AB \rightarrow 8 Ω	AC \rightarrow 5 Ω	CG \rightarrow 100 Ω	ABC \rightarrow 15 Ω
B3	7.21	1.86	1.1	1.29	2.45	4.41	3.81	3.33
B88	204.34	25.07	3.42	8.82	42.96	101.79	76.28	69.43
B175	1	1	1	1	1	1	1	1
B146	1	1	1	1	1	1	1	1
B114	N/A	N/A	1	0	1	N/A	N/A	1
B190	1	1	1	1	1	1	1	1
B172	N/A	1	1	1	N/A	1	1	1
B150	13.22	2.38	1.13	1.44	3.45	6.92	5.3	5.02
B158	31.99	4.15	1.18	1.33	2.19	15.4	9.58	10.67
B126	14.61	2.26	1	1	1	67.09	124.54	45.06
B134	2.04	2.01	1	1	1	2.03	2.02	2.02
B245	690.63	135.04	1	1	1	1207.06	2055.56	1207.06
B137	1	1	1	1	1	1	1	1
B105	1	1	1	1	1	1	1	1
B115	1	1	1	1	1	1	1	1
B99	0.99	0.85	2.41	23.05	1.04	4.79	8.56	3.53
B53	N/A	1	1	220.13	N/A	22.87	22.87	22.87
B67	N/A	1	1	1	N/A	1	1	1
B72	N/A	1	1	1	N/A	1	1	1
B69	0.97	0.99	1.22	0.98	4.17	1.43	1.28	1.39
B55	0.73	0.95	2.35	0.99	25.27	3.71	2.3	3.63
B218	1	0.99	1	1	1	0.98	0.97	0.99
B107	0.99	1	1	1	1	0.99	1	0.99
B182	0.98	1	1	1	0.99	0.99	1	0.99
B44	1	1	1.03	1	1.43	1.06	1.03	1.05
B18	1	1	1016.04	1	25.72	1147.09	1810.05	1366.77
B22	0.99	1	1	1	3.13	1	1	1
B87	1	1	1	0	1	1	N/A	1
B156	0.99	1	1	0.99	3.66	1	1	1
B25	0.98	1	1	0.99	4.98	0.99	1	0.99
B50	0.99	1	1	0.99	3.46	0.99	0.99	0.99
B203	0.98	1	1	0.99	5.83	0.99	1	0.99
B145	0.99	1	1	1	1374.67	0.99	1	0.99
B12	1	1	1	1	1	1	1	1
B100	0.99	1	1	1	1	1	1	1

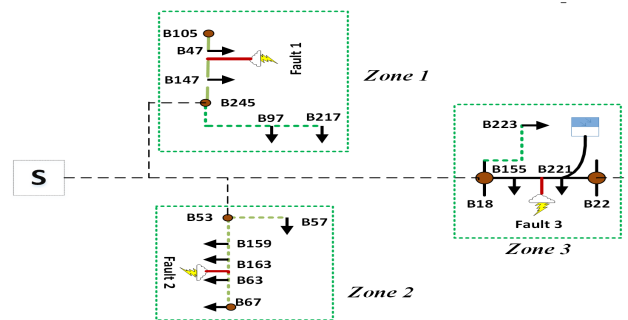


Figure 4.5: Identified faulty zones for voltage profile comparison.

error. The error for each fictitious bus of each zone is presented in Fig.4.6(e),(f),and (g). Fig.4.6(h) portrays the error of combined sets. The sets of fictitious root buses

are mentioned in Table 4.2. All the results demonstrate that B47u, B63u, and B221u are the minimum error buses. Therefore, it is clearly manifested that the identified faulty sections are B147-B47, B163-B63, and B155-B221.

The robustness of the algorithm is tested utilizing the monte-carlo (MC) method by running a quasi-static time series (QSTS) simulation for 24 hours in 15 minutes interval with random fault impedance for different zones in case 5. The errors for each set mentioned in Table 4.2 is then averaged for all the time steps, depicted in Fig.4.8, which also demonstrates the correct identification of faulty sections.

Table 4.2: Set of fictitious root buses.

Sets	Combination of buses			Sets	Combination of buses		
1	B221u	B47u	B63u	5	B221u	B47u	B63d
2	B221d	B47u	B63u	6	B221d	B47u	B63d
3	B221u	B47u	B63d	7	B221u	B47d	B63d
4	B221d	B47u	B63d	8	B221d	B47d	B63d

4.6 Summary

This chapter discussed a fault location method using wireless sensors and AMI data in two steps. The method is able to identify faults at multiple laterals happening simultaneously. Unlike the previous studies in the literature, this method first reduces the search space using a ratio test and a modified depth first search, and then analyzes the voltage profile within the reduced space. The entire methodology reduces the computational burden for feeders with a large number of buses and offers flexibility in identifying multiple faults. Moreover, the method assumes the usage of low-cost sensors which might be very cost-effective for utilities. The method is tested with variation of load and DER penetration in a QSTS simulation with Monte Carlo method to demonstrate the robustness of the overall approach. However, the method has a limitation in identification of multiple fault locations on the same lateral and phase. In this case, the proposed approach only identifies the distant fault in the lateral. Therefore, the future work of this research is to identify the faults that occur

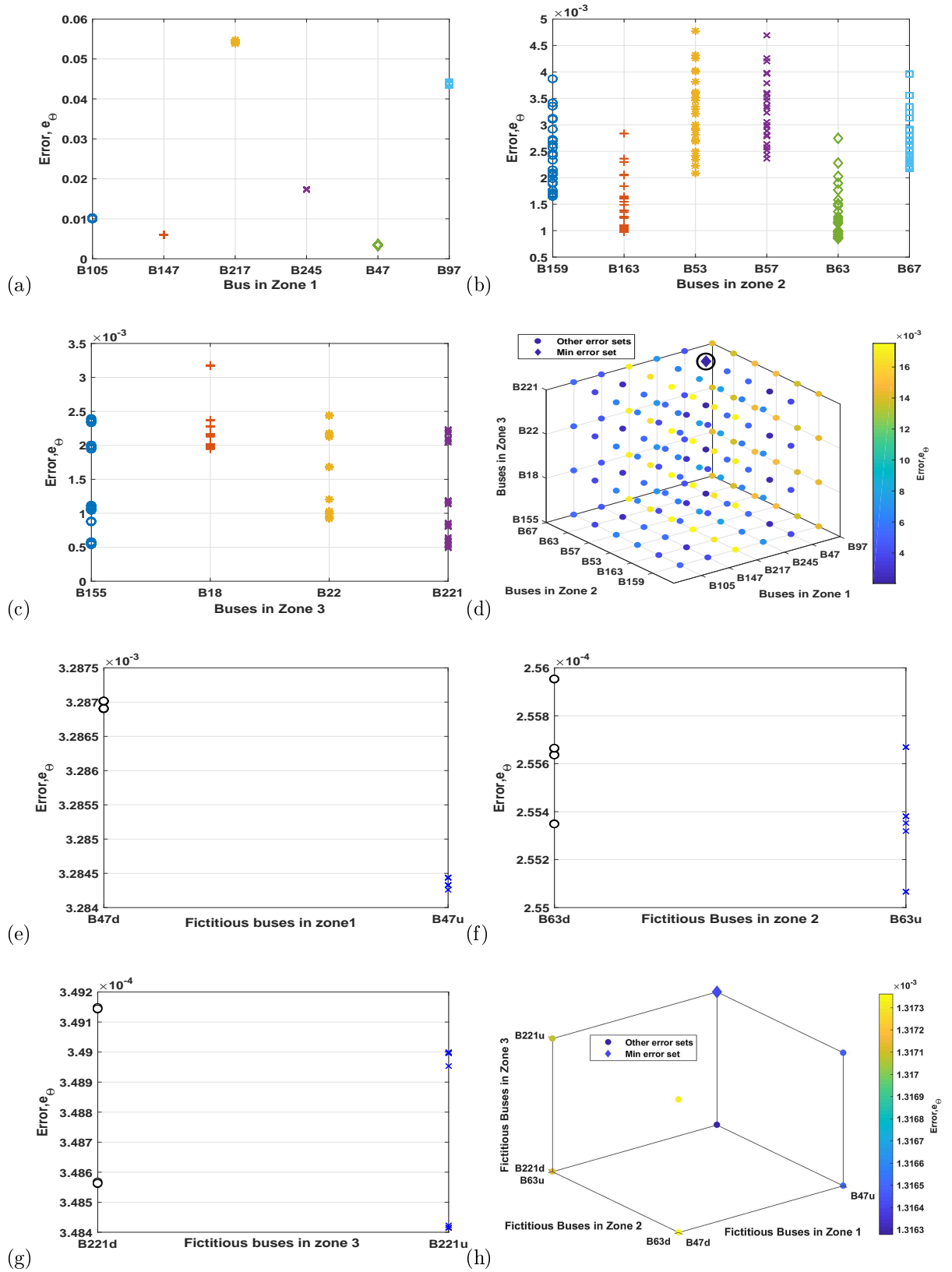


Figure 4.6: Error for buses in (a). Zone 1; (b). Zone 2; (c). Zone 3 (d).combination of buses in different zones; Error for fictitious root buses in (e). Zone 1; (f). Zone 2; (g). Zone 3. (h) combination of fictitious root buses in different zones.

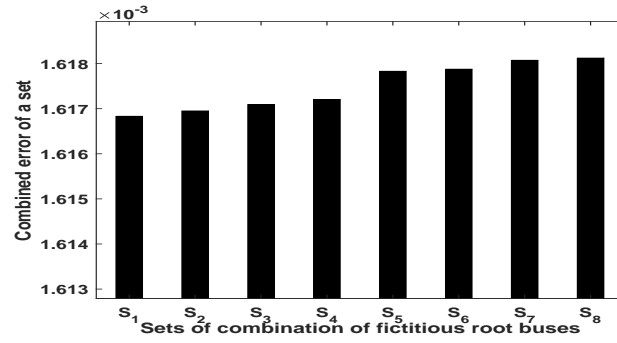


Figure 4.7: Combined error of sets of fictitious buses using MC simulation.

simultaneously in the same lateral. Apart from this extension, another future task would be to re-formulate the algorithm to work with a reduced set of sensors.

CHAPTER 5: Conclusion

This dissertation presented the challenges in the ADMS platform while integrating DMS and OMS with DERMS. At the same time, some techniques have been proposed to address these challenges. These techniques have been tested and validated in utility scale distribution feeders to render the proof of concept.

In chapter 2, the dissertation discussed the implementation and assessment of CVR deployment. Since CVR deployment depends on voltage sensitivity of loads, two different loads models: exponential and ZIP models were studied extensively for voltage reduction study. A dual-stage filtering approach was developed for identifying the load coefficients of each model. After that, the CVR factor was calculated using the identified parameters of both load models which were then compared. The comparison depicts that ZIP model is more inclined with the actual measurement of the composite load consumption. As described, the entire comparison study was conducted based on the composite load consumption. However, for the future direction of this dissertation, a synthetic verification can be conducted between the data from all the smart meters throughout a distribution feeder and data of the composite load consumption from the substation meter using the similar procedure to identify the actual error in CVR factor calculation.

More often the utility wants to deploy short term CVR. This dissertation discussed a time-varying stochastic assessment process of CVR deployment to rank the benefits in an descending order at different times so that utility can decide the timing of CVR deployment. The analysis was conducted in a distribution feeder where DERs are integrated. Stochasticity in load consumption and DER injection was considered. In addition, increasing penetration rate of DER can play a significant role in CVR

deployment. Specially, smart inverter interfaced DERs can provide more flexibility to control the voltage. Therefore, CVR planning with smart interfaced PV is also discussed in chapter 2 using an MINLP based program.

With the increasing rate of penetration, geo-spatial stochasticity in the generation of renewable energy based DERs can also impede the control of CVR deployment. Therefore, periodical or abrupt update of control parameters for both inverter(s), and other voltage regulating devices might be needed for maintaining the lower ANSI band to uphold the power quality. For further elaborating this research, a droop based inverter mechanism for centralized control is presented in Fig.5.1 for implementing and assessing CVR together. While controlling the devices, a distribution feeder can be segmented into different zones and only the zones with voltage violation are identified for taking further actions. This example only portrays droop based control for inverters using a set of droop curves. However, other control mechanisms can also be utilized.

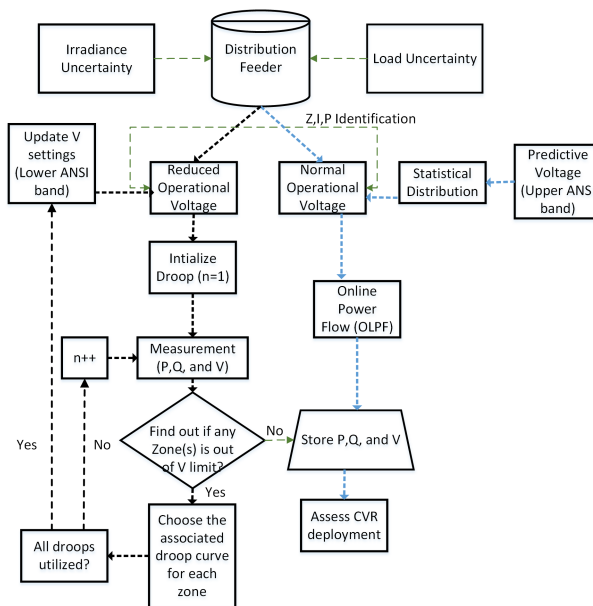


Figure 5.1: Hierarchical control and assessment of CVR deployment.

In chapter 3, a integrated CVR and DR framework was presented in a DER integrated feeder. Stochasticity in both load consumption and individual DER injection

was considered. In addition, several DR plans were considered for better participation of customers in the DR program. The study shows that the most suitable DR plan based on the individual customers usage can be offered. In addition, this integrated framework helps to flatten the voltage profile throughout the feeder by keeping the voltage within the lower ANSI band. Since, voltage reduction is conducted, load is automatically curtailed at the customer premise. Therefore, no additional curtailment is necessary from the customer end to compromise the comfortability. In this study, a scenario reduction technique was utilized and all the scenarios were combined together for less computational burden. This study can be extended for further analysis by using different controls on the DER injection. In addition, cost of investment for DER installation can be included for calculating long term profitability.

In chapter 4, a fault location scheme was developed using the measured data from smart meters and wireless sensors for the FLISR program of ADMS. The algorithm was able to locate simultaneous fault happening at different laterals of a distribution feeder. However, as discussed previously, the algorithm could detect only one fault in a lateral. Therefore, this work can be extended to locate simultaneous fault happening closely in a lateral. In addition, the algorithm assumes the placement of sensors where any lateral and sub-lateral is coming out. However, for a long feeder, there might be a high number of laterals which can lead to installment of higher number of sensors. For future research, a new algorithm can be integrated to reduce the number of sensors. Distribution system state estimation (DSSE) can be included to make the existing algorithm work with less number of sensors. This dissertation only discussed a fault location scheme for FLISR. Service restoration is not discussed in this dissertation. Service restoration depends on the neighboring feeders to feed the loads downstream to fault using the connection of tie-switches. However, depending on the loading conditions, overloading scenarios can happen that can lead to power quality issues. Therefore, intelligent algorithms are necessary that can help by initially serving the

critical loads only. Furthermore, networked microgrids can also be formed to serve the critical loads depending on the available sources.

REFERENCES

- [1] J. Wang, "ADMS for Grid Modernization -Importance of DMS for Distribution Grid Modernization," Argonne National Laboratory, Sep. 2015.
- [2] VOICES of Experience, "Insights into Advanced Distribution Management Systems," U.S. Dept. of Energy. Available:<http://energy.gov/>.
- [3] B. Milosevic and M. Begovic, "Capacitor placement for conservative voltage reduction on distribution feeders," in *IEEE Trans. on Power Del.*, vol. 19, no. 3, pp. 1360-1367, July 2004.
- [4] M. Farivar, R. Neal, C. Clarke, and S. Low, "Optimal inverter VAR control in distribution systems with high PV penetration," in *proc. of IEEE Power and Energy Society General Meeting*, San Diego, CA, 2012, pp. 1-7.
- [5] E. Dall'Anese, S. V. Dhople and G. B. Giannakis, "Photovoltaic Inverter Controllers Seeking AC Optimal Power Flow Solutions," in *IEEE Trans. on Power Systems*, vol. 31, no. 4, pp. 2809-2823, July 2016.
- [6] Z. Wang and J. Wang, "Review on Implementation and Assessment of Conservation Voltage Reduction," in *IEEE Trans. on Power Systems*, vol. 29, no. 3, pp. 1306-1315, May 2014.
- [7] B. Kennedy and R. Fletcher, "Conservation voltage reduction (CVR) at Snohomish County PUD," in *IEEE Trans. on Power Systems*, vol. 6, pp. 986-998, 1991.
- [8] J. De Steese, S. Merrick, and B. Kennedy, "Estimating methodology for a large regional application of conservation voltage reduction," in *IEEE Trans. on Power Systems*, vol. 5, pp. 862-870, 1990.
- [9] V. Warnock and T. Kirkpatrick, "Impact of voltage reduction on energy and demand: Phase II," in *IEEE Trans. on Power Systems*, vol. 1, pp. 92-95, 1986.
- [10] C. S. Chen, "The effect of voltage control to the efficiency and operation of electric distribution system," Ph.D. dissertation, Univ. Texas at Arlington, Arlington, TX, USA, 1984.
- [11] A. Bokhari et al., "Experimental Determination of the ZIP Coefficients for Modern Residential, Commercial, and Industrial Loads," in *IEEE Trans. on Power Delivery*, vol. 29, no. 3, pp. 1372-1381, June 2014.
- [12] Z. Wang and J. Wang, "Time-Varying Stochastic Assessment of Conservation Voltage Reduction Based on Load Modeling," in *IEEE Trans. on Power Systems* vol. 29, no. 5, pp. 2321-2328, Sept. 2014.

- [13] J. Zhao, Z. Wang and J. Wang, "Robust Time-Varying Load Modeling for Conservation Voltage Reduction Assessment," in *IEEE Trans. on Smart Grid*, vol. PP, no. 99, pp. 1-1.
- [14] T. Niknam, M. Zare, and J. Aghaei, "Scenario-Based Multiobjective Volt/Var Control in Distribution Networks Including Renewable Energy Sources," in *IEEE Trans. on Power Del.*, vol. 27, no. 4, pp. 2004-2019, Oct. 2012.
- [15] M. Alizadeh, X. Li, Z. Wang, A. Scaglione, and R. Melton, "Demand side management in the smart grid: Information processing for the power switch," in *IEEE Signal Process. Mag.*, vol. 29, no. 5, pp. 55-67, Sep. 2012.
- [16] Z. Wang and Y. He, "Two-stage optimal demand response with battery energy storage systems," in *IET Generation, Transmission & Distribution*, vol. 10, no. 5, pp. 1286-1293, 4 7 2016.
- [17] B. B. Alagoz, A. Kaygusuz, and A. Karabiber, "A user-mode distributed energy management architecture for smart grid applications," in *Energy*, vol. 44, no. 1, pp. 167-177, Aug. 2012.
- [18] J. S. Vardakas, N. Zorba, and C. V. Verikoukis, "A Survey on Demand Response Programs in Smart Grids: Pricing Methods and Optimization Algorithms," in *IEEE Communications Surveys & Tutorials*, vol. 17, no. 1, pp. 152-178, Firstquarter 2015.
- [19] F. Shariatzadeh, P. Mandal, and A. K. Srivastava, "Demand response for sustainable energy systems: A review, application and implementation strategy," in *Renewable and Sustainable Energy Reviews*, vol. 45, pp. 343-350, 2015.
- [20] J. Wang, A. Raza, T. Hong, A. Cisco Sullberg, F. De Leon, and Q. Huang, "Analysis of Energy Savings of CVR including Thermostatic Loads in Distribution Systems," in *IEEE Trans. on Power Del.*, vol. PP, no. 99, pp. 1-1.
- [21] Y. Gong and A. Guzmán, "Integrated Fault Location System for Power Distribution Feeders," in *IEEE Trans. on Industry Applications*, vol. 49, no. 3, pp. 1071-1078, May-June 2013.
- [22] IEEE Guide for Determining Fault Location on AC Transmission and Distribution Lines, in *IEEE Std C37.114-2014 (Revision of IEEE Std C37.114-2004)*, vol., no., pp.1-76, Jan. 30 2015.
- [23] F. C. L. Trindade, W. Freitas, and J. C. M. Vieira, "Fault Location in Distribution Systems Based on Smart Feeder Meters," in *IEEE Trans. on Power Delivery*, vol. 29, no. 1, pp. 251-260, Feb. 2014.
- [24] K. Sun, Q. Chen, and Z. Gao, "An Automatic Faulted Line Section Location Method for Electric Power Distribution Systems Based on Multisource Information," in *IEEE Trans. on Power Delivery*, vol. 31, no. 4, pp. 1542-1551, Aug. 2016.

- [25] R. Moghe, A. R. Iyer, F. C. Lambert, and D. M. Divan, "A Low-Cost Wireless Voltage Sensor for Monitoring MV/HV Utility Assets," in *IEEE Trans. on Smart Grid*, vol. 5, no. 4, pp. 2002-2009, July 2014.
- [26] R. Moghe, Y. Yang, F. Lambert, and D. Divan, "Design of a low cost self powered Stick-on current and temperature wireless sensor for utility assets", in *Proc. IEEE Energy Convers. Congr. Expo.*, pp. 4453-4460, 2010
- [27] M. Manbachi *et al.*, "Real-Time Co-Simulation Platform for Smart Grid Voltage Optimization Using IEC 61850," in *IEEE Trans. on Industrial Informatics*, vol. 12, no. 4, pp. 1392-1402, Aug. 2016.
- [28] M. Diaz-Aguiló *et al.*, "Field-Validated Load Model for the Analysis of CVR in Distribution Secondary Networks: Energy Conservation," in *IEEE Trans. on Power Delivery*, vol. 28, no. 4, pp. 2428-2436, Oct. 2013.
- [29] ANSI, "ANSI Standard C84.1-1995 Electric Power Systems and Equipment Voltage Ratings (60 Hz)," 1995.
- [30] K. Schneider, F. Tuffner, J. Fuller and R. Singh, "Evaluation of Conservation Voltage Reduction (CVR) on a National Level," 2010. Available: http://www.pnl.gov/main/publications/external/technical_reports//PNNL-19596.pdf.
- [31] K. An, H. J. Liu, H. Zhu, Z. Y. Dong, and K. Hur, "Evaluation of Conservation Voltage Reduction with Analytic Hierarchy Process: A Decision Support Framework in Grid Operations Planning," in *Energies* 2016, 9(12), 1074.
- [32] A. Bokhari *et al.*, "Combined Effect of CVR and DG Penetration in the Voltage Profile of Low-Voltage Secondary Distribution Networks," in *IEEE Trans. on Power Delivery*, vol. 31, no. 1, pp. 286-293, Feb. 2016.
- [33] T. J. Krupa and H. Asgeirsson, "The effects of reduced voltage on distribution circuit loads," in *IEEE Trans. on Power Systems*, vol. 2, pp. 1013-1018, 1987.
- [34] "Bibliography on load models for power flow and dynamic performance simulation," in *IEEE Trans. on Power Systems*, vol. 10, no. 1, pp. 523-538, Feb. 1995.
- [35] R. C. Dugan, "An open source platform for collaborating on smart grid research," in *Proc. of IEEE Power Energy Soc. Gen. Meeting*, San Diego, CA, Jul. 2011.
- [36] Y. Tang, X. Mao and R. Ayyanar, "Distribution system modeling using CYMDIST for study of high penetration of distributed solar photovoltaics," in *Proc. of 2012 North American Power Symposium (NAPS)*, Champaign, IL, 2012, pp. 1-6.
- [37] Willis, H. Lee., "Power distribution planning reference book," CRC press, 2004.

- [38] J. WANG et al. , "Analysis of Energy Savings of CVR including Thermostatic Loads in Distribution Systems," in *IEEE Trans. on Power Delivery*, vol. PP, no. 99, pp. 1-1.
- [39] J. Green, "Analysis of Sacramento Municipal Utility District Conservation Voltage Reduction (CVR) Tests," February , 2015. Available:<https://www.epri.com/#/pages/product/000000003002004930/>.
- [40] M. S. Hossan, H. M. M. Maruf, and B. Chowdhury, "Comparison of the ZIP Load Model and the Exponential Load Model for CVR Factor Evaluation," in *Proc. of IEEE Power Energy Soc. Gen. Meeting*, Chicago, IL, 2017.
- [41] S. J. Miller, "The method of least squares," Mathematics Department Brown University (2006), pp. 1-7.
- [42] C. F. So and S. H. Leung, "Variable forgetting factor RLS algorithm based on dynamic equation of gradient of mean square error," in *Electronics Letters*, vol. 37, no. 3, pp. 202-203, 1 Feb 2001.
- [43] K. J. Aström and B. Wittenmark, *Adaptive Control*, 2nd ed. New York: Dover, 2008.
- [44] S. Haykin, "Adaptive Filter Theory," 5th ed., Prentice Hall, 2013.
- [45] D. Simon, "Kalman filtering with state constraints: a survey of linear and non-linear algorithms," in *IET Control Theory & Applications*, vol. 4, no. 8, pp. 1303-1318, August 2010.
- [46] Z. Wang, "Assessment of Conservation Voltage Reduction by Unscented Kalman Filter based load modeling," in *Proc. of IEEE Power Energy Soc. Gen. Meeting*, Boston, MA, 2016, pp. 1-5.
- [47] S. Ghosh, S. Rahman, and M. Pipattanasomporn, "Distribution Voltage Regulation Through Active Power Curtailment with PV Inverters and Solar Generation Forecasts," in *IEEE Transactions on Sustainable Energy*, vol. 8, no. 1, pp. 13-22, Jan. 2017.
- [48] F. C. Schweppe, "Uncertain Dynamic Systems". Englewood Cliffs, NJ, USA: Prentice-Hall, 1973.
- [49] D. Simon and T. L. Chia, "Kalman filtering with state equality constraints," in *IEEE Trans. on Aerospace and Electronic Systems*, vol. 38, no. 1, pp. 128-136, Jan 2002.
- [50] S. J. Julier and J. J. LaViola, "On Kalman Filtering With Nonlinear Equality Constraints," in *IEEE Trans. on Signal Processing*, vol. 55, no. 6, pp. 2774-2784, June 2007.

- [51] L. S. Wang, Y. T. Chiang and F. R. Chang, "Filtering method for nonlinear systems with constraints," in *IEE Proc. of Control Theory and Applications*, vol. 149, no. 6, pp. 525-531, Nov 2002.
- [52] E. E. Elattar, J. Y. Goulermas, and Q. Wu, "Generalized locally weighted GMDH for short term load forecasting," in *IEEE Trans. Syst., Man, Cybern. C: Applicat. Rev.*, vol. 42, pp. 345-356, 2012.
- [53] Willis, H. Lee., Power distribution planning reference book, CRC press, 2004.
- [54] J. W. Smith, R. Dugan, and W. Sunderman, "Distribution modeling and analysis of high penetration PV," 2011 IEEE Power and Energy Society General Meeting, San Diego, CA, 2011, pp. 1-7.
- [55] SIWG, *Smart Inverter Working Group Recommendations*, January 2014.
- [56] W. H. Kerstings, *Distribution System Modeling and Analysis*, CRC press, 2006.
- [57] R. Billinton and R. N. Allan, *Reliability Evaluation of Power Systems*, 2nd ed. New York: Plenum, 1996.
- [58] Zhu, J.Z. Optimization of Power System Operation; IEEE Press-Wiley: Piscataway, NJ, USA, 2009.
- [59] D. Singh and K. Verma, "Multiobjective optimization for DG planning with load models," *IEEE Trans. Power Syst.*, vol. 24, no. 1, pp. 427-436, Feb. 2009
- [60] N. Acharya, P. Mahat, and N. Mithulananthan, "An analytical approach for DG allocation in primary distribution network," *Int. J. Elect. Power Energy Syst.*, vol. 28, pp. 669-678, 2006.
- [61] K. M. Rogers, R. Klump, H. Khurana, A. A. Aquino-Lugo and T. J. Overbye, "An Authenticated Control Framework for Distributed Voltage Support on the Smart Grid," in *IEEE Transactions on Smart Grid*, vol. 1, no. 1, pp. 40-47, June 2010.
- [62] M. E. Baran and F. F. Wu, "Network reconfiguration in distribution systems for loss reduction and load balancing," in *IEEE Transactions on Power Delivery*, vol. 4, no. 2, pp. 1401-1407, Apr. 1989
- [63] "OpenDSS PVSystem Element Model," information available: <https://sourceforge.net/p/electricdss/code/HEAD/tree/trunk/Doc/>
- [64] "Distribution Test Feeders," information available: <https://ewh.ieee.org/soc/pes/dsacom/testfeeders/>
- [65] "Sourceforge", information available: <https://sourceforge.net/p/electricdss/code//HEAD/tree/trunk/Distrib/Examples/Loadshapes/>
- [66] "NREL", information available: http://www.nrel.gov/midc/oahu_archive

- [67] Fourer, Robert; Brian W. Kernighan (2002).“ AMPL: A Modeling Language for Mathematical Programming," Duxbury Press. ISBN 978-0- 534-38809-6.
- [68] K. Kopsidas, A. Kapetanaki, and V. Levi, “Optimal Demand Response Scheduling With Real-Time Thermal Ratings of Overhead Lines for Improved Network Reliability," in *IEEE Trans. on Smart Grid*, vol. 8, no. 6, pp. 2813-2825, Nov. 2017.
- [69] A. Rabiee, S. M. Mohseni-Bonab, M. Parniani, and I. Kamwa, “Optimal Cost of Voltage Security Control Using Voltage Dependent Load Models in Presence of Demand Response," in *IEEE Transactions on Smart Grid*, vol. PP, no. 99, pp. 1-1.
- [70] Z. Wang, J. Wang, B. Chen, M. M. Begovic, and Y. He, “MPC-Based Voltage/Var Optimization for Distribution Circuits With Distributed Generators and Exponential Load Models," in *IEEE Trans. on Smart Grid*, vol. 5, no. 5, pp. 2412-2420, Sept. 2014.
- [71] M Chamana and B. H. Chowdhury, "Optimal Voltage Regulation of Distribution Networks with Cascaded Voltage Regulators in the Presence of High PV Penetration," in *IEEE Trans. on Sustainable Energy*, vol. PP, no. 99, pp. 1-1.
- [72] Y. P. Agalgaonkar, B. C. Pal, and R. A. Jabr, “Distribution voltage control considering the impact of PV generation on tap changers and autonomous regulators," in *IEEE Trans. Power Syst.*, vol. 29, no. 1, pp. 182-192, Jan. 2014.
- [73] F. A. Viawan and D. Karlsson, “Combined local and remote voltage and reactive power control in the presence of induction machine distributed generation," in *IEEE Trans. Power Syst.*, vol. 22, no. 4, pp. 2003-2012, Nov. 2007.
- [74] P. Faria, J. Soares, Z. Vale, H. Morais, and T. Sousa, “Modified Particle Swarm Optimization Applied to Integrated Demand Response and DG Resources Scheduling," in *IEEE Trans. on Smart Grid*, vol. 4, no. 1, pp. 606-616, March 2013.
- [75] M. Alipour, K. Zare, and M. Abapour, “MINLP Probabilistic Scheduling Model for Demand Response Programs Integrated Energy Hubs," in *IEEE Trans. on Industrial Informatics*, vol. 14, no. 1, pp. 79-88, Jan. 2018.
- [76] H. Geramifar, M. Shahabi, and T. Barforoshi, “Coordination of energy storage systems and DR resources for optimal scheduling of microgrids under uncertainties," in *IET Renewable Power Generation*, vol. 11, no. 2, pp. 378-388, 28 2017.
- [77] Y. M. Ding, S. H. Hong, and X. H. Li, “A Demand Response Energy Management Scheme for Industrial Facilities in Smart Grid," in *IEEE Trans. on Industrial Informatics*, vol. 10, no. 4, pp. 2257-2269, Nov. 2014.

- [78] M. Farivar and S. H. Low, "Branch Flow Model: Relaxations and Convexification?Part I," in *IEEE Trans. on Power Syst.*, vol. 28, no. 3, pp. 2554-2564, Aug. 2013.
- [79] R. Billinton and R. N. Allan, *Reliability Evaluation of Power Systems*, 2nd ed. New York: Plenum, 1996.
- [80] L. Wu, M. Shahidehpour, and T. Li, "Cost of Reliability Analysis Based on Stochastic Unit Commitment," in *IEEE Trans. on Power Syst.*, vol. 23, no. 3, pp. 1364-1374, Aug. 2008.
- [81] H. Heitsch and W. Römisch, "Scenario reduction algorithms in stochastic programming," in *Comput. Optim. Appl.*, vol. 24, nos. 2?3, pp. 187?206, Feb. 2003.
- [82] D. Singh and K. Verma, "Multiobjective optimization for DG planning with load models," in *IEEE Trans. Power Syst.*, vol. 24, no. 1, pp.427?436, Feb. 2009.
- [83] F. Robert, B. W. Kernighan (2002). "AMPL: A Modeling Language for Mathematical Programming," Duxbury Press. ISBN 978- 0- 534-38809-6.
- [84] M. Tawarmalani and N. V. Sahinidis, "A polyhedral branch-and-cut approach to global optimization," *Mathematical Programming*, 103:225-249, 2005.
- [85] R. Moghe, A. Iyer, F. C. Lambert, and D. Divan, "A robust smart sensor for smart substations," in *Proc. IEEE Power and Energy Society General Meeting*, San Diego, CA, 2012, pp. 1-8.
- [86] QinetiQ North America, "Distribution Grid Sensing and Monitoring," Available:<https://www.qinetiq-na.com/linewatchsensors/linewatch/about/>.
- [87] Tollgrade, "Improving grid reliability with tollgrade Lighthouse," Available:<http://www.tollgrade.com/smartgrid/smart-gridproducts/smart-grid-mv-sensor/>.
- [88] S. Chanda and A. K. Srivastava, "Defining and Enabling Resiliency of Electric Distribution Systems With Multiple Microgrids," in *IEEE Transactions on Smart Grid*, vol. 7, no. 6, pp. 2859-2868, Nov. 2016.
- [89] T. Tayjasanant, C. Li, and W. Xu, "A resistance sign-based method for voltage sag source detection," in *IEEE Trans. Power Delivery*, vol.20, no.4, pp. 2544-2551, Oct. 2005.
- [90] A. K. Pradhan and A. Routray, "Applying distance relay for voltage sag source detection," in *IEEE Trans. Power Delivery*, vol. 20, no. 1, pp. 529-531, Jan. 2005.
- [91] Two Ways to Make U.S. Distribution Systems Self-Healing, Available: <http://smartgrid.ieee.org/resources?catid=0&id=160..>

- [92] M. Korkali, H. Lev-Ari, and A. Abur, "Traveling-Wave-Based Fault-Location Technique for Transmission Grids Via Wide-Area Synchronized Voltage Measurements," in *IEEE Trans. on Power Systems*, vol. 27, no. 2, pp. 1003-1011, May 2012.
- [93] A. B. Borghetti et al. "Continuous-wavelet transform for fault location in distribution power networks: Definition of mother wavelets inferred from fault originated transients," in *IEEE Trans. on Power Systems*, vol. 23, no. 2, pp. 380-388, May 2008.
- [94] S. F. Alwash, V. K. Ramachandaramurthy, and N. Mithulananthan, "Fault-Location Scheme for Power Distribution System with Distributed Generation," in *IEEE Trans. on Power Delivery*, vol. 30, no. 3, pp. 1187-1195, June 2015.
- [95] S. M. Brahma, "Fault Location in Power Distribution System With Penetration of Distributed Generation," in *IEEE Trans. on Power Delivery*, vol. 26, no. 3, pp. 1545-1553, July 2011.
- [96] D. Thukaram, H. P. Khincha, and H. P. Vijaynarasimha, "Artificial neural network and support vector Machine approach for locating faults in radial distribution systems," in *IEEE Trans. on Power Delivery*, vol. 20, no. 2, pp. 710-721, April 2005.
- [97] J. Mora-Florez, V. Barrera-Nuez, and G. Carrillo-Caicedo, "Fault location in power distribution systems using a learning algorithm for multivariable data analysis," in *IEEE Trans. on Power Delivery*, vol. 22, no. 3, pp. 1715-1721, Jul. 2007.
- [98] G. Mateos and G. B. Giannakis, "Load Curve Data Cleansing and Imputation Via Sparsity and Low Rank," in *IEEE Transactions on Smart Grid*, vol. 4, no. 4, pp. 2347-2355, Dec. 2013.
- [99] X. Feng, F. Yang, and W. Peterson, "A practical multi-phase distribution state estimation solution incorporating smart meter and sensor data," in *Proc. IEEE Power and Energy Society General Meeting*, San Diego, CA, 2012.
- [100] P. Jouni et al., "Handling bad or missing smart meter data through advanced data imputation," in *Proc. Innovative Smart Grid Technologies Conference (ISGT)*, Minneapolis, MN, 2016, pp. 1-5.
- [101] IEEE Standard Definitions for the Measurement of Electric Power Quantities Under Sinusoidal, Nonsinusoidal, Balanced, or Unbalanced Conditions, in *IEEE Std 1459-2010* (Revision of IEEE Std 1459-2000) ,vol., no., pp.1-50, March 19 2010.
- [102] D. E. Knuth, *The art of computer programming, volume 3: (2nd ed.) sorting and searching*, Addison Wesley Longman Publishing Co., Redwood City, CA, 1998.

- [103] S. Lotfifard, M. Kezunovic, and M. J. Mousavi, "Voltage sag data utilization for distribution fault location," in *IEEE Trans. Power Delivery*, vol. 26, no. 2, pp. 1239-1246, Apr. 2011.
- [104] P. C. Chen, V. Malbasa, Y. Dong, and M. Kezunovic, "Sensitivity Analysis of Voltage Sag Based Fault Location With Distributed Generation," in *IEEE Trans. on Smart Grid*, vol. 6, no. 4, pp. 2098-2106, July 2015.
- [105] J. D. Glover, M. S. Sarma, and T. J. Overbye, *Power System Analysis and Design*, Canada, ON, Toronto:Thomson, 2008.